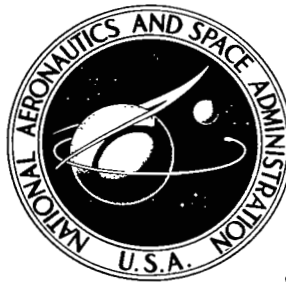


NASA TECHNICAL NOTE



NASA TN D-4308

C.1

NASA TN D-4308

LOAN COPY: RE
AFWL (WVJ)
KIRTLAND AFB,



TECH LIBRARY KAFB, NM

PRESSURE AND FLOW-FIELD STUDY
AT MACH NUMBER 8 OF
FLOW SEPARATION ON A FLAT PLATE
WITH DEFLECTED TRAILING-EDGE FLAP

by Charles B. Johnson

Langley Research Center

Langley Station, Hampton, Va.



TECH LIBRARY KAFB, NM



0131362

PRESSURE AND FLOW-FIELD STUDY AT MACH NUMBER 8
OF FLOW SEPARATION ON A FLAT PLATE WITH
DEFLECTED TRAILING-EDGE FLAP

By Charles B. Johnson

Langley Research Center
Langley Station, Hampton, Va.

NATIONAL AERONAUTICS AND SPACE ADMINISTRATION

For sale by the Clearinghouse for Federal Scientific and Technical Information
Springfield, Virginia 22151 - CFSTI price \$3.00

PRESSURE AND FLOW-FIELD STUDY AT MACH NUMBER 8
OF FLOW SEPARATION ON A FLAT PLATE WITH
DEFLECTED TRAILING-EDGE FLAP

By Charles B. Johnson
Langley Research Center

SUMMARY

An experimental investigation was made of the flow separation on a flat plate model with a short trailing-edge flap deflected at angles of 10° , 20° , and 30° relative to the plate surface. These tests were conducted at a nominal free-stream Mach number of 8 and the nominal free-stream unit Reynolds number per foot was varied from 0.22×10^6 to 10.9×10^6 (per meter from 0.72×10^6 to 35.8×10^6). Pressure measurements and schlieren studies were made for wall-to-total temperature ratios of 0.14, 0.43, and 0.74. Surface oil-flow studies were made at a wall-to-total temperature ratio of 0.43. Local similarity boundary-layer calculations were made upstream of the interaction region. Properties of the interaction and separated flow region were calculated with the boundary-layer—shock-wave interaction theory of Lees and Reeves (AIAA Journal, Nov. 1964). The upstream flat-plate boundary-layer theory was joined to the Lees and Reeves theory at the beginning of the interaction region by matching the boundary-layer momentum thicknesses.

The results showed good agreement between the experimental and calculated pressures for wall-to-total temperature ratios of 0.74 (adiabatic) and 0.43 (room temperature). The oil-flow study showed the variation in the extent of separation with a change in unit Reynolds number for both laminar separation and for transitional separation. Wall cooling, for transitional separation, reduced the extent of separation. The maximum pressures measured on any particular flap varied considerably with a change in unit Reynolds number. The maximum pressures measured on the 30° flap at a unit Reynolds number per foot of 2.65×10^6 (per meter of 8.69×10^6) indicated a pressure rise of approximately 58 percent over the oblique shock reattachment value.

INTRODUCTION

Flow separation is a common fluid mechanical phenomenon occurring on many configurations over a range of conditions from subsonic to hypersonic flow. Many investigations, both theoretical and experimental, have been made of varied configurations and

conditions causing flow separation. Recent reviews of flow-separation research are given in references 1 to 3. As the free-stream Mach number increases into the hypersonic flow regime, laminar flow generally becomes more prevalent; therefore, increased attention has been focused on laminar separation and the associated laminar plateau pressure rise. Typical examples of experimental investigations of flow separation on flat plates and axisymmetric bodies are found in references 4 to 23.

The purpose of the present paper is to present a detailed experimental investigation and a comparison with theory of the effect of unit Reynolds number, flap angle, and wall-to-total temperature ratio on the surface static pressure and the flow field for a flat plate model with a short trailing-edge flap. The tests herein were conducted for wall-to-total temperature ratios of 0.14, 0.43, and 0.74, flap angles of 10° , 20° , and 30° , and unit Reynolds numbers per foot ranging from 0.22×10^6 to 10.90×10^6 (per meter from 0.72×10^6 to 35.76×10^6). Pressure measurements and schlieren studies were made for all three wall-to-total temperature ratios. Previous tests conducted with a similar configuration have been made over a narrower range of unit Reynolds numbers and have not considered the effect of wall temperature. (See refs. 6, 7, 15, and 16.) The separation point, the separation shock angle, and the separation flow deflection angle were obtained from the schlieren studies. Separation and reattachment points were also measured by oil-flow studies. The trend in the movement of the separation point with a change in unit Reynolds number found from the oil-flow study clarifies the apparent contradictory results previously obtained over a much narrower range of Reynolds numbers (refs. 7 and 16). Reattachment pressures were determined from plots of the pressure distributions and the point of reattachment found from oil-flow studies. The model had a relatively short trailing-edge flap which undoubtedly had some effect on the extent of separation.

The Lees and Reeves theory (ref. 24) was used to compute the pressure rise from the beginning of the interaction region to the end of the first pressure plateau region. The local similarity theory of reference 25 was used to calculate the upstream boundary-layer parameters used in the Lees and Reeves theory. The Lees and Reeves solution was joined to the upstream boundary-layer solution by matching the value of the momentum thickness at the beginning of the interaction region as determined from the experimental data. Detailed results of the calculations are presented herein.

SYMBOLS

a speed of sound; also velocity profile parameter, $\left[\frac{\partial(\bar{U}/\bar{U}_e)}{\partial(\bar{Y}/\delta_i)} \right]_{\bar{Y}=0}$ for attached flow and $(\bar{Y}/\delta_i)_{f'=0}$ for separated flow

c_p specific heat at constant pressure

c_v specific heat at constant volume

$$E = \int_0^{\delta_i} (\bar{U}/\bar{U}_e) S d\bar{Y}$$

e enthalpy integral, $\int_0^{\delta_i} S d\bar{Y}$

f stream function (see eqs. (6) and (7) and ref. 25)

$$H = \theta_i / \delta_t^*$$

h enthalpy; also used for heat-transfer coefficient in definition for Stanton number

$$J = \theta_i^* / \delta_t^*$$

L length of flat plate portion of model, 10 inches (0.254 meter)

L' normalizing factor for theoretical solution, 1 foot (0.3048 meter)

M Mach number

m_β curve fit pressure gradient parameter

N_{Pr} Prandtl number

N_{St} Stanton number, $h/c_p \rho_e u_e$

P wall shear stress function, $\frac{\delta_t^*}{\bar{U}_e} \left(\frac{\partial \bar{U}}{\partial \bar{Y}} \right)_{\bar{Y}=0}$

p static pressure

R unit free-stream Reynolds number per foot; also used in appendix B for

$$\text{dissipation function, } \frac{2\delta_t^*}{\bar{U}_e^2} \int_0^{\delta_i} \left(\frac{\partial \bar{U}}{\partial \bar{Y}} \right)^2 d\bar{Y}$$

$$Re_{e,x} = \frac{\rho_e u_e x}{\mu_e}$$

S total enthalpy function, $\frac{h_t}{h_{t,e}} - 1$

T temperature

T* enthalpy function, $E/S_w \delta_t^*$

\bar{U} Stewartson's transformed velocity, $\left(\frac{a_\infty}{a_e}\right)u$

u velocity component parallel to surface

x coordinate parallel to surface

\bar{Y}, \bar{X} Stewartson's transformed coordinates (see ref. 24)

Z velocity integral, $\frac{1}{\delta_t^*} \int_0^{\delta_i} \left(\frac{\bar{U}}{\bar{U}_e}\right) d\bar{Y}$

β pressure gradient parameter

γ ratio of specific heats, c_p/c_v

δ_f trailing-edge flap angle

δ boundary-layer thickness

δ^* displacement thickness

δ_i transformed boundary-layer thickness

δ_i^* boundary-layer-displacement thickness $\int_0^{\delta_i} \left(1 - \frac{\bar{U}}{\bar{U}_e}\right) d\bar{Y}$

δ_t^* transformed displacement thickness, $\delta_i^* + e$

ζ stagnation enthalpy ratio, $h_t/h_{t,e}$

η similarity variable (ref. 25)

θ momentum thickness

θ_i boundary-layer momentum thickness, $\int_0^{\delta_i} \frac{\bar{U}}{\bar{U}_e} \left(1 - \frac{\bar{U}}{\bar{U}_e}\right) d\bar{Y}$

θ_i^* mechanical "energy" thickness, $\int_0^{\delta_i} \frac{\bar{U}}{\bar{U}_e} \left(1 - \frac{\bar{U}^2}{\bar{U}_e^2}\right) d\bar{Y}$

θ_2 indicated shock angle (see sketch 1 on p. 14)

μ viscosity

ρ density

ψ indicated flow deflection angle (see sketch 1 on p. 14)

Subscripts:

e local external conditions

i transformed conditions

o at beginning of interaction

pl plateau value

r reattachment value

s separation point

t stagnation conditions

w wall conditions

x along plate

∞ free-stream conditions behind oblique shock

A prime indicates differentiation with respect to η .

APPARATUS AND TEST PROCEDURES

Description of the Models Used

The pressure model used for the tests at the three wall temperature conditions is shown in figures 1 and 2. The model made from AISI type 347 stainless steel had a sharp leading edge about 0.001 in. thick (0.025 mm). The flat plate portion of the model was 7.75 in. wide (0.197 m) and 10 in. long (0.254 m). A 2.0-in-long (0.0508 m) trailing-edge flap, which may be positioned at angles δ_f of 0° , 10° , 20° , and 30° relative to the flat plate surface, extends across the back of the model. Tests were also made with upper side plates with sharp leading edges which extended back from the leading edge at an angle of approximately 6° as indicated by the line labeled "side plate" in figure 1.

Instrumentation

The pressure model was instrumented with 23 pressure orifices of 0.070-in. (1.78 mm) inside diameter as shown in figure 2. The instrumentation extends from 4.75 in. (0.121 m) from the leading edge to 0.281 in. (0.00714 m) from the trailing edge of the flap. The pressures were measured with electrical hot-wire pressure gages and with electrical wire strain-gage type of pressure gages. The range of the electrical hot-wire gages is 0 to 20 mm Hg and the range of the strain-gage type varied from 0 to 1 to 0 to 7.5 psia (0 to 6894.7 to 0 to 51 710 N/m²). The accuracy of the hot-wire pressure gage is thought to be ± 0.05 mm Hg and the accuracy of the strain-gage pressure transducer is thought to be 0.75 percent of full-scale deflection. The calibration of the hot-wire gage is extremely nonlinear and was calibrated with a high degree of accuracy in the lower pressure range. The strain-gage transducers have a linear calibration over their rated pressure range.

Pressure tests at $T_w/T_t = 0.43$ and 0.14 were made with the electrical hot-wire pressure gages mounted inside the body of the model, as shown in figure 3. For pressure tests at $T_w/T_t = 0.43$ the strain-gage type was used also and was mounted inside the model injection box below the tunnel test section as shown in figure 4. Stainless-steel tubing and plastic vacuum tubing were used for all pressure leads. For the pressure tests at $T_w/T_t = 0.74$, both the electrical hot-wire and electrical wire strain-gage types were used with the gages mounted outside the tunnel, wrapped in a polyethylene bag, and immersed in an ice bath so that the gages could be kept at a constant temperature.

Test Apparatus and Procedures

The tests were conducted in the Langley Mach 8 variable-density hypersonic tunnel. The tunnel operated at a nominal Mach number of 8 over a range of Reynolds number per foot of 0.20×10^6 to 11.0×10^6 (per meter of 0.65×10^6 to 36.1×10^6). The tunnel

stagnation conditions varied from 25 psia and 1070° R (172.4 kN/m² and 594° K) to 2680 psia and 1470° R (18.5 MN/m² and 817° K) for lowest and highest unit Reynolds numbers, respectively. A Mach number calibration of the facility can be found in reference 26 and a further description is given in reference 27. Throughout the tests the model was set at 1/2° angle of attack resulting in a range of local Mach number on the plate from about 7.4 to 7.8.

The pressure tests for $T_w/T_t = 0.43$ were made with the model at essentially isothermal room temperature conditions since the data were taken at 1/2 sec after the model was positioned in the test section. Less than 1/2 sec was required for the pressures to reach an equilibrium value over the range of test conditions when the 0 to 20 mm gages were mounted inside the model. Equilibrium pressures were reached in approximately the same time for the higher range pressure gages, which were mounted outside the model in the vacuum tight chamber because of their size. (See fig. 4.)

The tests at $T_w/T_t = 0.14$ were conducted with the model cooled by liquid nitrogen. The small hot-wire gages were mounted inside the model as shown in figure 3 and were sprayed with liquid nitrogen. The leading-edge piece had two passages drilled through it for liquid nitrogen cooling, as shown in figure 2. The pressure gage cavity (fig. 3) and back side of the flap were sprayed with liquid nitrogen. When the model reached an isothermal temperature of approximately 190° R (105.5° K) the model was injected into the tunnel and the pressure data were taken 1/2 sec after the model was positioned in the test section. The cold wall temperature of the model was measured by thermocouples mounted on the inside surface of the model at a point from the leading edge where the skin thickness was approximately 3/16 in. (0.00476 m) thick (fig. 2). A tight-fitting cover was placed over the surface of the model during the cool down period to prevent the formation of frost on the surface of the model. This cover was removed just prior to the injection of the model for a subsequent test.

For the tests at $T_w/T_t = 0.74$, the model was heated prior to exposure to the hypersonic stream to approximately 1000° R (555.5° K) by blowing subsonic heated air over the model. During an actual test when the model was in the hypersonic stream the model temperature settled out to a near equilibrium value which gave a wall-to-total temperature ratio of approximately 0.74. The actual surface test temperature of the model ranged from 950° to 1200° R (528° to 666° K) for the lowest to the highest Reynolds numbers, respectively. The thermocouples as shown in figure 2 were used to determine the surface temperature of the model for the hot wall test. The data were taken just prior to the time when there was a breakdown of the supersonic flow in the tunnel. The length of the run prior to flow breakdown was approximately 60 sec.

THEORETICAL APPROACH

At the time the present tests were conducted, the most promising theoretical approach to the flat plate trailing-edge flap problem was the theory of Lees and Reeves in reference 24. (See appendix A.) Consequently, the method of Lees and Reeves was programed for use on the IBM 7090 electronic data processing system and approximately 120 cases were calculated to check the agreement with experimental data. The first set of theoretical calculations was made for $T_w/T_t = 1.0$, which was compared with the data for the adiabatic ($T_w/T_t = 0.74$) test conditions. Additional boundary-layer parameters were calculated for $T_w/T_t = 0.6$ (appendix B) and compared with the data for room temperature wall conditions ($T_w/T_t = 0.43$).

The method of joining the Lees and Reeves separated flow solution to the upstream-boundary-layer solution as used herein deviates slightly from the method indicated in reference 24. The juncture of the two solutions is located at the beginning of the interaction region. (See fig. 5.) This point is determined from the results of experimental pressure distributions, rather than from an iterative solution from the complete theory. The beginning of the interaction region is defined as the point where the pressure first begins to rise above a flat plate value due to the adverse pressure gradient feeding upstream from the flap. In order to find the proper Lees and Reeves solution for a given experimental case the value of momentum thickness at start of the Lees and Reeves solution was matched to the value of the momentum thickness from the upstream-boundary-layer solution at the x/L point defined as the beginning of the interaction. The upstream-boundary-layer calculation took into account the favorable pressure gradient due to the induced-boundary-layer effects. This method of matching was used because the complete Lees and Reeves solution from the beginning of the separation interaction region to the undisturbed flow downstream of the reattachment point could not be matched to the physical size of the model. Specifically, the calculations from the hinge line through reattachment and downstream to a point where the solution reached a Blasius type of flow yielded a streamwise x distance greater than the 2-in-long (0.0508 m) flap of the model. The calculations that were made with the Lees and Reeves theory were done with the intention of predicting the initial shape of the pressure curve and the level of the plateau pressure. For the initial 120 cases for $T_w/T_t = 1.0$ and $T_w/T_t = 0.6$ only the region from the beginning of the interaction to the hinge line was calculated. The details of the Lees and Reeves calculations are given in appendixes A and B.

Upstream-Boundary-Layer Calculation

The local external flow properties for the upstream-boundary-layer solutions were calculated from the induced pressure effects for the case of weak interaction from the

theory of Bertram and Blackstock in reference 28. The equation for the induced pressure (for $\gamma = 1.4$) is

$$\frac{p}{p_\infty} = 1 + \frac{\alpha}{\sqrt{1 + \alpha}} \left[1 + \frac{\alpha}{2(1 + \alpha)} \right] + \frac{0.4285\alpha^2}{(1 + \alpha)} \left[1 + \frac{\alpha}{2(1 + \alpha)} \right]^2 \quad (1)$$

where

$$\alpha = 0.7G\bar{\chi}$$

$$G = 0.34416 \left(\frac{T_w}{T_t} - 0.3859 \right)$$

$$\bar{\chi} = \frac{M^3 \sqrt{C}}{\sqrt{R_{\infty, x}}}$$

$$C = \frac{\mu_w T_\infty}{\mu_\infty T_w}$$

The local values at the edge of the boundary layer of Mach number, temperature, velocity, and local Reynolds number per foot were computed from ($\gamma = 1.4$).

$$M_e = \sqrt{\left[\left(\frac{p}{p_\infty} \right)^{-2/7} (5 + M_\infty^2) \right] - 5.0} \quad (2)$$

$$\frac{T_e}{T_\infty} = \frac{5 + M_\infty^2}{5 + M_e^2} \quad (3)$$

$$u_e = M_e (49.1) \sqrt{T_e} \quad (4)$$

$$Re = \frac{1.812 \times 10^8 (T_e + 201.6) M_e p_e}{T_e^2} \quad (5)$$

The locally similar solutions of Beckwith and Cohen in reference 25 were used to calculate the upstream boundary layer with a pressure gradient as calculated by equation (1). The boundary-layer equations in the similarity coordinates with the simplifying assumptions of constant c_p and $\rho\mu$ and $N_{Pr} = 1.0$ reduce to

$$f'''' + ff'' + \beta(\xi - f'^2) = 0 \quad (6)$$

$$\xi'' + f\xi' = 0 \quad (7)$$

where the notation is that of reference 25.

Thus, with the local conditions external to the boundary layer calculated from equations (1) to (5), the upstream boundary layer was obtained from a numerical solution to equations (6) and (7) at 35 points along the flat plate.

Application of Theory to a Flat Plate

With a Trailing-Edge Flap

The Lees and Reeves solution between the beginning of the interaction region and the shock impingement point depends only on the separation point value of the transformed displacement thickness, the assumed local conditions at the edge of the boundary layer, and the previous upstream history of the boundary layer. Therefore, the Lees and Reeves solution, as calculated for a shock-wave—boundary-layer interaction, may be readily applied to a flat plate with a trailing-edge flap, from the beginning of the interaction region to the vicinity of the hinge line.

The regions from the shock impingement point to beyond the reattachment point, for the case of a shock-wave—boundary-layer interaction, are assumed analogous to certain regions for a trailing-edge flap configuration if the wedge angle of the shock generator is half the flap angle since the final total compression angle of the inviscid flow would then be the same for the two configurations. The corresponding assumed flow models for the shock-wave—boundary-layer interaction and for the flat plate with trailing-edge flap are shown in figure 5 where it is assumed that the point of shock impingement and hinge line coincide. For the shock-wave—boundary-layer interaction a fluid element external to the boundary layer and moving parallel to the plate surface turns through an angle of $\delta_f/2$ as it passes through the impinging shock wave. The same fluid element external to the boundary layer is turned again by an angle of $\delta_f/2$ as it passes through the reattachment compression fan and then moves downstream parallel to the plate surface. For the flat plate with a trailing-edge flap the fluid element external to the boundary layer is turned by an angle of δ_f as it passes over the flap and through the reattachment compression fan. Thus, if the shock generator angle is taken as half the flap angle, the external flow for both conditions will experience the same total compression angle and will have a similar static-pressure history over the surface as is shown in part (c) of figure 5. In the flow models assumed for both configurations, the increase in entropy along the edge of the boundary layer is neglected — that is, the compression is assumed to occur through a series of weak waves rather than one strong shock wave.

TEST RESULTS

Transition-Point Data

It is known that transition can affect the extent of separation as well as the pressure levels associated with the region of separation; therefore, the location of the point of transition was determined from heat-transfer measurements made with a configuration which is geometrically similar to the pressure model of figures 1 and 2. (See ref. 29.) In figure 6 a typical example of the heat-transfer distribution obtained with the model tested as a flat plate ($\delta_f = 0$) illustrates where the position that was chosen as the point of transition is located ($x/L \approx 0.90$).

The location of the point of transition for the $\delta_f = 30^\circ$ data in figure 6 is believed to be somewhere between the flat plate value of $x/L \approx 0.90$ and the point where the heat transfer in the separated region first begins to rise, $x/L \approx 0.75$. A summary of the flat plate transition data is shown in table I.

TABLE I.- FLAT PLATE TRANSITION-POINT DATA

Unit Reynolds number		Distance from leading edge to beginning of transition, x/L	Local transition Reynolds number
per foot	per meter		
2.65×10^6	8.69×10^6	0.90	1.99×10^6
3.45	11.32	.80	2.30
4.30	14.11	.75	2.69
10.90	35.8	.55	5.00

Over the range of unit Reynolds number an attempt was made to classify the type of separation as laminar, transition, or turbulent according to the definition of the three classes of separation as set forth in reference 20. The classification of the type of separation is readily defined at unit Reynolds numbers per foot of 2.65×10^6 (per meter of 8.69×10^6) and above, where measurements of the flat plate transition point indicate a maximum downstream limit as to where transition should occur in the regions of separated flow. For the separated flows at unit Reynolds numbers per foot below 2.65×10^6 it is felt that transition could possibly occur in the separated region on the flap, somewhere before reattachment, even though there was no transition detected on the flat plate model. One possible reason for the occurrence of transition on the flap at lower unit Reynolds numbers is that the effect of separation and the effect of the flap deflection is to increase the local pressure and thereby increase the local Reynolds number in the separated region. Becker and Korycinski (ref. 21) found that in the presence of extensive separation the transition Reynolds number (based on free-stream conditions and distance to transition point) was less by a factor of approximately 4 than the transition Reynolds number

for which there was no separation. The movement of the separation point with a change in unit Reynolds number (which will be discussed in detail in the section "Surface Oil-Flow Studies") also helps to classify the type of separation.

Room Temperature Wall Pressure Tests

Pressure distributions obtained on the plate with various flap angles at $T_w/T_t = 0.43$ for various Reynolds numbers are shown in figure 7. The measured pressures were divided by the pressures at the beginning of the interaction region. The pressures were obtained without side plates except for those presented in figure 7(d). All the pressure data in figure 7 are compared with the Lees and Reeves theory (ref. 24) for $T_w/T_t = 0.6$, and the beginning of the interaction region is determined as described in the section "Theoretical Approach."

The agreement between experiment and the Lees and Reeves theory is, in general, good for the range of unit Reynolds number per foot from 0.22×10^6 to 1.46×10^6 (per meter from 0.72×10^6 to 4.79×10^6). The tests in this Reynolds number range are in a flow regime where plateau pressure level is not strongly affected by transitional effects. When transitional effects become more pronounced (Reynolds numbers per foot greater than 2.65×10^6 (per meter 8.69×10^6)) the Lees and Reeves theory tends to underpredict the level of pressure in the area of the start of transition. The rise in pressure when transition occurs in the separated region was previously noted by Chapman, Kuehn and Larson in reference 20. For the tests at a unit Reynolds number per foot of 2.65×10^6 in figures 7(a) to 7(d) the rise in pressure above the laminar plateau value occurs at $x/L \approx 0.90$, which was previously given as the approximate transition location. For the tests at a unit Reynolds number per foot of 4.3×10^6 (per meter of 14.1×10^6) in figures 7(a) to 7(c), the start of transition is slightly upstream of the point of separation (based on the flat plate transition point); thus, little or no agreement would be expected at $R = 4.3 \times 10^6/\text{ft}$ with the laminar theory of Lees and Reeves. The side plate data in figure 7(d) at a unit Reynolds number per foot of 1.06×10^6 (per meter of 3.48×10^6) show that as the flap angle increases the level of plateau pressure also increases, and, in addition, the Lees and Reeves theory tends to slightly underpredict for the 20° and 30° flap angles as was found for the model with no side plates. A comparison of the data for $R = 2.65 \times 10^6/\text{ft}$ in figures 7(a) to (d) shows that, in general, the addition of side plates increases the extent of separation for all flap angles. The pressures measured upstream of the separation interaction region in figure 7 agree well with the viscous interaction theory of Bertram and Blackstock (ref. 28). The pressure ratio for the theoretical viscous interaction curves shown is divided by the theoretical pressure ratio at the beginning of the interaction. Flagged symbols in figure 7 indicate pressures measured off the center line of the model. (See fig. 2.)

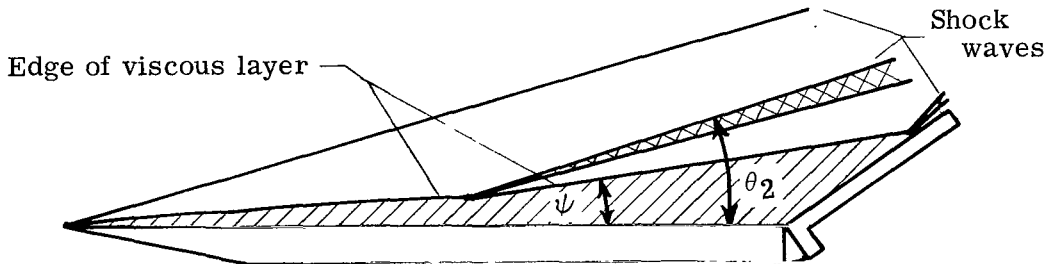
In figure 8 are shown schlieren photographs for tests at $T_w/T_t = 0.43$ and flap angles of 10° , 20° , and 30° over a range of Reynolds number per foot from 0.22×10^6 to 10.9×10^6 (per meter from 0.72×10^6 to 35.8×10^6). These photographs were used to determine the angles of the leading-edge shock, the separated layer shock, and the deflection angle of the separated boundary layer. In addition the photographs were used to determine the separation point based on the location where the separation shock wave intersects the boundary layer. These measurements of the separation point were found to be in good agreement with oil-flow separation-point data.

Figure 9 shows the pressure distribution for a room temperature wall divided by the theoretical static pressure as calculated for the inviscid flat plate model set at $1/2^\circ$ positive angle of attack for various flap angles and Reynolds numbers with and without side plates. The flap pressure ratios above values of 10 are not shown in figure 7 but are shown in figure 9. The separated-layer oblique-shock theory in figure 9 was calculated from the apparent measured flow deflection angle above the separated layer (fig. 8) and based on the value of Mach number ahead of the interaction region. The value of Mach number ahead of the interaction region was calculated from the measured value of the leading-edge shock angle, above the interaction region, and the free-stream Mach number. All oblique shock parameters were taken from reference 30. Also shown in figure 9 are the values of the beginning of the interaction x_o , the separation point x_s , and the reattachment point x_r . The values of the separation point and the reattachment point (fig. 9) were taken from oil-flow studies. The beginning of the interaction region is taken from the expanded plots, shown in figure 7, of pressures in the area of the plateau and interaction region, where the beginning of the interaction region is defined as previously noted in the section "Theoretical Approach." The separated-layer oblique-shock values of pressure agree, for the most part, with the measured pressure plateau values with the exception of a few of the lower unit Reynolds numbers where the shock pressures tend to slightly overpredict the measured values.

The peak pressure ratio in figure 9(a) for the 30° flap at $R = 10.9 \times 10^6/\text{ft}$ ($35.8 \times 10^6/\text{m}$) is 29.6 compared with the inviscid-flap oblique-shock value of 28.6. The value of the pressure ratio reaches a maximum at approximately the same level as the inviscid-flap oblique-shock value apparently because of the thin boundary layer and the absence of any separation incurred at this highest Reynolds number. For $R = 4.3 \times 10^6/\text{ft}$ and $2.65 \times 10^6/\text{ft}$ ($14.1 \times 10^6/\text{m}$ and $8.69 \times 10^6/\text{m}$) the peak pressure ratios are approximately 42.0 and 45.0 as compared to inviscid values of 28.6 and 28.5, respectively. This peak value of about 45.0 for the lower Reynolds number represents an increase of 58 percent over the calculated inviscid value. The measured peak pressure exceeds the inviscid shock pressure because of the quasi-isentropic compression which occurs through a series of waves or several shocks rather than through a single shock. At Reynolds numbers per foot of 1.46×10^6 , 1.06×10^6 , and 0.65×10^6 (per meter

of 4.79×10^6 , 3.48×10^6 , and 2.13×10^6), the pressure ratios have reached values greater than the corresponding inviscid values but apparently have not reached as high a value as they would have if the flap had been longer. This phenomenon is apparently due to the proximity of the reattachment point to the trailing edge of the flap, which does not allow the flow to turn completely parallel to the flap. This same effect becomes even more pronounced at the three lowest Reynolds numbers as the reattachment point moves closer to the trailing edge of the flap. In figure 9(b) a similar trend can be seen where for the 20° flap, with the highest unit Reynolds number per foot of 10.9×10^6 , the pressure approaches the inviscid value of 14.2, while at a Reynolds number per foot of 4.3×10^6 the pressure rise increases to a peak and then starts an approach toward the inviscid value. In figure 9(c) for the 10° flap the peak pressure rise has a trend similar to that exhibited in figures 9(a) and 9(b) for the 30° and 20° flaps, only to a much lesser degree. The side plate data in figures 9(d) and 9(e), in general, indicate a slower rise to the peak pressure value on the flap.

In figure 10 the indicated flow deflection angle ψ (sketch 1), measured to within an accuracy of approximately $\pm 0.3^\circ$ from schlieren photographs, and the indicated shock angle θ_2 are plotted against unit Reynolds number.



Sketch 1

The angles were measured over the linear part of the shock wave and the separated region that was over the flat plate portion of the model. Figure 10 shows that for a given free-stream unit Reynolds number, the indicated flow deflection angle and corresponding indicated shock wave angle decrease as the flap angle decreases. Also, as the unit Reynolds number decreases the flow deflection and corresponding shock angle increase.

A comparison of the plateau pressures obtained from oblique shock calculations, the Lees and Reeves theory, and measured static pressure values (for no side plates) is shown in figure 11. The oblique shock curves in figure 11 are faired curves taken from another plot of the individual data points. These faired oblique shock curves deviate approximately 2 percent from the individual data points and were calculated from the flow

deflection angles (fig. 10) by using the local values of Mach number just upstream of the beginning of the interaction. The local Mach number was calculated from the leading-edge shock-wave inclination and the free-stream Mach number. The Lees and Reeves prediction for the plateau pressure ratio for flap angles of 10° , 20° , and 30° was taken from plots of $(p/p_o)_{pl}$ against $M_{e,s}$ for the various unit Reynolds numbers. (See appendix A.) The measured plateau pressures for flap angles of 20° and 30° were taken from the plotted data of figure 7. No experimental plateau pressures for a 10° flap angle are presented since the length of separated-flow region was so short that a pressure plateau could not form. In general, the oblique-shock value of plateau pressure is higher than the measured value and the Lees and Reeves value is slightly lower. (The difference in the Lees and Reeves value of plateau pressure between figure 7 and figure 11 lies in the fact that the plateau pressures for figure 11 are taken from plots of $(p/p_o)_{pl}$ against $M_{e,s}$ for the exact value of $M_{e,s}$, whereas the theoretical plateau pressures in figure 7 were taken from plots of p/p_o against x/L' for a nominal value of $M_{e,s}$. (See appendix A.)

Surface Oil-Flow Studies

Technique for testing.- The pressure model (fig. 1) was used for the surface oil-flow studies and was tested with and without side plates. Prior to making an oil-flow test a pattern of drops consisting of an oil-lampblack mixture was placed on the surface of the plate as shown on the left in figure 12. The viscosity of the oil was increased with increasing unit Reynolds number in order that an oil-flow pattern could be established in approximately the same length of time for all runs. The model was rapidly injected into the wind-tunnel flow and when the apparent rearward movement of the oil drops stopped, giving a stabilized oil-flow pattern, the model was retracted from the stream. The temperature of the model in the area of separation varied from approximately 90° F to 100° F for all oil-flow tests. This temperature was measured with a thermocouple located 8 in. (0.2032 m) downstream from the leading edge on the inside surface of the model at an area where the skin thickness is approximately $3/16$ in. (0.00476 m). The oil drops were placed on the model just prior to the run and a photograph was taken of the oil dots in the undisturbed position and then immediately after the run a second photograph was taken of the oil-flow pattern. These photographs were used as a means for determining the location of the separation point. A typical oil-flow pattern is shown in figure 12 for a free-stream unit Reynolds number per foot of 4.3×10^6 (per meter of 14.1×10^6) and a flap angle of 20° . It can be seen from these oil-flow photographs that the surface streamlines are parallel to the inviscid flow before the interaction region; however, in the reverse flow region the surface oil flow shows the streamlines diverge indicating that the surface flow is three dimensional in nature. The use of the side plates considerably reduced the divergence of the flow in the separated region.

The viscosity of the oil for each Reynolds number and flap angle could not be chosen to insure a clear and distinct pattern of oil flow in the separated region for each run. For the majority of runs the oil droplets in the reverse flow region were displaced to some extent toward the separation point due to surface shear, where this movement could be detected by superimposing the negatives taken before and after the run. The use of the two negatives as an oil-flow evaluation technique was extremely helpful in determining the exact location of the point of separation which is indicated by the arrows.

Separation point results.- The distance from the leading edge to the point of separation as obtained from oil-flow data is shown in figure 13 for free-stream unit Reynolds numbers per foot from 0.22×10^6 to 4.3×10^6 (per meter from 0.72×10^6 to 14.1×10^6), for flap angles of 10° , 20° , and 30° , and for the studies with and without side plates. The results show that the separation point moves forward appreciably as the flap angle is increased and generally moves forward as the unit Reynolds number increases, up to $R \approx 0.8 \times 10^6/\text{ft}$ ($2.62 \times 10^6/\text{m}$). At the lower Reynolds numbers (up to $R = 0.4 \times 10^6/\text{ft}$ ($1.31 \times 10^6/\text{m}$)) for the 10° and 20° flap angles, the rearward movement of the separation point with increasing Reynolds number is attributed to the fact that the outer edge of the viscous layer observed in the schlieren photographs passes well above the uppermost portion of the deflected flap (2 in. (0.0508 m) long). An examination of the schlieren photographs showed that when the outer edge of the viscous layer was deflected in a direction parallel to the flap, the separation point began to move forward on the plate with increasing Reynolds number, as can be noted in figure 13 for the 30° deflected flap. It can be seen in figure 13 that for all three flap angles the separation point begins to move to the rear of the plate at a unit Reynolds number per foot of approximately 1.0×10^6 (per meter of 3.28×10^6). This reversal in the trend of the separation-point movement is attributed to the flow going from a laminar separation to a transition type of separation. For these data it appears that separation up to a unit Reynolds number per foot of approximately 1.0×10^6 gives laminar separation and for a unit Reynolds number per foot above approximately 1.0×10^6 the separation is transitional, independent of the extent of separation and flap angle. The oil-flow tests were made with a model which had a trailing-edge flap 2 in. long. This short flap caused the reattachment point to be close to the trailing edge of the flap for the lowest unit Reynolds number tested. Undoubtedly the short length of the flap had some effect on the extent of the separation; however, to what degree the flap length affected the extent of separation would require a separate investigation.

In figure 13 the effects of the side plates for all flap angles and Reynolds numbers is to move the separation point upstream with the exception of the 10° flap angle where for Reynolds numbers per foot from 0.65×10^6 (per meter from 2.13×10^6) to 4.3×10^6 (per meter from 14.10×10^6) the separation point moves slightly downstream with the addition of side plates. A comparison between the separation point, as indicated by the oil-flow pattern and as obtained from schlieren photographs, shows reasonably good

agreement when the schlieren separation point is chosen at the intersection of the shock wave from the separated layer and the apparent outer edge of the boundary layer.

The effect of unit Reynolds number on the movement of the separation point.- From prior experimental investigations it was exhibited that when the Reynolds number was low enough the type of separation was purely laminar and that an increase in unit Reynolds number for any particular configuration moved the separation point upstream. For instance, the results from an experimental investigation by Miller, Hijman, and Childs at a Mach number of about 16 (ref. 15), in which all the data presented were classified as pure laminar separation, showed that as the Reynolds number increased (up to $R \approx 1.0 \times 10^6/\text{ft}$ ($3.28 \times 10^6/\text{m}$)) that the separation point moved upstream. The data of Chapman, Kuehn, and Larson (ref. 20) at Mach numbers of 2.7 to 3.5 show that, when the unit Reynolds number is increased so that the separation becomes transitional, the point of separation moves downstream with an increase in unit Reynolds number. In addition, the data show that a further increase in unit Reynolds number caused the separation to become turbulent and the separation point moved even further downstream. Becker and Korycinski (ref. 21) pointed out a similar effect on the movement of the point of separation on an axisymmetric flared body when the separation went from pure laminar to transitional and finally to a turbulent type of separation. The movement of the point of separation with a change in unit Reynolds number shown in figure 13, and discussed in the previous section "Separation point results," showed the same trend with a change in unit Reynolds number as found in references 15, 20, and 21.

A set of theoretical calculations with the laminar theory of Lees and Reeves showed that an increase in the unit Reynolds number moved the separation point upstream. The calculation was made for a constant local Mach number at the point of separation (appendix A) and was based on the value of the displacement thickness found at the beginning of the Lees and Reeves interaction region and matched to the value of displacement thickness found on a flat plate with the local similarity solution of reference 25.

Thus, the results from this paper and prior experimental investigations, as well as the theoretical calculations from the Lees and Reeves theory, show that for laminar separation the point of separation moves upstream with an increase in the unit Reynolds number. Experimental results also show that for transitional and turbulent separation the separation point moves downstream with an increase in unit Reynolds number.

Reattachment point results.- In figure 14 the results of an oil-flow study to determine the reattachment point on the flap are shown. The reattachment point clearly moves toward the hinge line as the Reynolds number increases. The location of reattachment on the flap, for a given unit Reynolds number, varies only slightly with a change in the flap angle. It is only in the vicinity of a unit Reynolds number per foot of 1.06×10^6 (per meter of 3.48×10^6) that there is any appreciable variation in the point of reattachment

with a change in flap angle. This variation is attributed to a delay in the transitional effects with a decrease in flap angle. The solid lines in figure 14 are the predicted reattachment points as obtained from a linear extension of the dividing streamline from the point of separation (fig. 13) to the flap at an angle equal to the flow deflection angle of figure 10. The experimental data points are further downstream from the hinge line at the lower unit Reynolds numbers than the predicted values indicating that the dividing streamline curves upward as it moves downstream from the point of separation.

In figure 15 the pressure ratios at the reattachment point on the flap are plotted against unit Reynolds number. The pressures in figure 15 are limited in accuracy due to the difficulty in determining the precise point of reattachment in an area on the flap where the pressure gradient is often quite large. For a given unit Reynolds number the level of pressure increases with an increase in flap angle as might be expected; however, the reattachment pressure levels are considerably lower than the oblique shock inviscid pressure levels which are noted in figure 9. The reattachment pressure levels are much smaller than the inviscid oblique shock values indicating that the inviscid stream has not yet turned parallel to the flap and the compression process is still underway.

Wall Temperature Effects

In order to determine the wall temperature effect on separation, experimental tests were conducted at wall-to-total temperature ratios of 0.14, 0.43, and 0.74. Figure 16 shows the measured flat plate static pressure, 5 in. (0.127 m) aft of the leading edge, divided by the theoretical inviscid flat plate static pressure at $1/2^\circ$ positive angle of attack and the theoretical viscous interaction pressure calculated by the Bertram and Blackstock method (ref. 28) for various values of T_w/T_t . The results in figure 16 show that the pressure ratios for $T_w/T_t = 0.43$ and 0.74 decrease with an increase in unit Reynolds number and the theory overpredicts the measured pressure ratios by approximately 10 percent. The pressure data at $T_w/T_t = 0.14$ at the two lowest unit Reynolds numbers are considerably lower than the theory, whereas the remaining values of pressure ratio at the higher Reynolds numbers are lower than the theory by approximately 10 percent or less. The large discrepancy between data and theory, for $T_w/T_t = 0.14$, at the two lowest unit Reynolds numbers may be caused by a shift in the gage calibration due to a temperature effect on the hot-wire gage.

Pressure parameter distribution for various flap angles.- The pressure tests conducted for various flap angles and wall-to-total temperature ratios are shown in figures 17 to 22. The measured pressures have been divided by the measured pressure at the beginning of the interaction region. The pressure data in these figures for wall-to-total temperature ratios of 0.43 and 0.74 are compared to calculations based on the Lees and Reeves theory (ref. 24) for corresponding wall conditions of $T_w/T_t = 0.6$ and $T_w/T_t = 1.0$, respectively. In addition pressure distributions based on the flat plate

viscous-interaction theory of Bertram and Blackstock (ref. 28) are calculated (and plotted) for wall-to-total temperature ratios of 0.43 and 0.74. The flagged symbols in figures 17 to 19 indicate pressures measured off the center line of the model. (See fig. 2.)

The data in figure 17 for $\delta_f = 10^0$ show reasonably good agreement with the theory of Lees and Reeves for unit Reynolds numbers per foot up to 1.46×10^6 (per meter up to 4.79×10^6). The effect of wall cooling on the extent of separation and the level of plateau pressure is small for the three lowest Reynolds numbers. The data for the two highest Reynolds numbers show that, as the wall-to-total temperature ratio decreases, the extent of separation also decreases, particularly at the highest Reynolds number.

An inspection of the experimental data of figure 17 shows that, as the wall-to-total temperature ratio decreases, the pressure gradient from the beginning of the interaction region to approximately the hinge line becomes slightly greater. Gadd, in reference 31, showed this effect of wall temperature on the pressure gradient rise for tests made at a Mach number of 3.0. Calculations with the theory of Lees and Reeves also show that, for $T_w/T_t = 0.6$, larger pressure gradients occur in this region than occurred for $T_w/T_t = 1.0$. In an earlier and different type of analysis from that of Lees and Reeves, Curle (ref. 32) and Gadd (ref. 33) showed that the pressure gradient at separation should be inversely proportional to the wall temperature, which is qualitatively the same finding that comes out of the Lees and Reeves solutions. The absolute value of the measured plateau pressure for $T_w/T_t = 0.74$ is higher than for $T_w/T_t = 0.43$. However, when the absolute values of plateau pressure are divided by the experimental value of the pressure at the beginning of the interaction, resulting values of the plateau pressure ratios for $T_w/T_t = 0.43$ and 0.74 are brought fairly close together. This trend can be seen from figures 16 to 22.

The data of figures 20, 21, and 22 were obtained with side plates (fig. 1) at unit Reynolds numbers per foot of 1.06×10^6 and 2.65×10^6 (per meter of 3.48×10^6 and 8.69×10^6). In general, the results of figures 20, 21, and 22 show a slight decrease in the extent of separation with wall cooling at a unit Reynolds number per foot of 1.06×10^6 and a marked decrease in the extent of separation with wall cooling at a unit Reynolds number per foot of 2.65×10^6 . Figures 20 to 22 also show a decrease in flap pressure ratio with an increase in the wall-to-total temperature ratio for both unit Reynolds numbers.

Separation point data.- A summary of the separation point data taken from the schlieren photographs of figure 23 for various wall-to-total temperature ratios and two flap angles are shown in figure 24. The schlieren photographs were taken during the pressure tests shown in figures 18 and 19. For the 30^0 flap angle, the results in figure 24 for the room temperature wall ($T_w/T_t = 0.43$) and the hot wall ($T_w/T_t = 0.74$) show that the separation point moves forward on the plate with increasing unit Reynolds number per

foot up to a value of approximately 1.0×10^6 (per meter, 3.28×10^6). An increase in unit Reynolds number per foot above approximately 1.0×10^6 for all three wall-to-total temperature ratios rapidly moves the separation point toward the hinge line for both the 20° and 30° flaps. For pure laminar separation the wall temperature effects for a flap angle of 30° show that the highly cooled wall ($T_w/T_t = 0.14$) has the greatest extent of separation, whereas for $T_w/T_t = 0.43$ and 0.74 nearly an equal extent of separation is noted. The wall temperature effect for $\delta_f = 20^\circ$ is quite similar to that for the 30° flap with the extent of laminar separation being the greatest for the highly cooled wall ($T_w/T_t = 0.15$), the room temperature wall ($T_w/T_t = 0.43$) having the smallest extent of separation, and the hot wall ($T_w/T_t = 0.74$) having an extent of separation falling between the other two wall conditions. For both the 20° and 30° flap angles, after transition occurs the effect of wall cooling for a given unit Reynolds number tends to decrease the extent of separation significantly. (Transition is assumed to occur near a unit Reynolds number per foot of approximately 1.0×10^6 based on previously discussed results at $T_w/T_t = 0.43$.) This wall temperature effect, decreasing the extent of separation, is particularly noticeable at unit Reynolds numbers per foot above 2.65×10^6 (per meter above 8.69×10^6). The effect of wall cooling in reducing the extent of separation was also shown in reference 34 for a cone-cylinder flare at Mach number 5 over a similar unit Reynolds number range.

Plateau pressure data.- In figure 25 the values of plateau pressure ratios for various wall-to-total temperature ratios and flap angles were taken from the plots of figures 18 and 19. The level of plateau pressure decreases with an increase in the unit Reynolds number for all three temperature ratios and both flap angles. The highly cooled wall ($T_w/T_t = 0.14$) and the hot wall ($T_w/T_t = 0.74$) give higher values of plateau pressure than the room temperature wall ($T_w/T_t = 0.43$) up to a unit Reynolds number per foot of 1.0×10^6 (per meter of 3.28×10^6). At a unit Reynolds number per foot of about 1.0×10^6 the transitional effects become significant and the plateau pressure level, for a given unit Reynolds number, decreases with an increase in wall cooling.

Flow deflection and shock wave angles.- The schlieren photographs (fig. 23) were used to determine the wall temperature effect upon the flow deflection angles and the shock wave angles shown in figure 26. An analysis of figure 26 shows that the flow deflection angle and the shock wave angle, measured at the point of separation, decrease continuously with increasing unit Reynolds number for all three wall-to-total temperature ratios. The effect of wall temperature on flow deflection and shock angle is not large; however, it should be noted that the highly cooled wall ($T_w/T_t = 0.14$) and the hot wall ($T_w/T_t = 0.74$) both have slightly higher values of deflection and shock wave angle than does the room temperature wall ($T_w/T_t = 0.43$). This fact tends to confirm the observations noted previously regarding effect of cooling on the measured pressures.

Plateau pressure correlation.- Figure 27 shows a correlation of the plateau pressure coefficients in terms of the local Reynolds number and local Mach number at the beginning of the interaction region. The local flow properties were evaluated from the measured wall pressures, shock angles, and the oblique shock relations. These data show reasonable agreement with an expression given by Hakkinen, Greber, Trilling, and Abarbanel in reference 35 but fall slightly above the theory of Erdos and Pallone in reference 36. The lower Mach number data of Chapman, Kuehn, and Larson in reference 20 and the data of Miller, Hijman, and Childs in reference 15 also are higher than the expression for $(c_p)_{pl}(Re,x)_o^{1/4}$ of Erdos and Pallone.

In figure 28 the plateau pressure data of the present investigation, as shown in figure 27, are compared with the data of references 4, 11, 15, 19, 20, 23, and 35. The correlation of $(c_p)_{pl}(Re,x)_o^{1/4}$ is plotted as a function of the local Mach number at the beginning of the interaction $M_{e,o}$ from 1.3 to 14.3. Even though there is scatter in the data the agreement with the theories of references 35 and 36 can be seen over the range of $M_{e,o}$. In particular the agreement with the theory of reference 35 appears reasonably good up to a Mach number of approximately 8, whereas for $M_{e,o}$ values greater than 8 the data show closer agreement with the theory of reference 36. The curves obtained in references 35 and 36 are somewhat dependent upon the assumed relationship between Reynolds number and skin friction. The use of other methods of determining skin friction could lead to other curves than those shown.

CONCLUDING REMARKS

An experimental investigation of pressures on a flat plate with various flap angles and three wall-to-total temperature ratios was made. The model tested had a short trailing edge flap (2 in. (0.127 m) long) which, for the lower unit Reynolds numbers, resulted in the point of reattachment being near the trailing edge of the flap. The short length of the flap and the associated reattachment point close to the trailing edge of the flap undoubtedly had some effect on the extent of separation and clearly had some effect on the maximum pressure rise on the flap.

Experimental pressures in the separation region were compared with calculations made by the Lees and Reeves theory (AIAA Journal, Nov. 1964) for a shock-wave—boundary-layer interaction. Only the calculation for the region from the beginning of the interaction region to the maximum extent of the laminar plateau region was used due to the short length of the flap. Agreement between the separation pressure data and the Lees and Reeves theory was found to be reasonably good. Lees and Reeves upper and lower branch boundary-layer parameters for a wall-to-total temperature ratio of 0.6 were calculated from local similarity boundary-layer solutions for use in the separated flow solution.

The results of an extensive surface oil-flow study conducted at room temperature wall conditions showed that for pure laminar separation an increase in unit Reynolds number moved the separation point upstream; however, when the separation becomes transitional, an increase in unit Reynolds number moved the separation point toward the hinge line. It was also found that the use of side plates and an increase in the size of the flap angle increased the extent of separation. The variation of the extent of separation with a change in unit Reynolds number was nearly the same for conditions with and without side plates. The flap reattachment point, according to the results of the oil-flow study, showed that for a given unit Reynolds number the point of reattachment changed very little with a change in flap angle from 10° to 30° . However, the pressures at reattachment varied considerably.

The maximum pressures measured on any particular flap varied considerably with a change in unit Reynolds number. The maximum pressures measured on the 30° flap at a unit Reynolds number per foot of 2.65×10^6 (per meter of 8.69×10^6) indicated a pressure rise of approximately 58 percent over the oblique shock reattachment value. The reason for this rise in pressure is believed to be due to a quasi-isentropic compression occurring through a series of waves (or shocks) rather than a single shock. Similar pressure rises, only to a lesser degree, are noted for the 20° flap angles for similar unit Reynolds numbers.

The measured separation flow deflection angles and shock-wave angles for wall-to-total temperature ratios of 0.14, 0.43, and 0.74 indicate qualitative agreement with calculations made from measured pressures and the theoretical calculations made from the Lees and Reeves theory.

A change in the wall-to-total temperature ratios (T_w/T_t) showed:

(1) For the range of unit Reynolds number that appeared to give laminar separation, $T_w/T_t \approx 0.14$ gave the highest plateau pressure and the greatest extent of separation; the smallest value of plateau pressure and the least extent of separation occurred for $T_w/T_t \approx 0.43$; and for $T_w/T_t \approx 0.74$ the value of plateau pressure and length of separation was between these two extremes.

(2) For the range of Reynolds numbers where the separation was classified as first becoming transitional (with transition believed to occur in the separated layer very near the flap) the level of plateau pressure and the extent of separation were in reasonably close agreement for all three flap angles.

(3) For the highest Reynolds number, where the separation was clearly transitional (with transition occurring in the separated layer above the flat plate portion of the model), a decrease in the wall-to-total temperature ratio markedly decreased the extent of separation and also reduced the level of the plateau pressure.

The viscous interaction theory of Bertram and Blackstock (NASA Technical Note D-798) agreed well with the experimental flat plate data upstream of the separation effects for $T_w/T_t = 0.43$ and 0.74 .

A correlation of the plateau pressure with the local Mach number and Reynolds number at the beginning of the interaction showed reasonable agreement with the theory of Hakkinen, Greber, Trilling, and Abarbanel (NASA Memorandum 2-18-59W).

The effect of side plates on the model as compared to the results with no side plates showed a reduction in the three dimensionality of the flow in the separated region, a slight increase in the plateau pressure level, and a considerable increase in the extent of separation.

Langley Research Center,
National Aeronautics and Space Administration,
Langley Station, Hampton, Va., March 29, 1967,
129-01-08-38-23.

APPENDIX A

SOLUTION FOR THE LAMINAR SEPARATED BOUNDARY LAYER

Review of Theoretical Literature

The problem of flow separation has been investigated theoretically since the time of Prandtl's early works published in reference 37. In recent times one of the first efforts toward an analysis of supersonic separation was made by Chapman, Kuehn, and Larson (ref. 20) in which the results of Chapman's mixing layer analysis (ref. 38) were used. Chapman's analysis represents a limiting case for separation with the assumption that the boundary-layer thickness is zero at the point of separation.

The Karman-Pohlhausen method was used by Gadd, Curle, and Savage (refs. 39, 32, and 40, respectively) without a great deal of success primarily because the assumed velocity profiles in the region of separation did not give the reverse flow found in experiment. Crocco and Lees, in reference 41, developed a semiempirical method which depends on the rate of entrainment of fluid from the external stream into the boundary layer. Results from the Crocco-Lees method were only in qualitative agreement with experimental data. The Crocco-Lees method, modified by Glick (ref. 42), predicted results that were in good agreement with pressure data as obtained from experiment. This method uses the concept of the dividing streamline; however, empirical data are required for its application. The Crocco-Lees method was also used by Bray, Gadd, and Woodger (ref. 43) with reasonable success.

Tani in reference 44 used an analysis similar to that of Wieghardt (ref. 45) and Walz (ref. 46) in that his solution for an attached flow with an adverse pressure gradient used the first moment of momentum in addition to the zeroth moment and continuity equations. Tani used a quartic representation for the velocity profiles; however, the boundary condition which required that the momentum equation at the wall be satisfied was dropped. When this boundary condition was neglected the resulting one parameter, which characterizes the family of velocity profiles, was not directly related to the static pressure distribution but was directly proportional to the shear stress at the wall. The one parameter describing the family of velocity profiles was obtained from the simultaneous solution of the zeroth moment of momentum and the first moment of momentum equations. The results of Tani's analysis have been found to be in good agreement with exact solutions of the boundary-layer equations. Poots, in reference 47, extended Tani's method by adding the energy equation to the continuity and two momentum equations.

Abbot, Holt, and Nielsen, in reference 48, studied the separated flow problem by using the continuity equation, the zeroth and the first moment of momentum equation, and the energy equation with a fourth degree polynomial expression for the velocity and

APPENDIX A

temperature profiles and with one undetermined parameter per profile. The resulting separated flow pressure distributions did not have the correct trends primarily because of the use of polynomials for the velocity and temperature profiles. Lees and Reeves, in reference 24, developed a method for the shock-wave—boundary-layer interaction problem wherein the continuity equation, the momentum equation, and the first moment of momentum equations are solved simultaneously with a one parameter family of velocity and enthalpy profiles. Lees and Reeves used the Cohen and Reshotko profiles for the highly cooled wall cases and added the Stewartson profiles for the adiabatic wall, as found in references 49 and 50, respectively. This method gives good agreement with experimental pressure data obtained in the present paper for both adiabatic and cooled walls ($T_w/T_t = 0.6$); however, for the highly cooled wall ($T_w/T_t = 0.2$) and for quantitative heat-transfer predictions, indications are that the method is inadequate. The most promising method for predicting both pressure and heat transfer under highly cooled wall conditions seems to be that of Holden (ref. 51), which adds the energy equation to the conservation of mass and the zeroth and first moment of momentum equations. Holden's method of solution is similar to that of Lees and Reeves in that he uses the velocity and enthalpy profiles from the upper and lower branches of the Cohen and Reshotko solution (ref. 49). However, Holden's family of velocity and enthalpy profiles are determined by two parameters, one of which defines the velocity profile and the other defines the enthalpy profile. Both Holden and Lees and Reeves in their methods of solution uncouple the boundary-layer velocity profiles from the pressure gradient parameter associated with the Cohen and Reshotko solution. For the Lees and Reeves method of solution once the velocity profile is determined there is only one enthalpy profile associated with the given velocity profile. On the other hand in Holden's method the enthalpy profile is uncoupled from both the pressure gradient parameter and the velocity profile, and with the inclusion of the energy equation the enthalpy profile parameter can be determined. The results of Holden's method agree well with his highly cooled wall experimental heat-transfer and pressure data (ref. 51).

Lees and Reeves General Method of Solution

The Lees and Reeves theory (ref. 24) gives the solution for the laminar boundary layer in which a pressure disturbance is propagated upstream through a supersonic flow. A pressure disturbance may be generated by a shock wave impinging on the boundary layer or it may be caused by a trailing-edge flap — the Lees and Reeves theory may be applied to either of the two types of disturbances. (See fig. 5.) The theory, and its calculations as used in this paper, applies at the beginning of the interaction region and is used to the point of the shock impingement (the hinge line) for $T_w/T_t = 0.6$ and 1.0. The flow region on the flap was calculated for a few cases but it was found that the extent of the calculated region over the flap was considerably longer than the actual size of the flap on the model.

APPENDIX A

The Lees and Reeves method requires the solution of the previously mentioned conservation equations coupled with an inviscid-streamline—Prandtl-Meyer solution. The method gives the solution for the boundary layer and the flow external to the boundary layer within the framework of a single parameter family of velocity profiles. This one parameter determines the velocity and enthalpy profile for specified regions of attached and separated flows and yet is not directly related to the local static-pressure gradient. The local pressure gradient is determined from the local inviscid flow inclination and the Prandtl-Meyer solution.

As previously noted for $T_w/T_t = 1.0$, the Stewartson (ref. 50) and the Cohen and Reshotko (ref. 49) boundary-layer solutions were used to evaluate the integral parameters used in the Lees and Reeves solution. With heat transfer, $T_w/T_t = 0.6$, the boundary-layer profiles were calculated from the local similarity solutions with $N_{Pr} = 1.0$, $c_p = \text{Constant}$, and $\rho\mu = \text{Constant}$. These boundary-layer solutions were used to calculate the integral parameters. (See appendix B.) These integral parameters were then curve fitted (by a polynomial expression) as a function of the single parameter a used to describe the entire family of velocity profiles for both attached and separated flow. The coefficients of the polynomials from the fitted curves of the integral parameters for $T_w/T_t = 0.6$ are tabulated in tables II and III. The local similarity solutions reduce to a solution which is the same as that of Cohen and Reshotko (ref. 49) when a Prandtl number of unity and a constant heat capacity are used.

The Lees and Reeves method of calculation starts at the point of separation and moves upstream until a flat plate (Blasius type) solution is reached at the upstream end of the interaction. The values of local Mach number and unit Reynolds number are fixed at the point of separation and the value of the transformed displacement thickness at the point of separation is iterated for until the proper upstream solution is found at the beginning of the interaction region. The conditions needed for satisfying the two-point boundary value problem are the rate of change with respect to the transformed \bar{x} distance of the local Mach number and the shape parameter approaching zero at the same time as the parameter describing the family of velocity profiles approaches the zero pressure gradient value for attached flow. After the correct value of the displacement thickness, at the point of separation, is found the solution moves downstream into the separated flow region. The basic equations used in the Lees and Reeves method of solution are found in reference 24 and were integrated by a fourth-order Runge-Kutta integration procedure which extrapolates to a zero interval size as a correction factor. The equations were all integrated with δ_t^* as the independent variable.

APPENDIX A

Procedure Used for Application of the Lees and Reeves Theory

In figure 29 the experimental values are shown of the beginning of the interaction region as taken from measured pressure distributions at three different wall-to-total temperature ratios. The beginning of the interaction region $(x/L)_O$ is selected as the point where the pressure begins to rise above the undisturbed upstream values due to the adverse pressure gradient feeding forward from the flap. The Lees and Reeves solution is then joined to the upstream boundary-layer solution at this $(x/L)_O$. The upstream boundary-layer momentum thickness is shown in figures 30 and 31 for a plate 10 in. (0.254 m) long at $T_w/T_t = 1.0$ and 0.6, respectively. The calculations in figures 30 and 31 were made for a unit Reynolds number range per foot from 0.22×10^6 to 4.3×10^6 (per meter from 0.72×10^6 to 14.11×10^6), respectively. (The Mach number and unit Reynolds number actually varied slightly along the plate according to the weak interaction equations.) The momentum thickness at the beginning of the interaction θ_{x_O} from the Lees and Reeves solution for the various test Reynolds numbers is plotted against the assumed local Mach number at the point of separation $M_{e,s}$ in figures 32 and 33. Specific cases using the Lees and Reeves theory were calculated for unit Reynolds numbers per foot from 0.22×10^6 to 4.3×10^6 and local Mach numbers at separation from 6.5 to 7.5 at 0.1 intervals in $M_{e,s}$. The undisturbed flat plate Mach number was varied from 7.4 to 7.8 to correspond to the change in the test section Mach number with a change in free-stream unit Reynolds number (ref. 27). Typical plots of pressure against x/L' from the beginning of the interaction region are shown in figure 34 for various values of unit Reynolds number and $T_w/T_t = 1.0$ and 0.6.

The first step in the application of the Lees and Reeves theory as used in the present paper is to obtain from figure 29, for a given T_w/T_t and unit Reynolds number, the $(x/L)_O$ value for the beginning of the interaction. This value of $(x/L)_O$ is then used to find the value of the momentum thickness at the beginning of the interaction θ_O for the upstream solutions from figure 30 or 31. This value of θ_O is then used in either figure 32 or 33 for a given value of T_w/T_t and R to obtain the corresponding value of $M_{e,s}$, which in turn is used to specify the particular Lees and Reeves solution and pressure distribution (fig. 34) for the given test conditions.

It can be seen in figure 34, for all values of unit Reynolds number, that as the Mach number at separation increases, the rate of the pressure increase (with distance) decreases for a sizable x/L' distance before the pressure begins to climb toward a plateau value. This slow rate of increase in pressure occurs in the region between $p/p_O = 1.00$ and 1.10 and makes it difficult to determine the beginning of the interaction region. For the purpose of comparing the theory with experimental data this difficulty was overcome by linearly extrapolating the slope of the curve at $p/p_O = 1.10$ to the abscissa as is shown typically by the dash-dot line in figure 34(a) for $R = 0.22 \times 10^6/\text{ft}$ ($0.72 \times 10^6/\text{m}$) and $M_{e,s} = 6.8$. The point where the extrapolated lines crossed the

APPENDIX A

x/L' abscissa was considered to be the theoretical point of the beginning of the interaction region; this was matched to the experimental value of the beginning of the interaction region. Thus, the theoretical and experimental techniques of determining the beginning of the interaction were consistent, in that both methods used a sudden pressure rise to define the beginning of the interaction region.

It should be noted in figure 34 that, at the separation point for $T_w/T_t = 0.6$, the pressure-ratio curves have a distinct discontinuity in slope. When the theoretical curves were compared with the experimental data the discontinuities in slope were faired to give a smooth pressure rise. The reason for the discontinuity in the slope of the pressure curves at the point of separation is believed to be due to the change in slope of the separated and attached profile parameters upstream and downstream of the point of separation. (See appendix B.) For the majority of the cases calculated in figure 34 the plateau pressure level for the adiabatic wall conditions ($T_w/T_t = 1.0$) was slightly higher than that for the cool wall ($T_w/T_t = 0.6$), where the extent of separation was long enough to allow the pressure ratios for both wall conditions to reach an almost constant plateau value.

In figure 35 a comparison is shown between the growth of the momentum and displacement thicknesses for the upstream similar solution boundary layer ($T_w/T_t = 0.43$) and for the downstream Lees and Reeves solution at a unit Reynolds number per foot of 0.22×10^6 (per meter of 0.72×10^6), where the two solutions were joined based on $(x/L)_0$ for $\delta_f = 30^\circ$ and $M_{e,S} = 6.6$. The results of a typical calculation shown in figure 35 indicate that the momentum thickness changes less than the displacement thickness in the presence of an adverse pressure gradient for the interaction and separated regions.

Plots of the plateau pressure against the local Mach number at separation as obtained from the Lees and Reeves theory are shown for $T_w/T_t = 0.6$ and 1.0 in figures 36 and 37, respectively. The dashed curves represent the theoretical values of plateau pressure based on the experimental value of the beginning of the interaction found in figure 29. In addition to figure 29, figures 30 to 33 were used to obtain the proper value of the local Mach number at separation (as discussed previously) for the dashed curves in figures 36 and 37. The predicted values of plateau pressures in figures 35 and 36 are confined to a narrow band which decreases steadily with an increase in unit Reynolds number.

APPENDIX B

LEES AND REEVES BOUNDARY-LAYER PARAMETERS FOR $T_w/T_t = 0.6$

The curve fit parameters for the boundary-layer integral parameters for $T_w/T_t = 0.6$ that were used in the Lees and Reeves calculation are given in tables II and III for attached and separated flow parameters, respectively. These parameters were calculated from local similarity solutions using a Prandtl number of unity and constant heat capacity. The integral parameters, in the notation of reference 25, are

$$H = \frac{\int_0^{\delta} f'(1 - f')d\eta}{\int_0^{\delta} (\xi - f')d\eta} \quad (B1)$$

$$J = \frac{\int_0^{\delta} f'(1 - f'^2)d\eta}{\int_0^{\delta} (\xi - f')d\eta} \quad (B2)$$

$$P = f''_w \int_0^{\delta} (\xi - f')d\eta \quad (B3)$$

$$R = 2 \int_0^{\delta} (\xi - f')d\eta \int_0^{\delta} (f'')^2 d\eta \quad (B4)$$

$$T^* = \frac{\int_0^{\delta} f'(\xi - 1)d\eta}{(t_w - 1) \int_0^{\delta} (\xi - f')d\eta} \quad (B5)$$

$$Z = \frac{(f)_{\delta}}{\int_0^{\delta} (\xi - f')d\eta} \quad (B6)$$

APPENDIX B

The value of f' , at the edge of the boundary layer, was taken as 0.9995 for all calculations. The parameters in equations (B1) to (B6) were fitted to various order polynomials by the method of least squares as a function of the parameter a defined by the Lees and Reeves method. The parameters H , J , P , R , T^* , and Z in tables II and III are defined in equations (B1) to (B6) while ζ'_w and m_β are defined in reference 29 where the expression for heat transfer is given.

The polynomials in tables II and III occur in the general form

$$H = A + Ba + Ca^2 + Da^3 + Ea^4 + Fa^5 + Ga^6 + Ha^7$$

and vary from fourth order for the attached flow parameter to as high as seventh order for separated flow.

TABLE II.- COEFFICIENTS FOR ATTACHED FLOW

$$T_w/T_t = 0.6$$

Parameter	A	B	C	D	E
H	0.3321009	0.13986596	0.01179970	-0.00946576	0.00275081
J	.50348534	.19925458	.02442816	.00089497	-.00135237
R	.9388926	-.41635211	.19676828	-.06663378	.01160929
¹ P (if $a > 0.4$)	.00432494	.28136774	-.04773970	-.01147897	.00336312
Z	1.894155	.79107769	.18536477	-.00701481	.007183026
T*	.17239089	.13440415	.01340911	.01577639	-.00074312
ζ'_w	.12409628	.05559569	-.03955804	.02479668	-.00555449
m_β	-.1094301	-.01730765	.05114864	.02927415	.01006094

¹If $0 \leq a \leq 0.4$, $P = 0.2715a$.

TABLE III.- COEFFICIENTS FOR SEPARATED FLOW

$$T_w/T_t = 0.6$$

Parameter	A	B	C	D	E	F	G	H
H	0.3318532	-0.52778371	0.2626242	-3.0420035	4.3360826			
J	.50378811	-.99282899	5.100377	-52.405373	251.93463	-630.63668	788.67751	-384.52197
¹ R (if $a > 0.06$)	.92651705	3.5312703	-48.027304	502.05092	-2393.2702	6017.3521	-7518.2889	3648.4459
² P (if $a > 0.05$)	-.00302374	-.5727471	-7.2003253	53.081567	-263.80331	669.6665	-745.74645	286.17898
Z	1.8961545	-2.5925828	-6.8986577	55.663569	-186.92544	281.81194	-155.92	
T*	.17241606	-.40731561	-.11445041	.8055802	-1.1635996	1.1703974		
³ ζ'_w (if $a > 0.05$)	.12554626	-.16814151	1.4798979	-19.391634	105.05788	-293.36703	401.23095	-210.28584
m_β	-.10887434	-.10113126	2.5761168	-17.154012	59.001127	-89.996992	48.966367	

¹If $(0 \leq a \leq 0.06)$, $R = 0.9388926 + 1.806118a$.

²If $(0 \leq a \leq 0.05)$, $P = -0.889a$.

³If $(0 \leq a \leq 0.05)$, $\zeta'_w = 0.12409628 + 0.1022052a$.

REFERENCES

1. Weaver, J. E.; and Clayton, F. I.: Flow Separation in High Speed Flight – A Review of the State-of-the-Art. Rept. SM-46429, Missile & Space Syst. Div., Douglas Aircraft Co., Apr. 1965.
2. Kaufman, Louis G., II; Hartofilis, Stavros A.; Evans, William J.; Oman, Richard A.; Meckler, Lawrence H.; and Weiss, Daniel: A Review of Hypersonic Flow Separation and Control Characteristics. ASD-TDR-62-168, U.S. Air Force, Mar. 1962.
3. Nielsen, Jack N.; and Goodwin, Frederick K.: Investigation of Hypersonic Flow Separation and Its Effect on Aerodynamic Control Characteristics. Vidya Rept. No. 63 (Contract No. AF 33(657)-7084), Itek Corp., Jan. 1962.
4. Putnam, Lawrence E.: Investigation of Effects of Ramp Span and Deflection Angle on Laminar Boundary-Layer Separation at Mach 10.03. NASA TN D-2833, 1965.
5. Kaufman, Louis G., II; Meckler, Lawrence; Hartofilis, Stavros A.; and Weiss, Daniel: An Investigation of Hypersonic Flow Separation and Control Characteristics. AFFDL-TR-64-174, U.S. Air Force, Jan. 1965.
6. Gray, J. Don: Laminar Boundary-Layer Separation on Flared Bodies at Supersonic and Hypersonic Speeds. AEDC-TDR-64-277, U.S. Air Force, Jan. 1965. (Available from DDC as AD 609841.)
7. Holden, Michael: Separated Flow Studies at Hypersonic Speeds – Part II. Two-Dimensional Wedge Separated Flow Studies. Rept. No. AF-1285-A-13 (2) (Contract No. Nonr 2653(00)), Cornell Aeron. Lab., Inc., Dec. 1964.
8. Holden, Michael: Separated Flow Studies at Hypersonic Speeds – Part I. Separated Flows Over Axisymmetric Spiked Bodies. Cornell Aeronautical Laboratory, Inc., Rept. No. AF-1285-A-13 (1) (Contract No. Nonr 2653(00)), Cornell Aeron. Lab., Inc., Dec. 1964.
9. Ginoux, J. J.: Laminar Separation in Supersonic Flow. AFOSR 65-0352, U.S. Air Force, Oct. 1964. (Available from DDC as AD 612 407.)
10. Holloway, Paul F.; Sterrett, James R.; and Creekmore, Helen S.: An Investigation of Heat Transfer Within Regions of Separated Flow at a Mach Number of 6.0. NASA TN D-3074, 1965.
11. Pate, S. R.: Investigation of Flow Separation on a Two-Dimensional Flat Plate Having a Variable-Span Trailing-Edge Flap at $M_\infty = 3$ and 5. AEDC-TDR-64-14, U.S. Air Force, Mar. 1964.

12. Burchfield, C. G.; Hube, F. K.; and Burdette, J. E.: An Experimental Heat-Transfer Investigation in Regions of Flow Separation at Mach Number 8. AEDC-TDR-64-30, U.S. Air Force, Feb. 1964.
13. Kaufman, Louis G., II: Pressure and Heat Transfer Measurements for Hypersonic Flows Over Expansion Corners and Ahead of Ramps – Part I: Mach 5 and 8 Data for Expansion Corner Flows. ASD-TDR-63-679, Pt. I, U.S. Air Force, Dec. 1963.
14. Baer, A. L.: An Investigation of Separated Flows on Two-Dimensional Models at Mach Numbers 5 and 8. AEDC-TDR-63-200, U.S. Air Force, Oct. 1963.
15. Miller, D. S.; Hijman, R.; and Childs, M. E.: Mach 8 to 22 Studies of Flow Separations Due to Deflected Control Surfaces. AIAA J., vol. 2, no. 2, Feb. 1964, pp. 312-321.
16. Bogdonoff, S. M.; and Vas, I. E.: Some Experiments on Hypersonic Separated Flows. ARS J., vol. 32, no. 10, Oct. 1962, pp. 1564-1572.
17. Sterrett, James R.; and Emery, James C.: Experimental Separation Studies for Two-Dimensional Wedges and Curved Surfaces at Mach Numbers of 4.8 to 6.2. NASA TN D-1014, 1962.
18. Eminton, E.: Simple Theoretical and Experimental Studies of the Flow Through a Three-Shock System in a Corner. Tech. Note Aero.2784, Brit. R.A.E., Sept. 1961.
19. Sterrett, James R.; and Emery, James C.: Extension of Boundary-Layer-Separation Criteria to a Mach Number of 6.5 by Utilizing Flat Plates With Forward-Facing Steps. NASA TN D-618, 1960.
20. Chapman, Dean R.; Kuehn, Donald M.; and Larson, Howard K.: Investigation of Separated Flows in Supersonic and Subsonic Streams With Emphasis on the Effect of Transition. NACA Rept. 1356, 1958. (Supersedes NACA TN 3869.)
21. Becker, John V.; and Korycinski, Peter F.: Heat Transfer and Pressure Distribution at a Mach Number of 6.8 on Bodies With Conical Flares and Extensive Flow Separation. NASA TN D-1260, 1962. (Supersedes NACA RM L56F22.)
22. Love, Eugene S.: Pressure Rise Associated With Shock-Induced Boundary-Layer Separation. NACA TN 3601, 1955.
23. Townsend, James C.: Effects of Leading-Edge Bluntness and Ramp Deflection Angle on Laminar Boundary-Layer Separation in Hypersonic Flow. NASA TN D-3290, 1966.
24. Lees, Lester; and Reeves, Barry L.: Supersonic Separated and Reattaching Laminar Flows: I. General Theory and Application to Adiabatic Boundary-Layer Shock-Wave Interactions. AIAA J., vol. 2, no. 11, Nov. 1964, pp. 1907-1920.

25. Beckwith, Ivan E.; and Cohen, Nathaniel B.: Application of Similar Solutions to Calculation of Laminar Heat Transfer on Bodies With Yaw and Large Pressure Gradient in High-Speed Flow. NASA TN D-625, 1961.
26. Stainback, P. Calvin: Heat-Transfer Measurements at a Mach Number of 8 in the Vicinity of a 90° Interior Corner Aligned With the Free-Stream Velocity. NASA TN D-2417, 1964.
27. Schaefer, William T., Jr.: Characteristics of Major Active Wind Tunnels at the Langley Research Center. NASA TM X-1130, 1965.
28. Bertram, Mitchel H.; and Blackstock, Thomas A.: Some Simple Solutions to the Problem of Predicting Boundary-Layer Self-Induced Pressures. NASA TN D-798, 1961.
29. Johnson, Charles Borden: A Theoretical and Experimental Study at Mach 8 of Flow Separation of a Flat Plate With Deflected Trailing Edge Flap. M.S. Thesis, Virginia Polytech. Inst., 1966.
30. Dennard, John S.; and Spencer, Patricia B.: Ideal-Gas Tables for Oblique-Shock Flow Parameters in Air at Mach Numbers From 1.05 to 12.0. NASA TN D-2221, 1964.
31. Gadd, G. E.: An Experimental Investigation of Heat Transfer Effects on Boundary Layer Separation in Supersonic Flow. J. Fluid Mech., vol. 2, pt. 2, Mar. 1957, pp. 105-122.
32. Curle, N.: The Effects of Heat Transfer on Laminar-Boundary-Layer Separation in Supersonic Flow. Aeron. Quart., vol. XII, pt. 4, Nov. 1961, pp. 309-336.
33. Gadd, G. E.: A Theoretical Investigation of the Effects of Mach Number, Reynolds Number, Wall Temperature and Surface Curvature on Laminar Separation in Supersonic Flow. Rept.No. F.M. 2415, Brit. A.R.C., June 13, 1956.
34. Schaefer, John W.; and Ferguson, Harold: Investigation of Separation and Associated Heat Transfer and Pressure Distribution on Cone-Cylinder-Flare Configurations at Mach Five. ARS J., vol. 32, no. 5, May 1962, pp. 762-769.
35. Hakkinen, R. J.; Greber, I.; Trilling, L.; and Abarbanel, S. S.: The Interaction of an Oblique Shock Wave With a Laminar Boundary Layer. NASA MEMO 2-18-59W, 1959.
36. Erdos, John; and Pallone, Adrian: Shock-Boundary Layer Interaction and Flow Separation. RAD-TR-61-23 (Contract AFO4(647)-685), AVCO Corp., Aug. 15, 1961.
37. Prandtl, L.: Note on the Calculation of Boundary Layers. NACA TM 959, 1940.
38. Chapman, Dean R.: Laminar Mixing of a Compressible Fluid. NACA Rept. 958, 1950.
39. Gadd, G. E.: Boundary Layer Separation in the Presence of Heat Transfer. AGARD Rept. 280, Apr. 1960.

40. Savage, Stuart B.: The Effect of Heat Transfer on Separation of Laminar Compressible Boundary Layers. Separated Flows Proj. Tech. Rept. No. 2 (Contract No. AF49(638)-916), Graduate Aeron. Labs., California Inst. Technol., June 1, 1962. (Available from DDC as AD No. 277 354.)
41. Crocco, Luigi; and Lees, Lester: A Mixing Theory for the Interaction Between Dissipative Flows and Nearly Isentropic Streams. J. Aeron. Sci., vol. 19, no. 10, Oct. 1952, pp. 649-676.
42. Glick, Herbert S.: Modified Crocco-Lees Mixing Theory for Supersonic Separated and Reattaching Flows. Hypersonic Res. Proj. Mem. No. 53 (Contract No. DA-04-495-Ord-1960), Guggenheim Aeron. Lab., California Inst. Technol., May 2, 1960.
43. Bray, K. N. C.; Gadd, G. E.; and Woodger, M.: Some Calculations by the Crocco-Lees and Other Methods of Interactions Between Shock Waves and Laminar Boundary Layers, Including Effects of Heat Transfer and Suction. C.P. No. 556, Brit. A.R.C., 1961.
44. Tani, Itiro: On the Approximate Solution of the Laminar Boundary-Layer Equations. J. Aeron. Sci., vol. 21, no. 7, July 1954, pp. 487-495, 504.
45. Wieghardt, K.: Über einen Energiesatz zur Berechnung Laminarer Grenzschichten. Ingr.-Arch., Bd. 16, 1948, pp. 231-242.
46. Walz, A.: Anwendung des Energiesatzes von Weighardt auf einparametrische Geschwindigkeitsprofile in laminaren Grenzschichten. Ingr.-Arch., Bd. 16, 1948, pp. 243-248.
47. Poots, G.: A Solution of the Compressible Laminar Boundary Layer Equations With Heat Transfer and Adverse Pressure Gradient. Quart. J. Mech. Appl. Math., vol. XIII, pt. 1, Feb. 1960, pp. 57-84.
48. Abbott, Douglas E.; Holt, Maurice; and Nielsen, Jack N.: Investigation of Hypersonic Flow Separation and Its Effects on Aerodynamic Control Characteristics. ASD-TDR-62-963, U.S. Air Force, Nov. 1962. (Available from DDC as AD No. 296 112.)
49. Cohen, Clarence B.; and Reshotko, Eli: Similar Solutions for the Compressible Laminar Boundary Layer With Heat Transfer and Pressure Gradient. NACA Rept. 1293, 1956. (Supersedes NACA TN 3325.)
50. Stewartson, K.: Further Solutions of the Falkner-Skan Equation. Proc. Cambridge Phil. Soc., vol. 50, pt. 3, July 1964, pp. 454-465.
51. Holden, M. S.: An Analytical Study of Separated Flows Induced by Shock Wave - Boundary Layer Interaction. Rept. No. A1-1972-A-3 (Contract NAS 5-3976), Cornell Aeron. Lab., Inc., Dec. 1965.

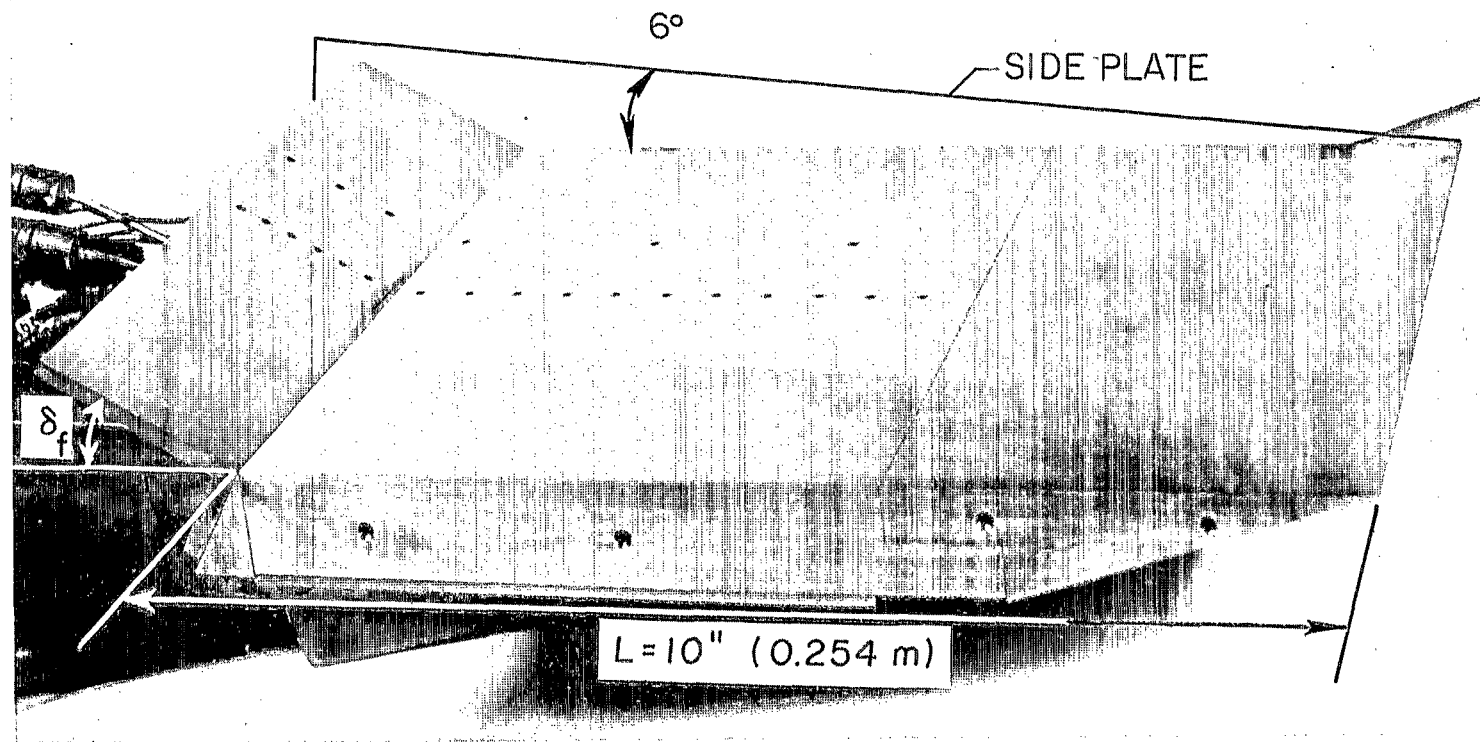


Figure 1.- Photograph of pressure model.

L-64-7

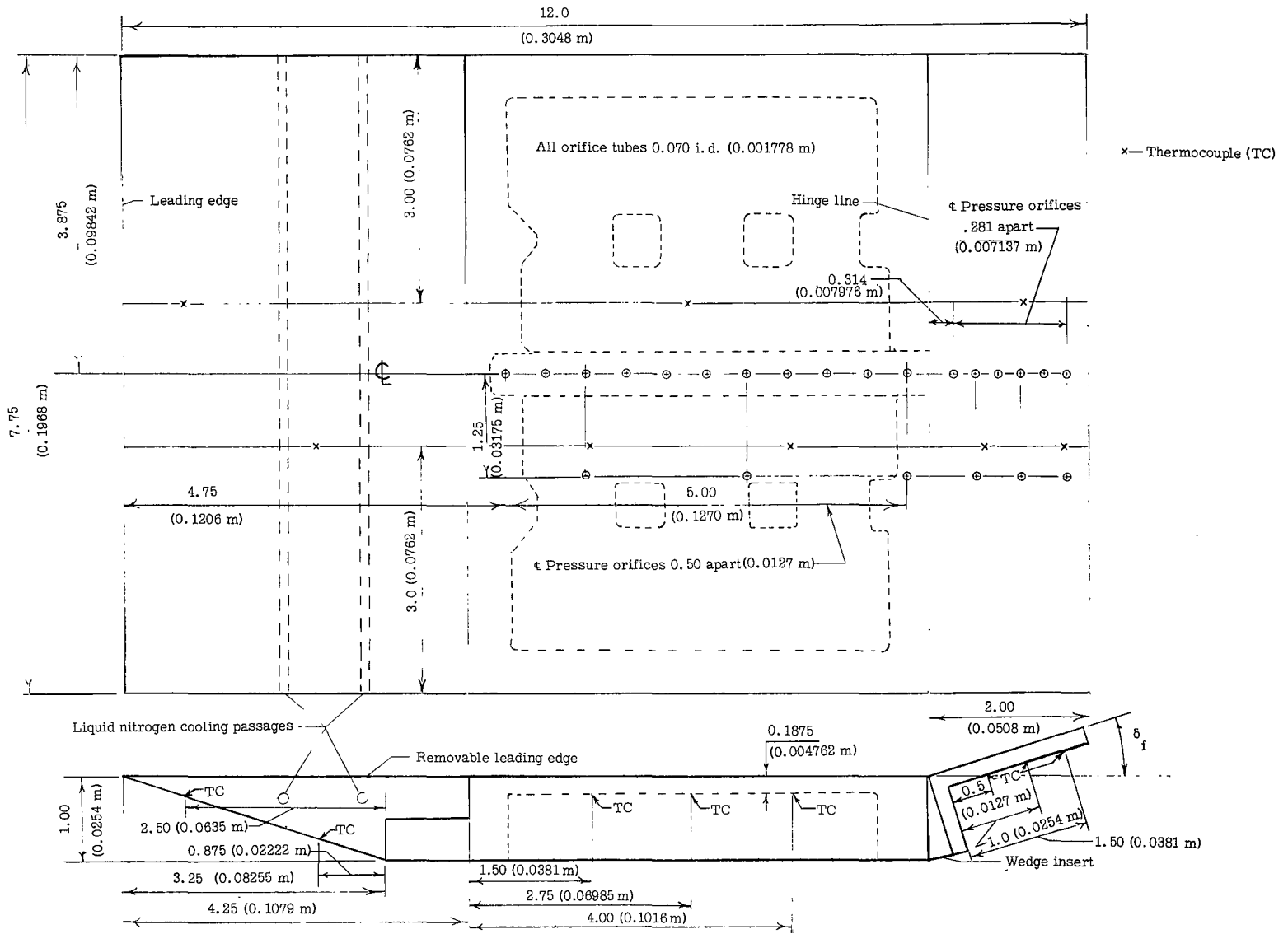


Figure 2.- Schematic of the pressure model. All dimensions are in in. (m).

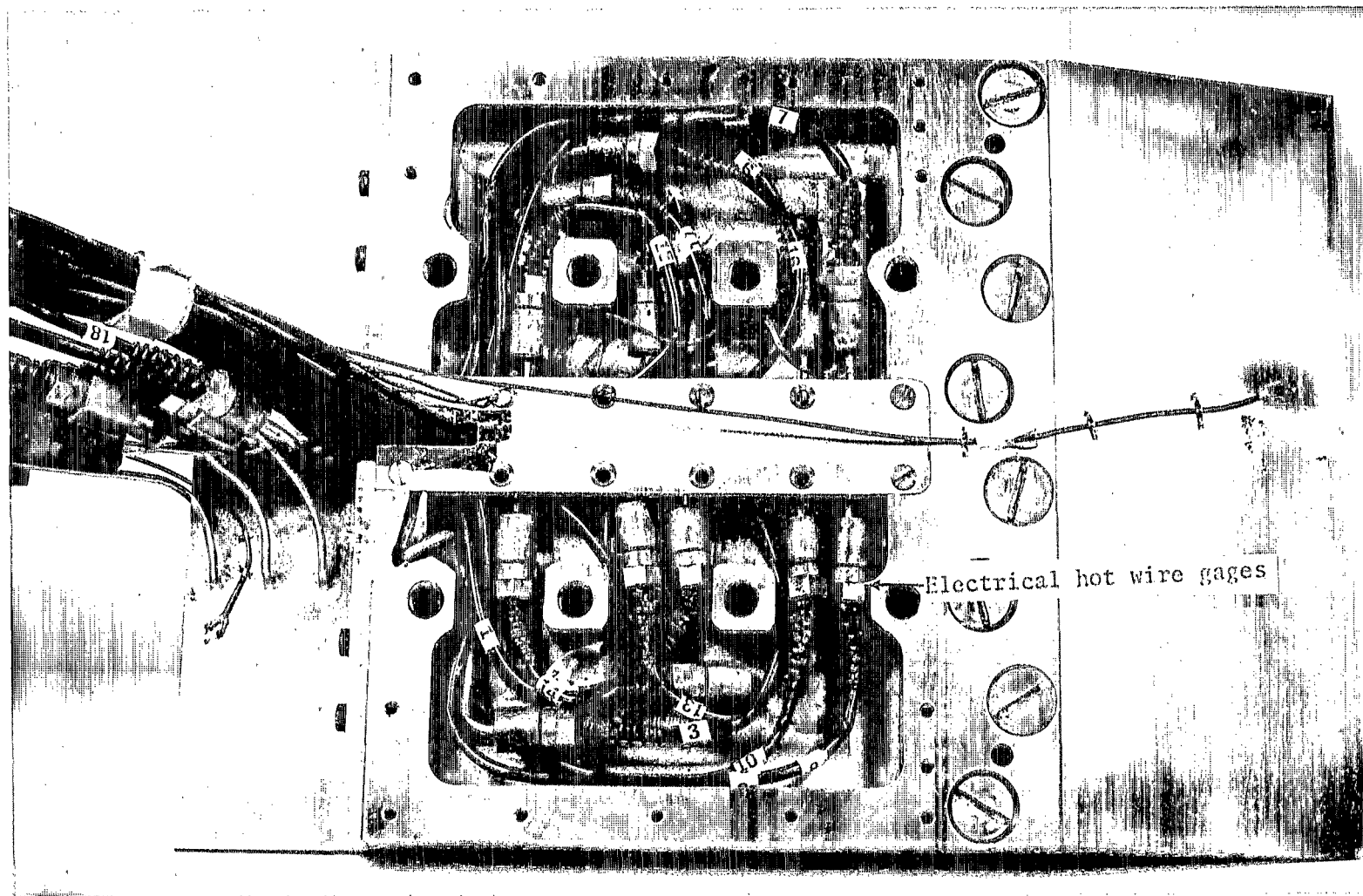


Figure 3.- View from below the pressure model showing pressure gage installation.

L-64-7603.1

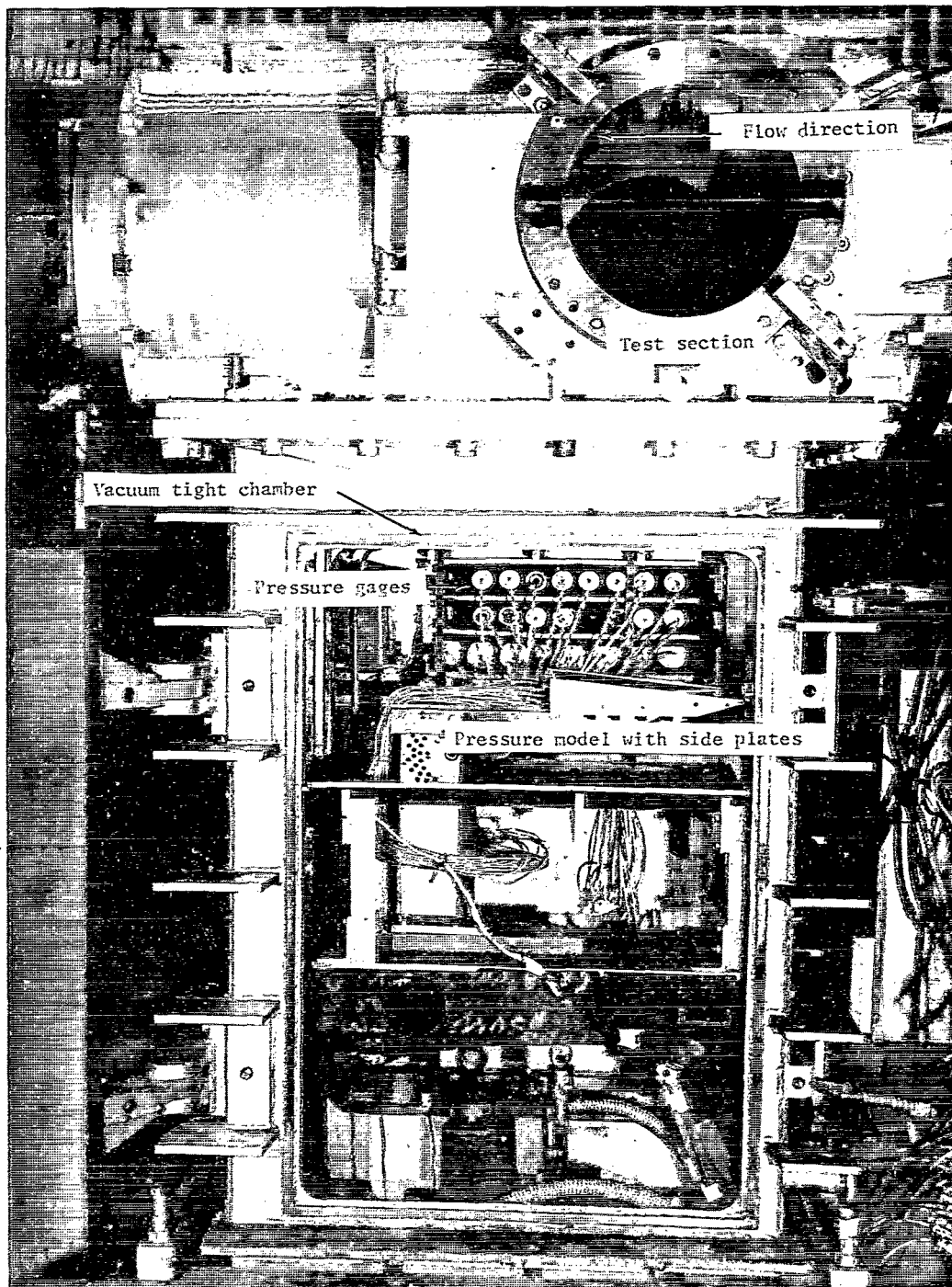


Figure 4.- Mach 8 tunnel apparatus, showing pressure model with upper side plates.

L-67-1074

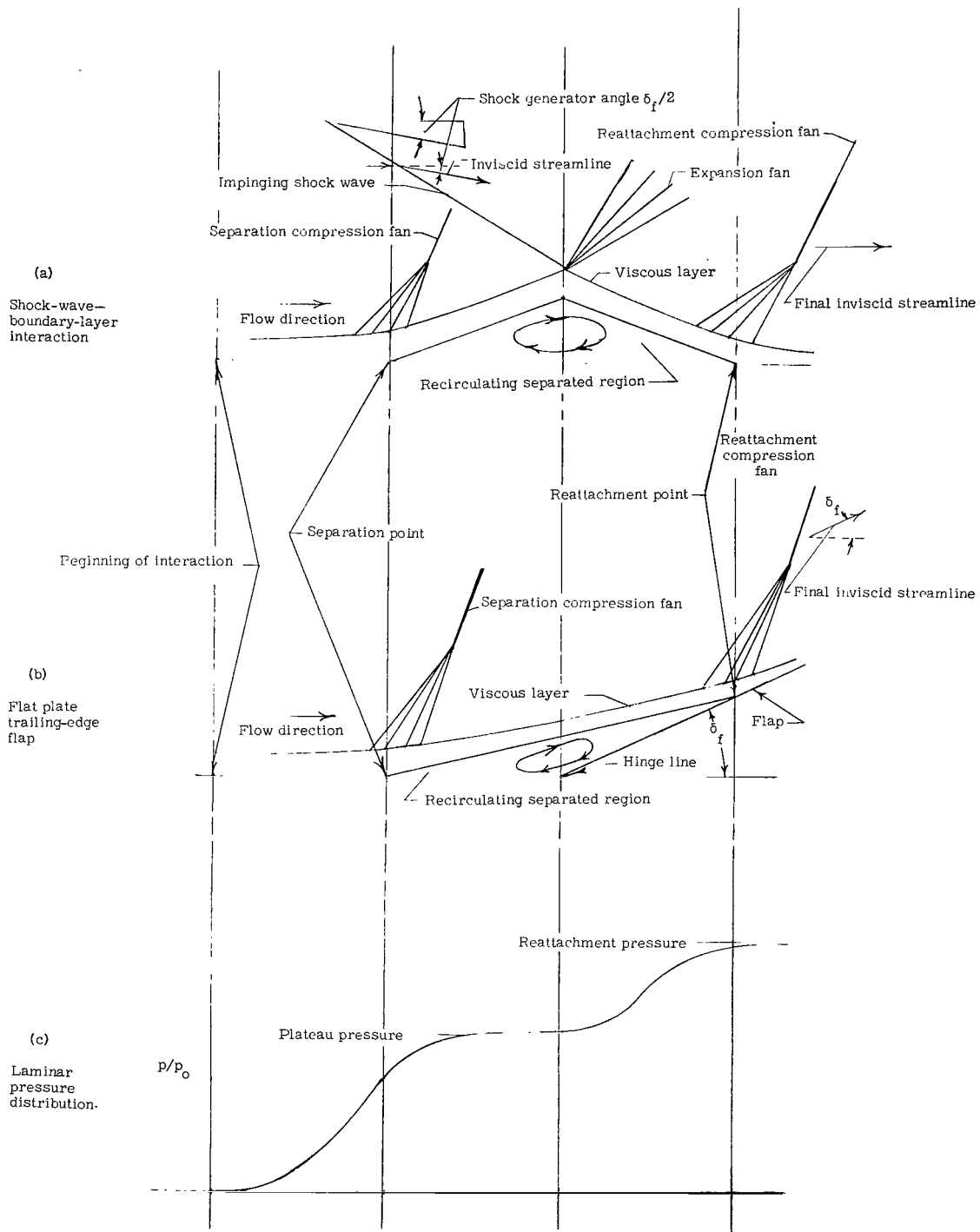


Figure 5.- Comparison of the basic flow models assumed for a shock-wave-boundary-layer interaction and flat plate with a trailing-edge flap and their associated laminar pressure distribution.

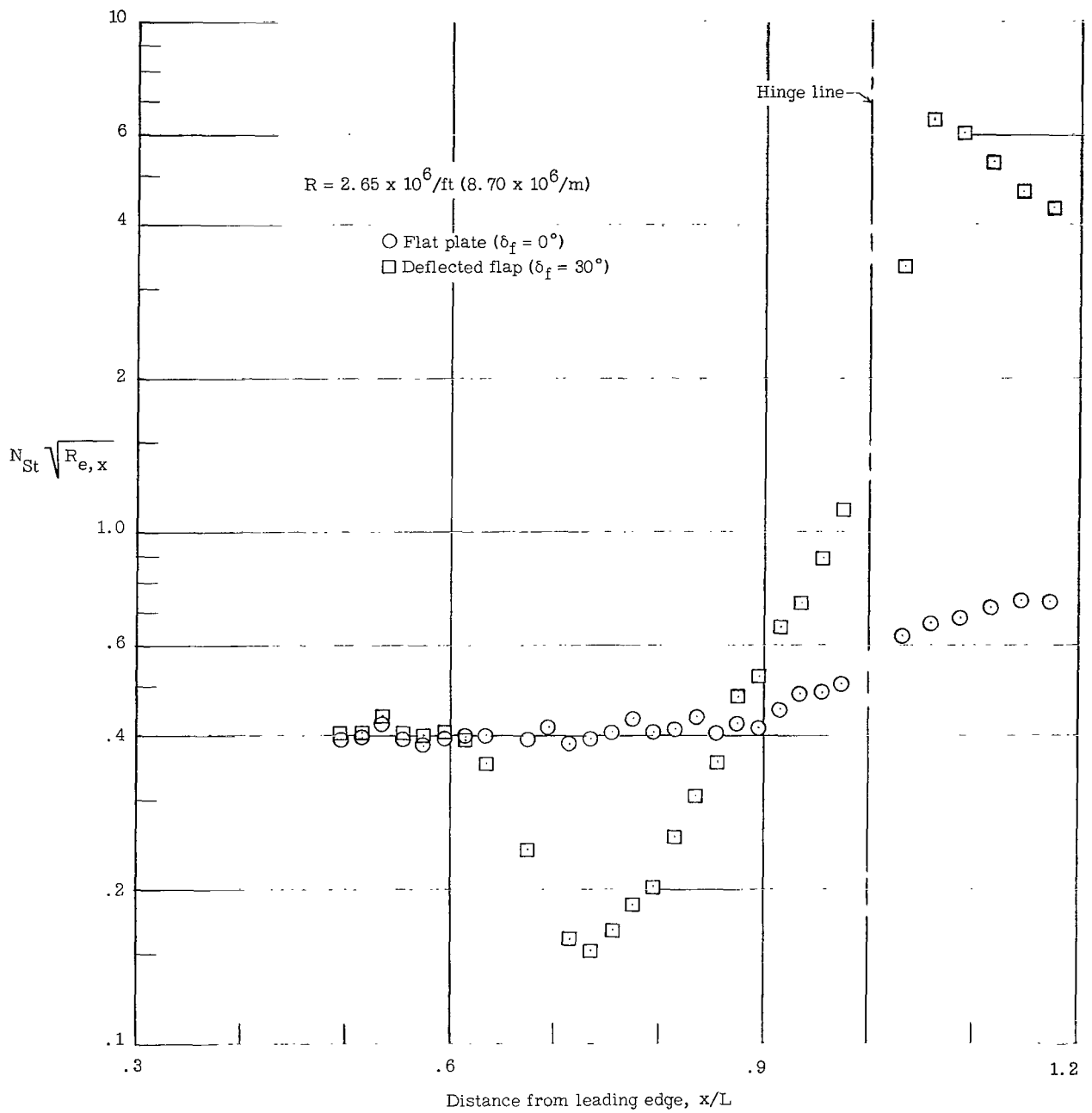
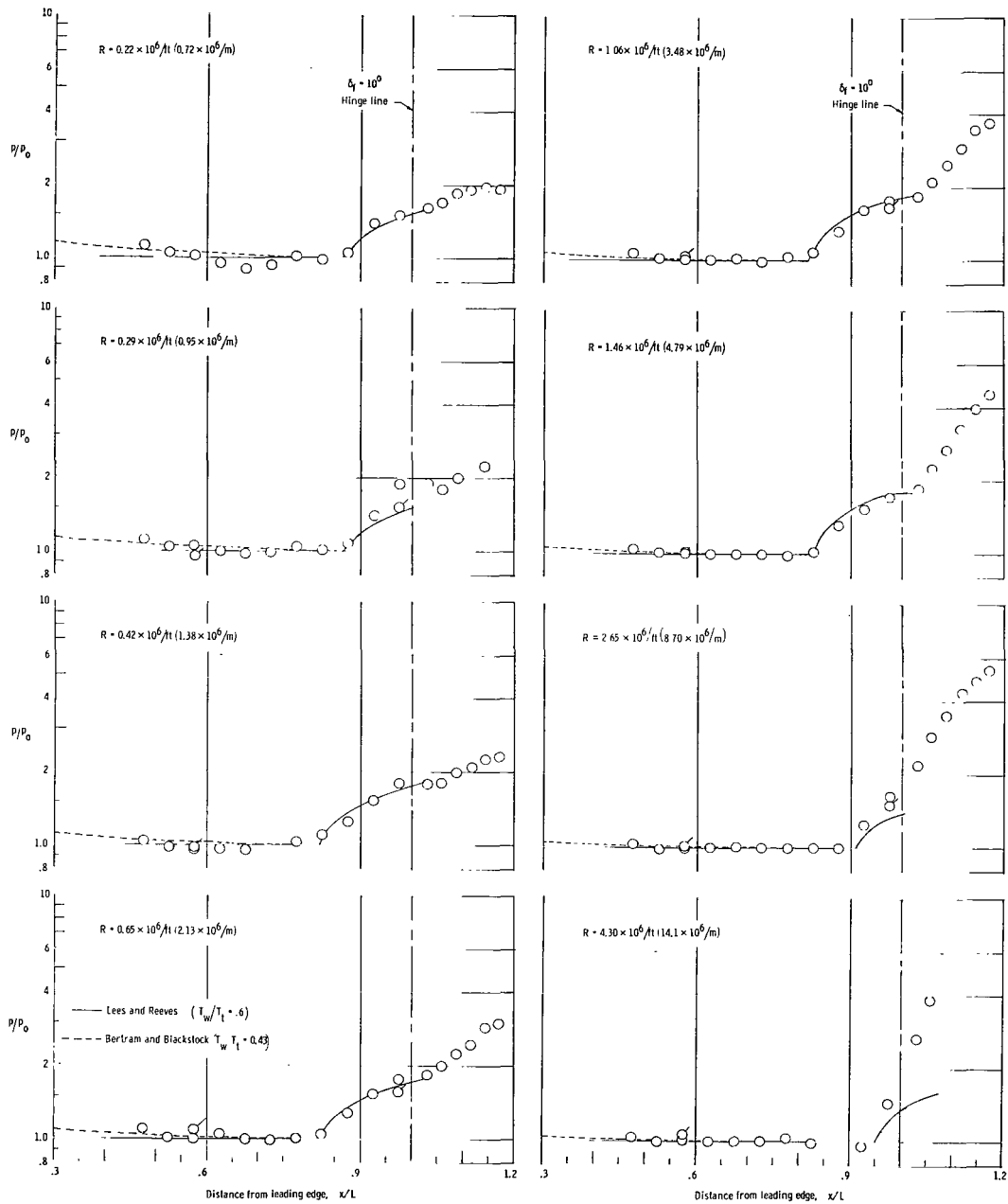
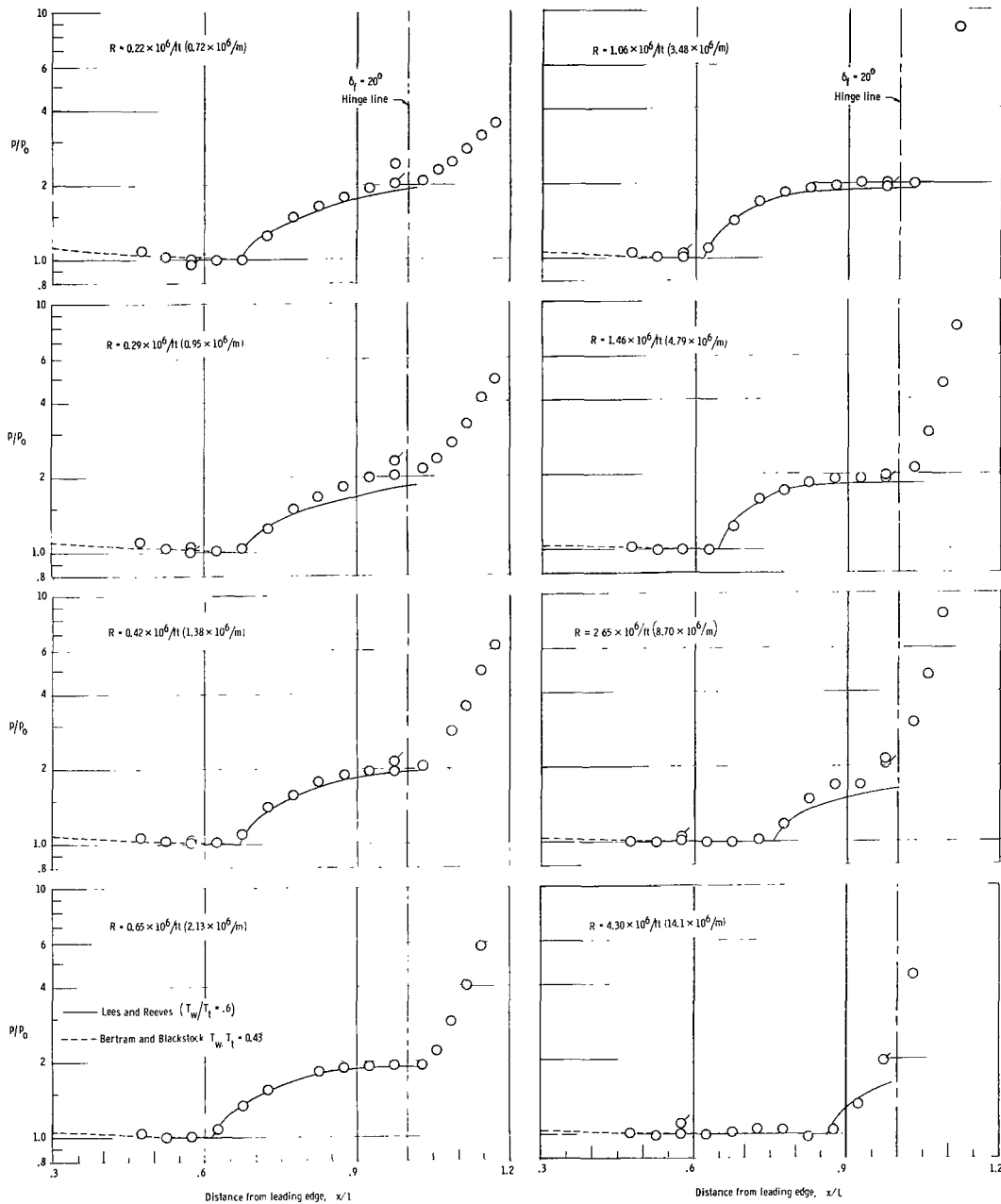


Figure 6.- The effect of transition on heat transfer for a flat plate ($\delta_f = 0^\circ$) and for a deflected flap ($\delta_f = 30^\circ$).



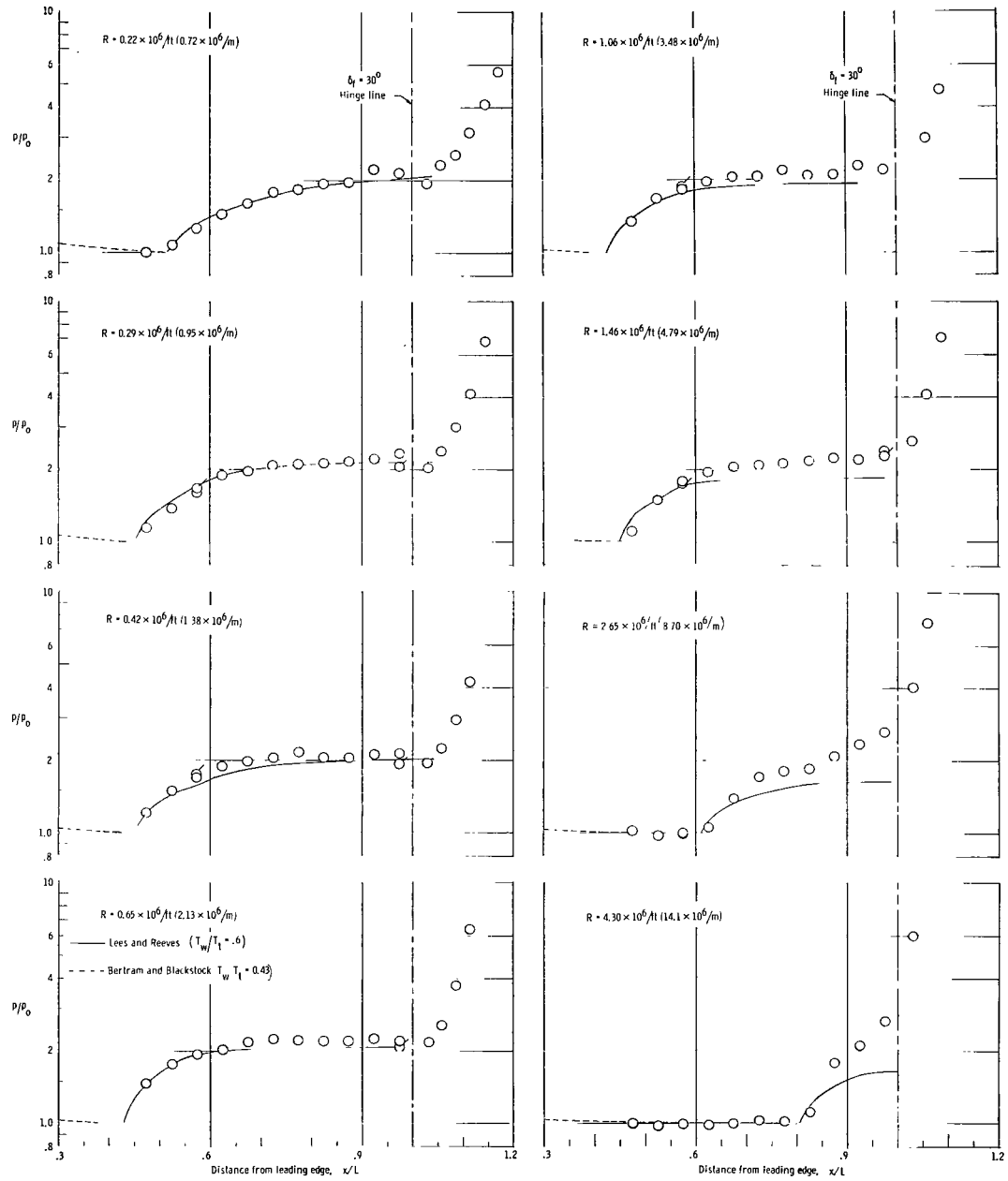
(a) $\delta_f = 10^\circ$.

Figure 7.- The effect of Reynolds number on the plateau pressure distribution at $T_w/T_t = 0.43$ for three flap angles, with and without side plates.



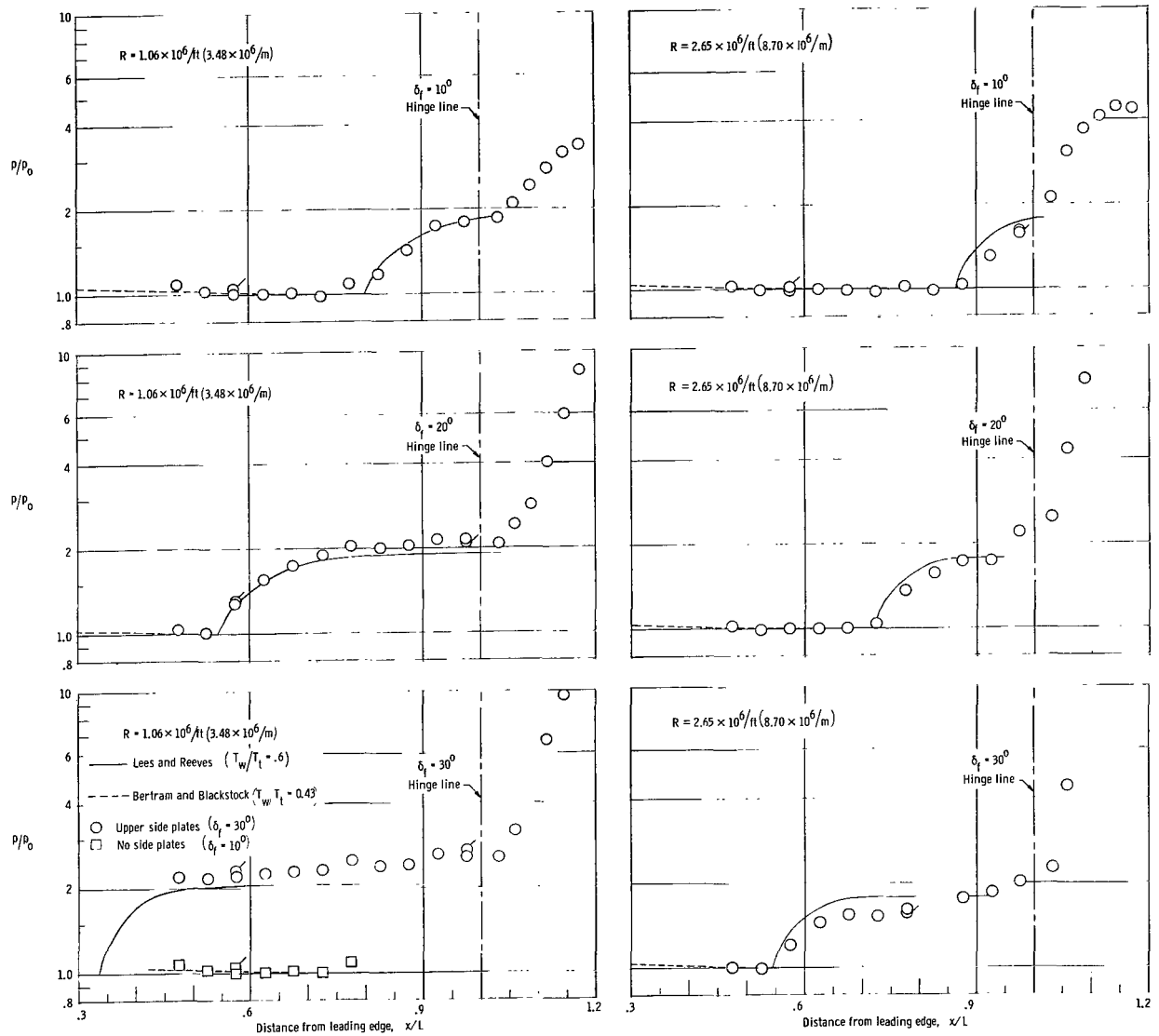
(b) $\delta_f = 20^\circ$.

Figure 7.- Continued.



(c) $\delta_f = 30^\circ$.

Figure 7.- Continued.



(d) Side plates.

Figure 7.- Concluded.

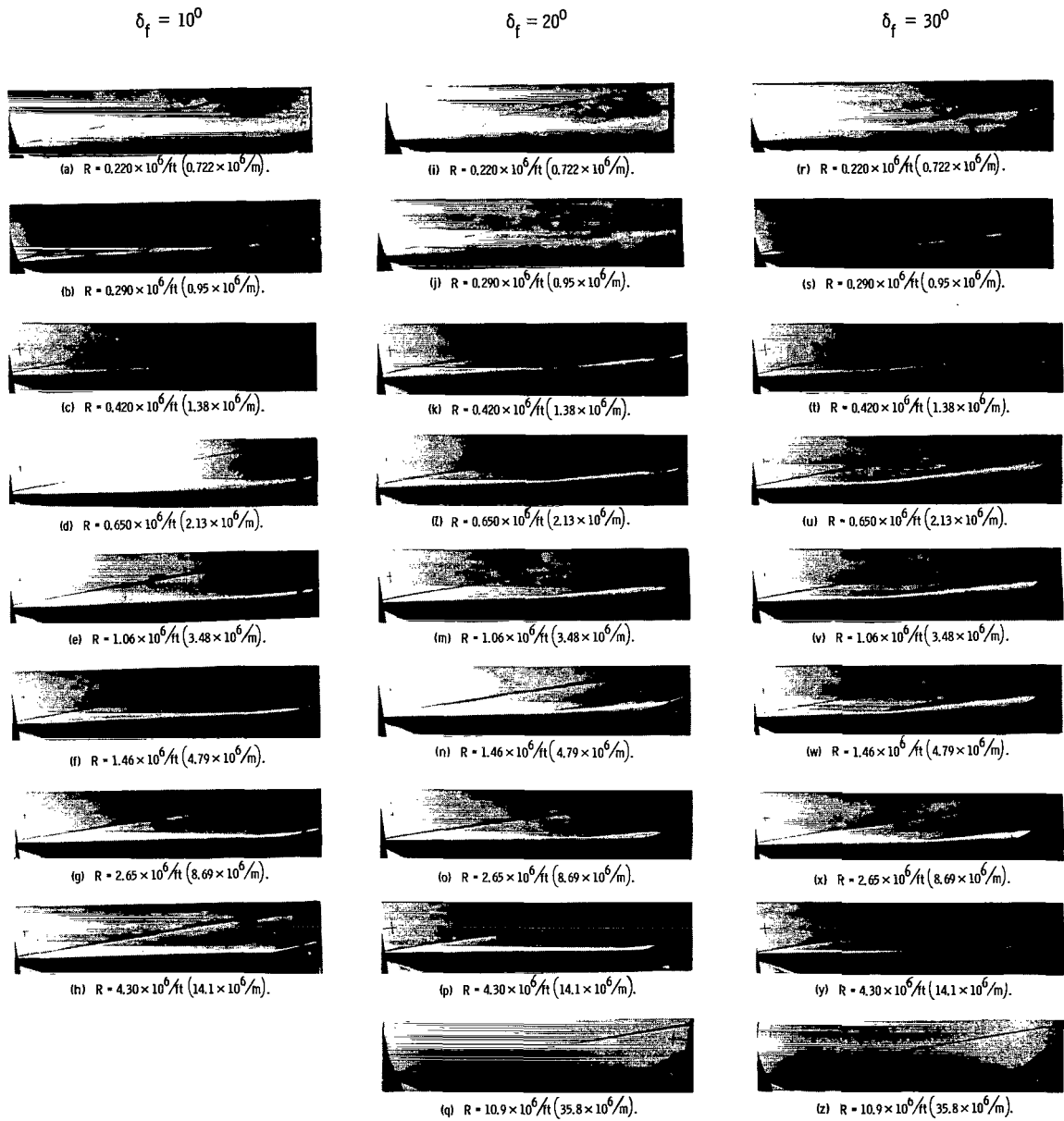
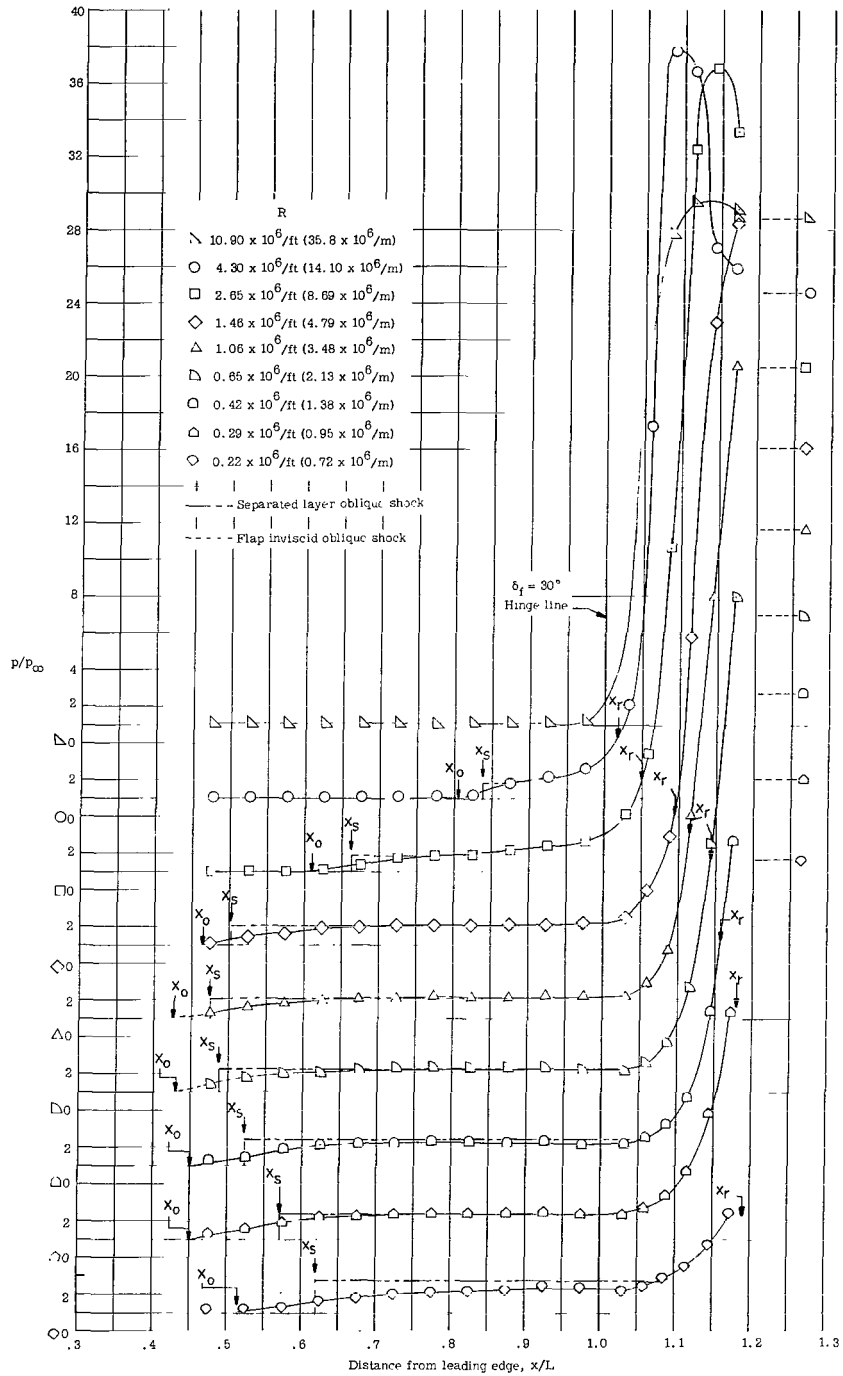


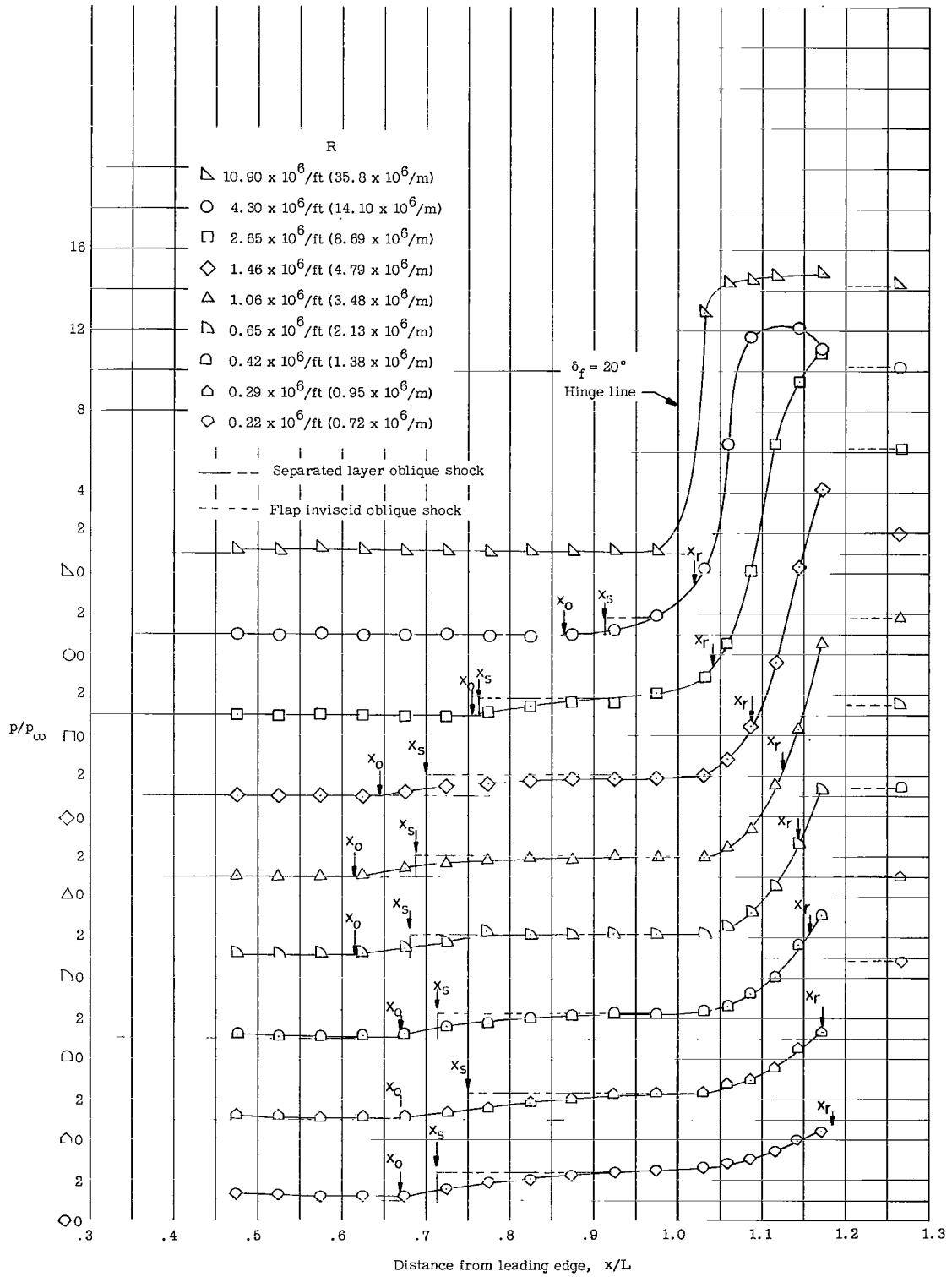
Figure 8.- Schlieren photographs of the flow separation model at $T_w/T_t = 0.43$ for three flap angles and various unit Reynolds numbers.

L-67-6601



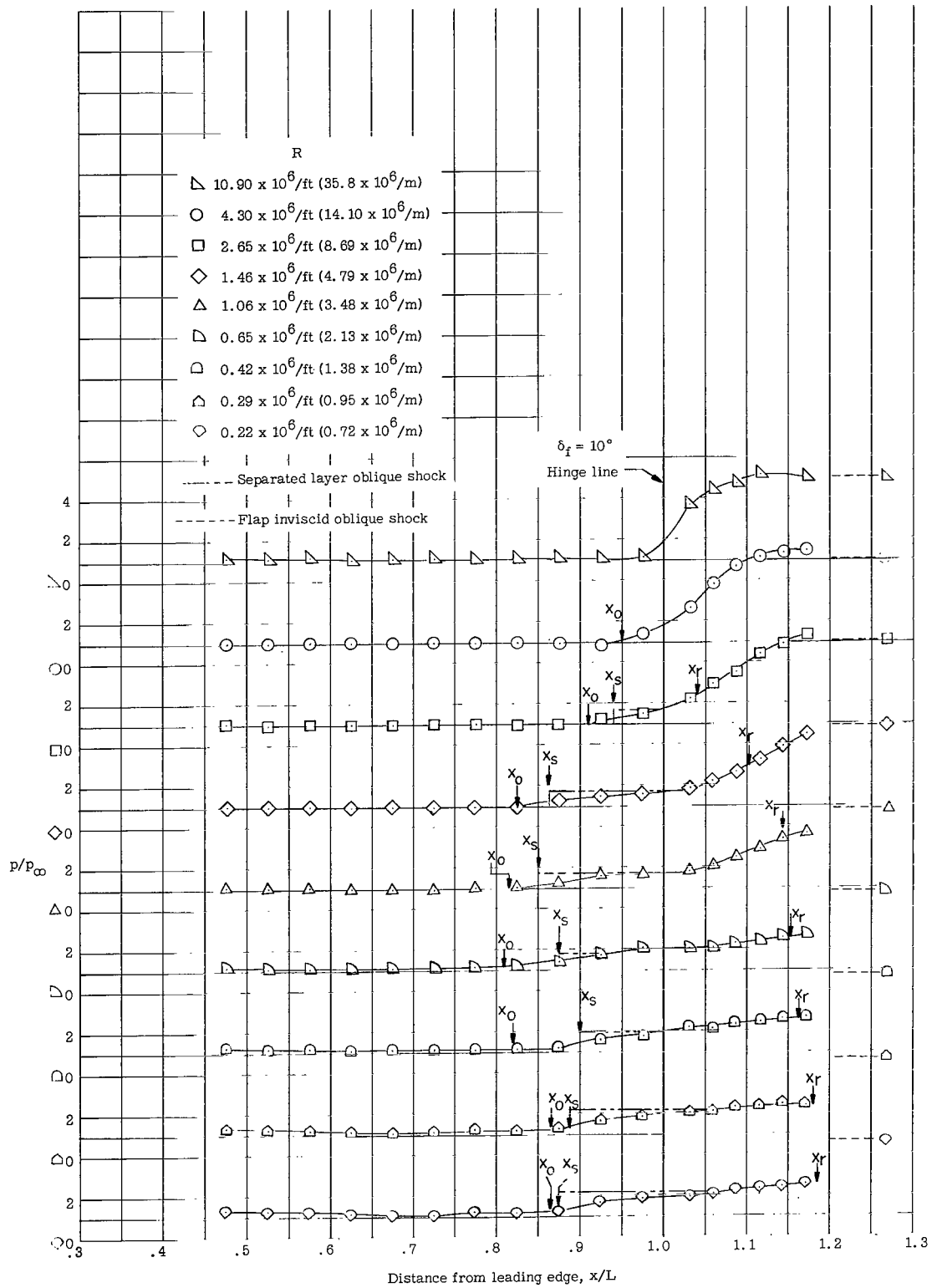
(a) $\delta_f = 30^\circ$.

Figure 9.- The effect of Reynolds number on the plateau and flap pressures at $T_w/T_t = 0.43$ for three flap angles, with and without side plates.



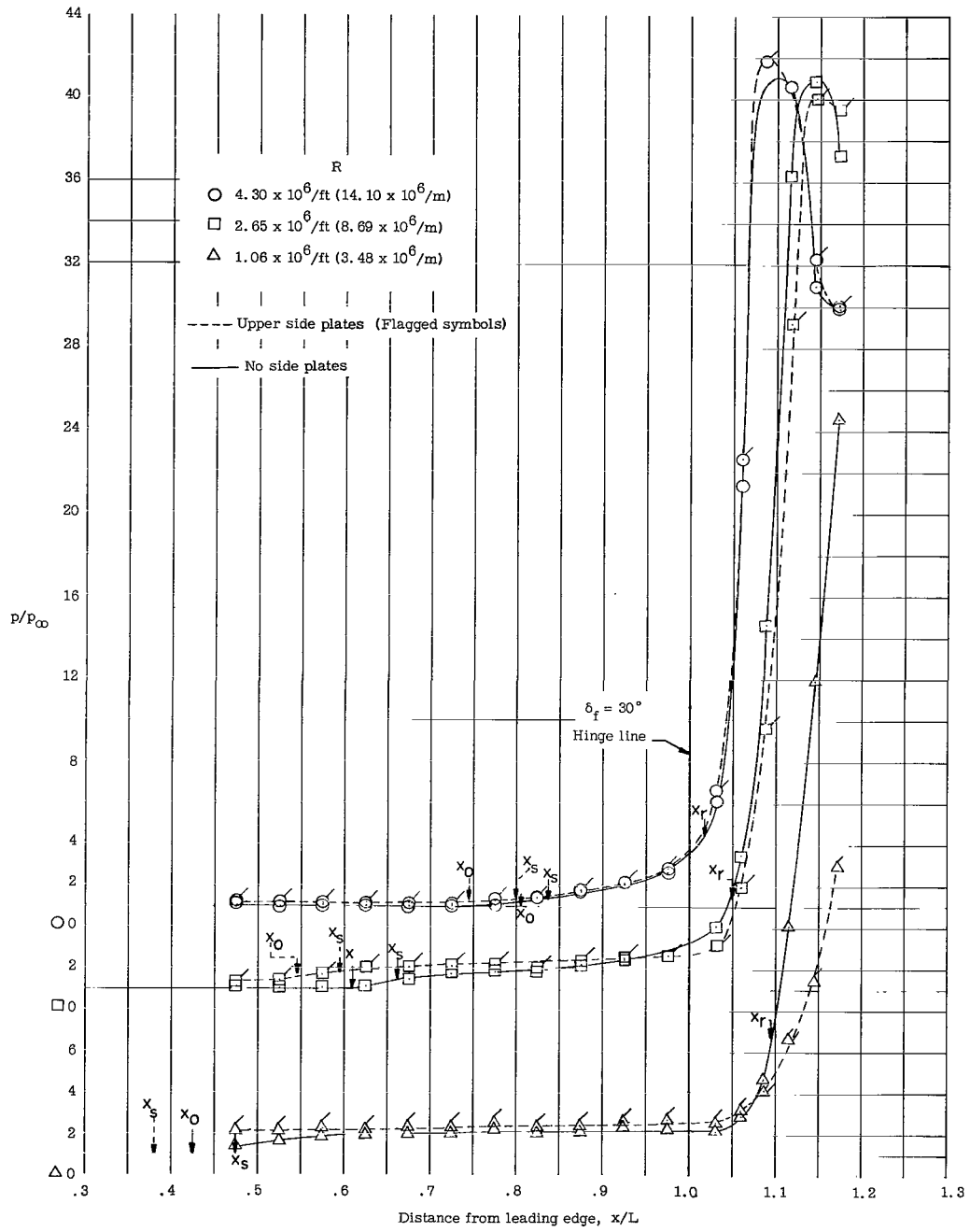
(b) $\delta_f = 20^\circ$.

Figure 9.- Continued.



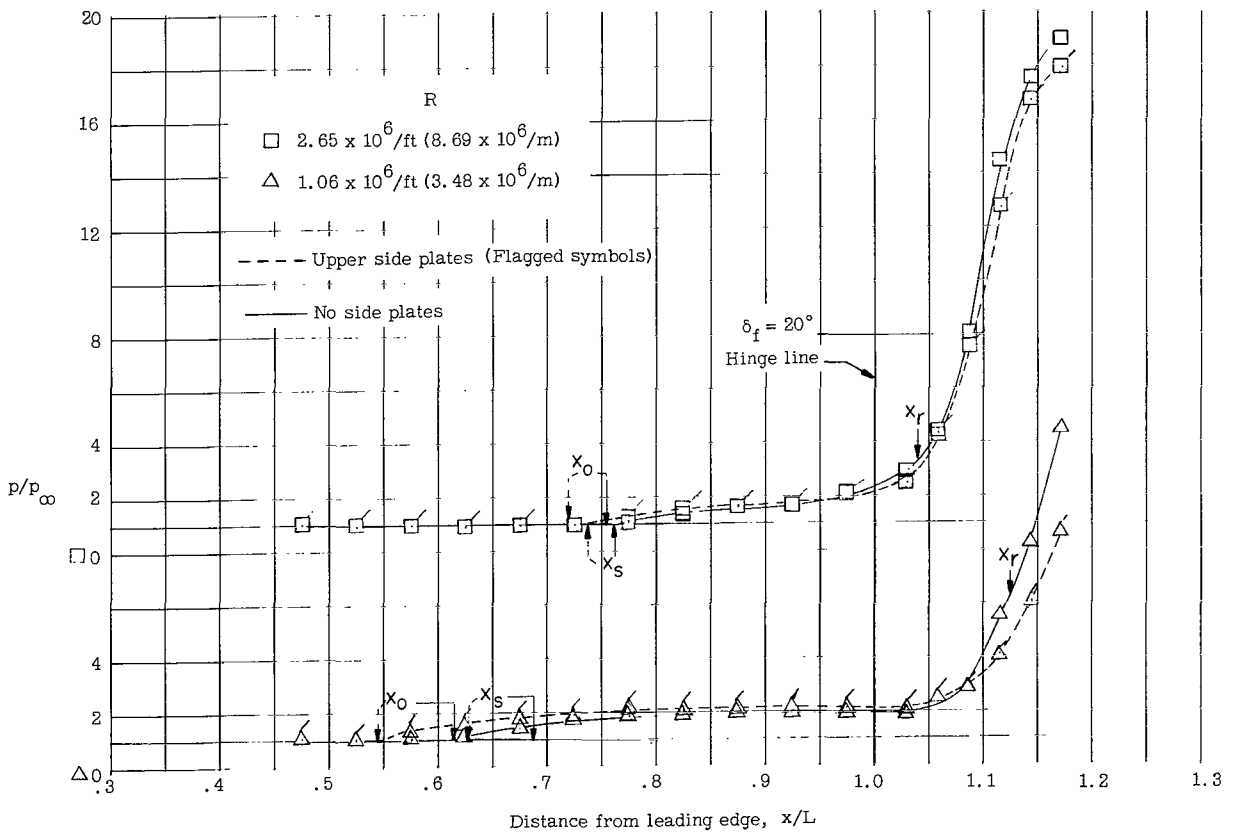
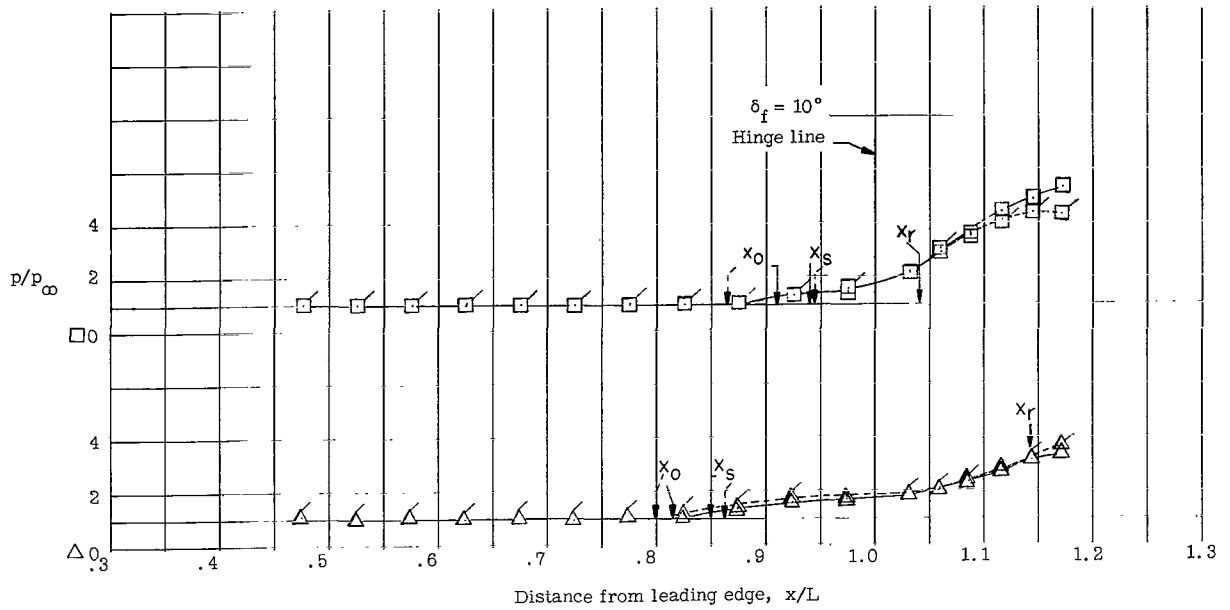
(c) $\delta_f = 10^\circ$.

Figure 9.- Continued.



(d) Side plates.

Figure 9.- Continued.



(e) Side plates.

Figure 9.- Concluded.

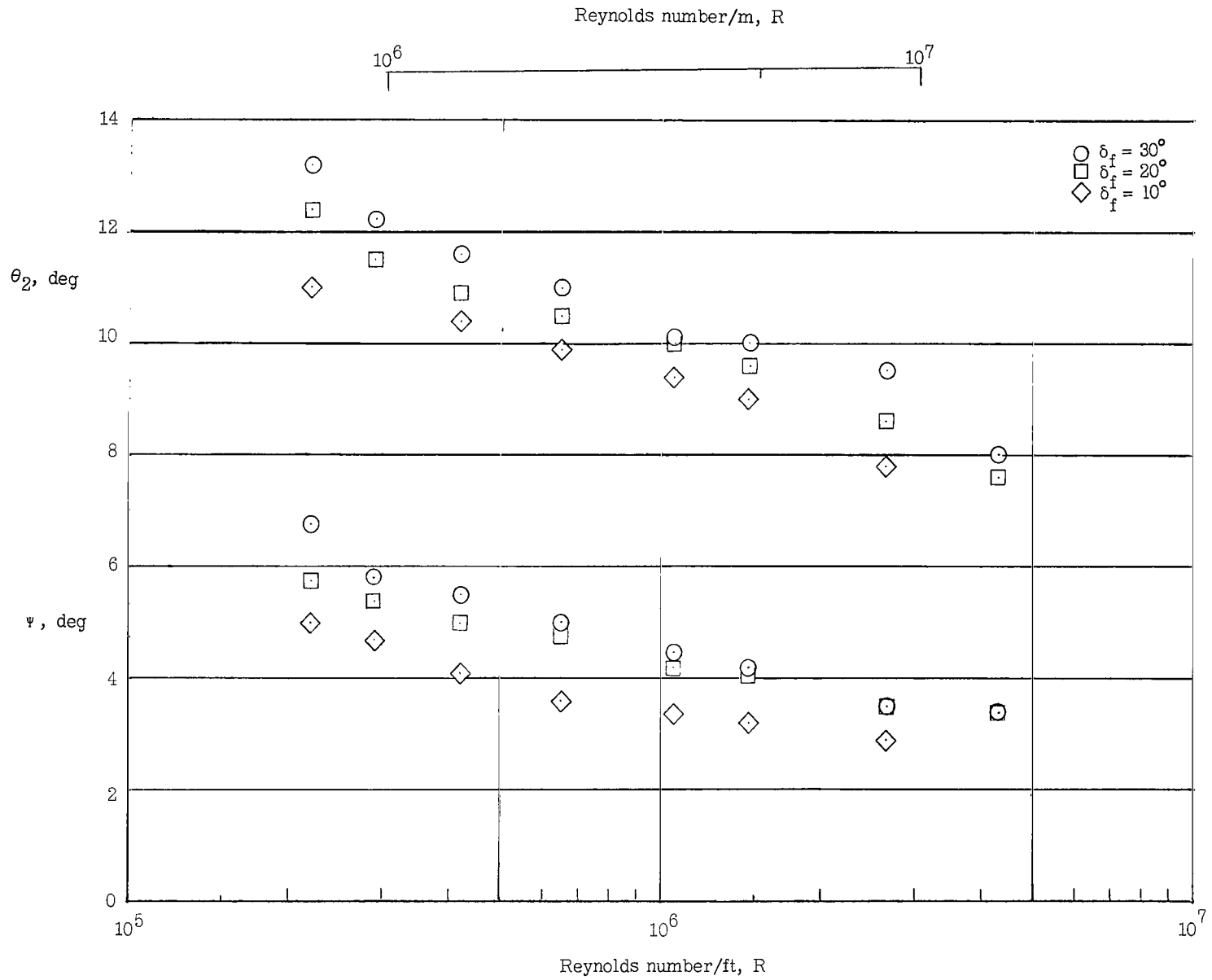


Figure 10.- The effect of Reynolds number and flap angle on the separation point flow deflection angle and the separation shock wave angle for $T_w/T_t = 0.43$.

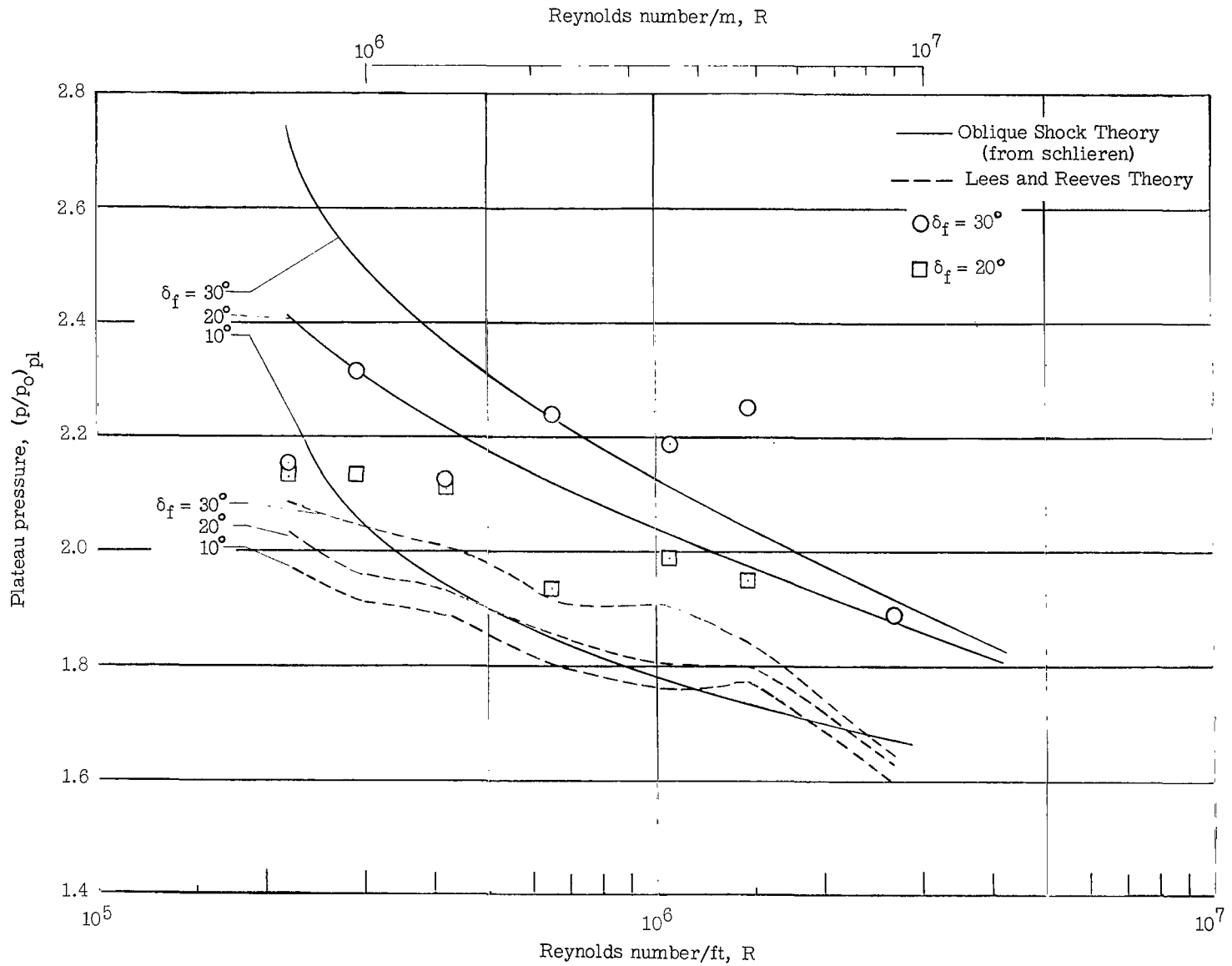
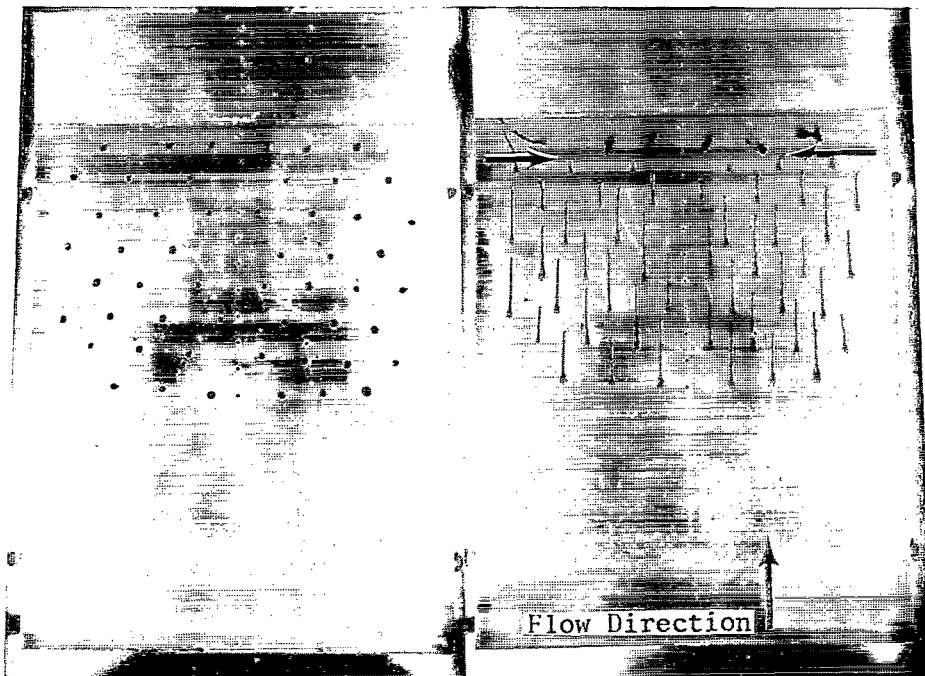


Figure 11.- The effect of Reynolds number and flap angle on three means of determining plateau pressure at $T_w/T_t = 0.43$.



t-67-1100

Figure 12.- Oil-flow patterns before and after tests at $R/ft = 4.3 \times 10^6$ ($R/m = 14.1 \times 10^6$) and $\delta_f = 20^\circ$.

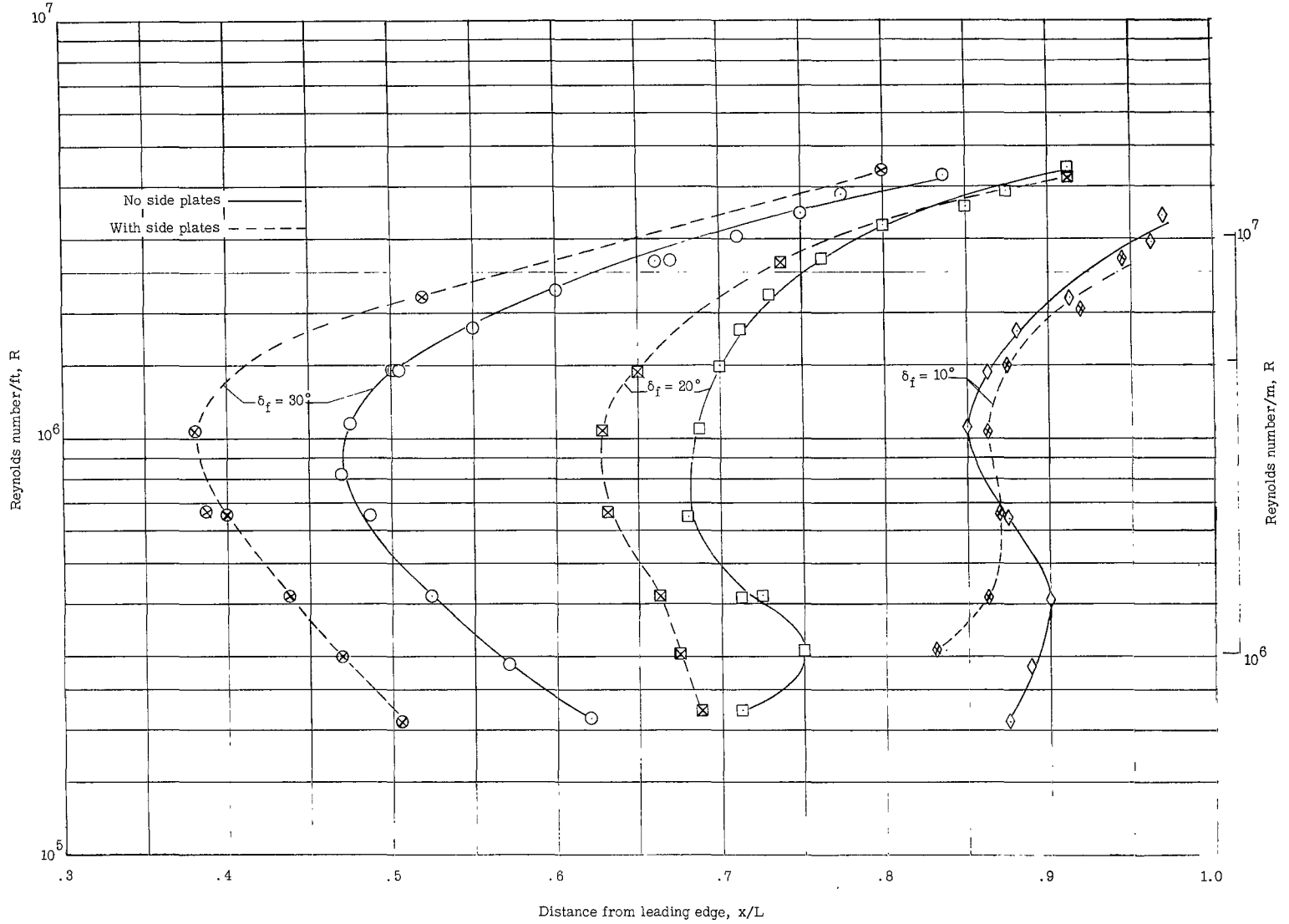


Figure 13.- Location of separation point for various free-stream unit Reynolds numbers.

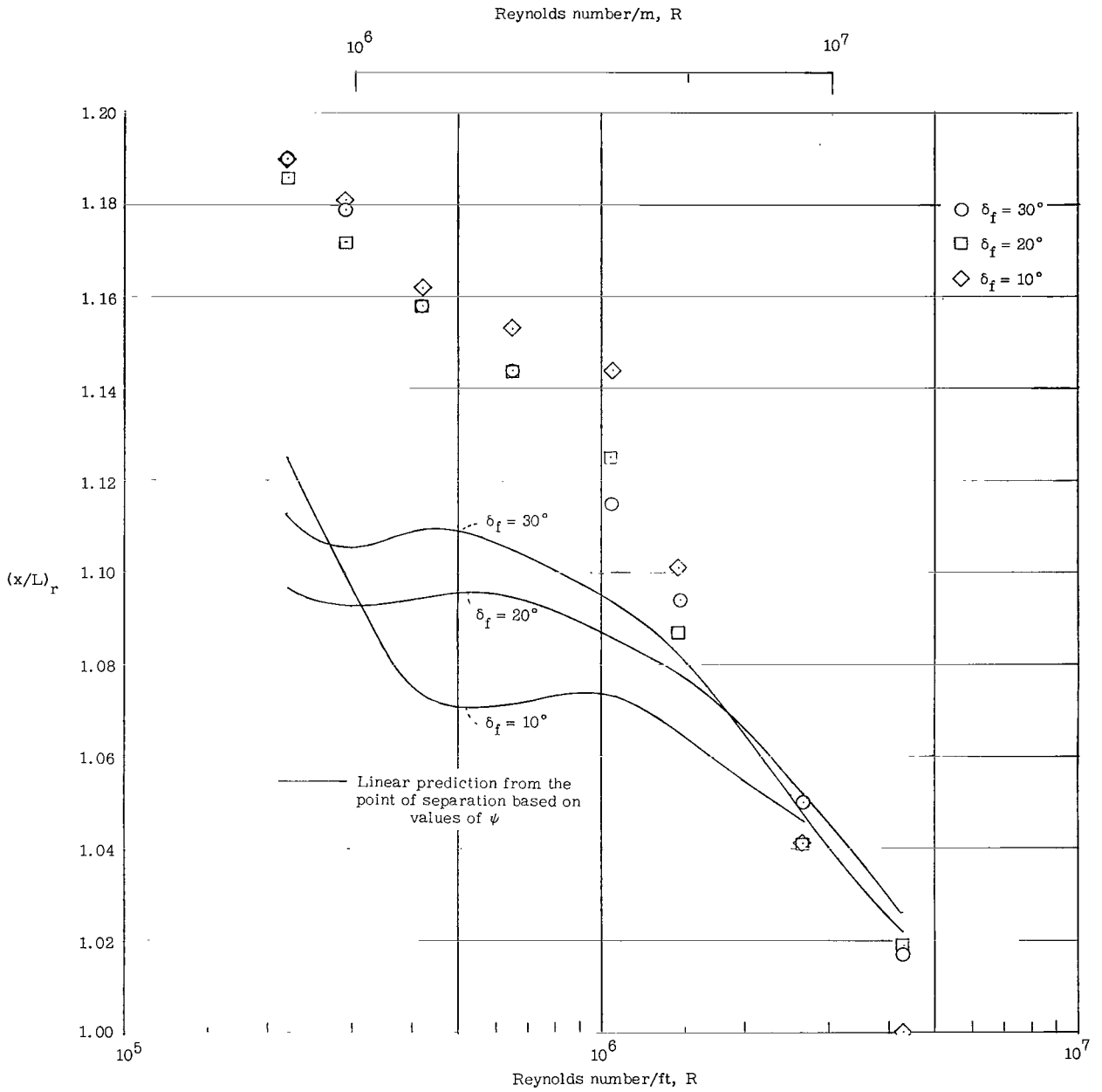


Figure 14.- The effect of Reynolds number and flap angle on the point of reattachment on the flap for $T_w/T_t = 0.43$.

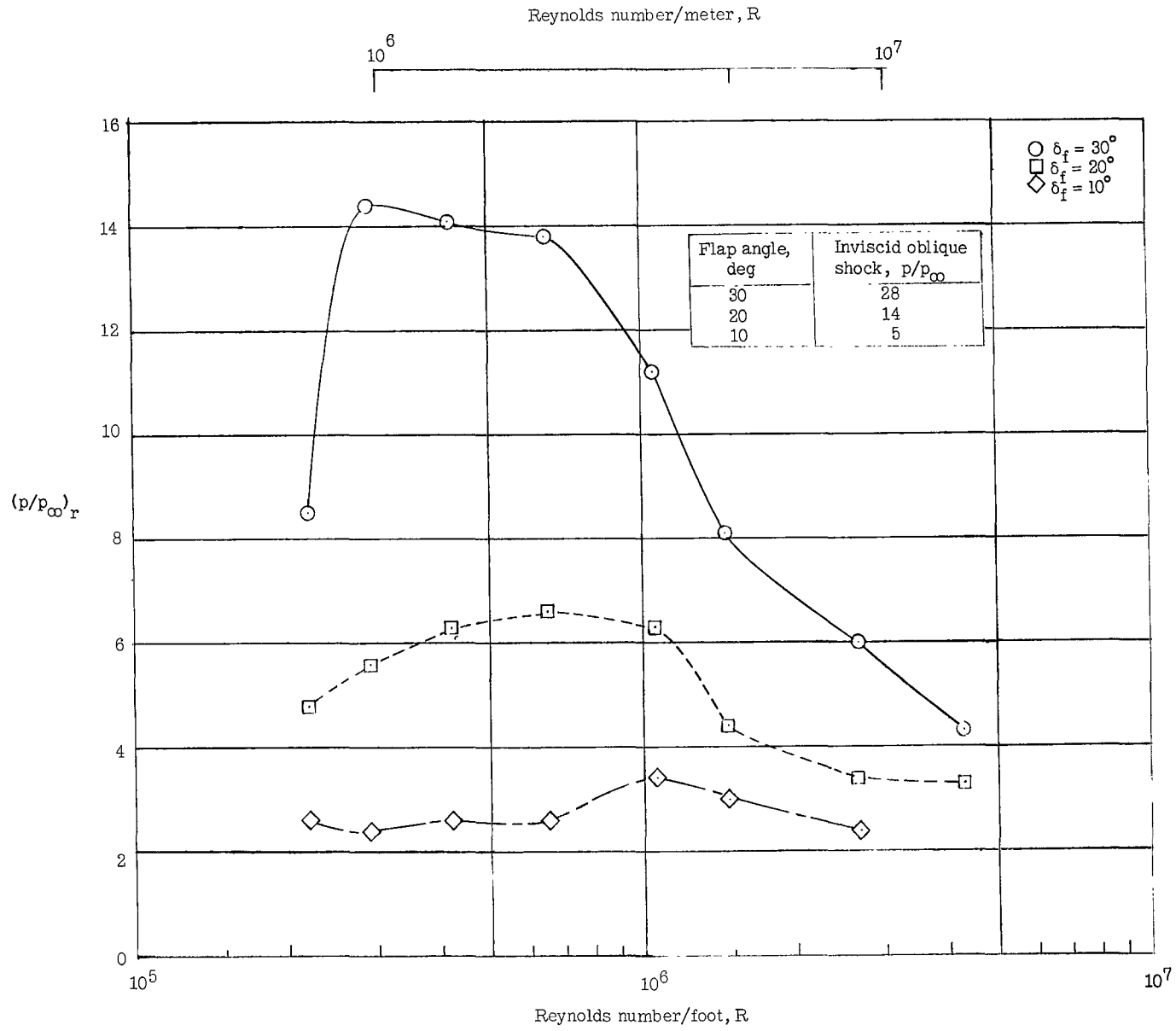


Figure 15.- The effect of Reynolds number and flap angle on the approximate pressure at the reattachment point on the flap for a $T_w/T_t = 0.43$.

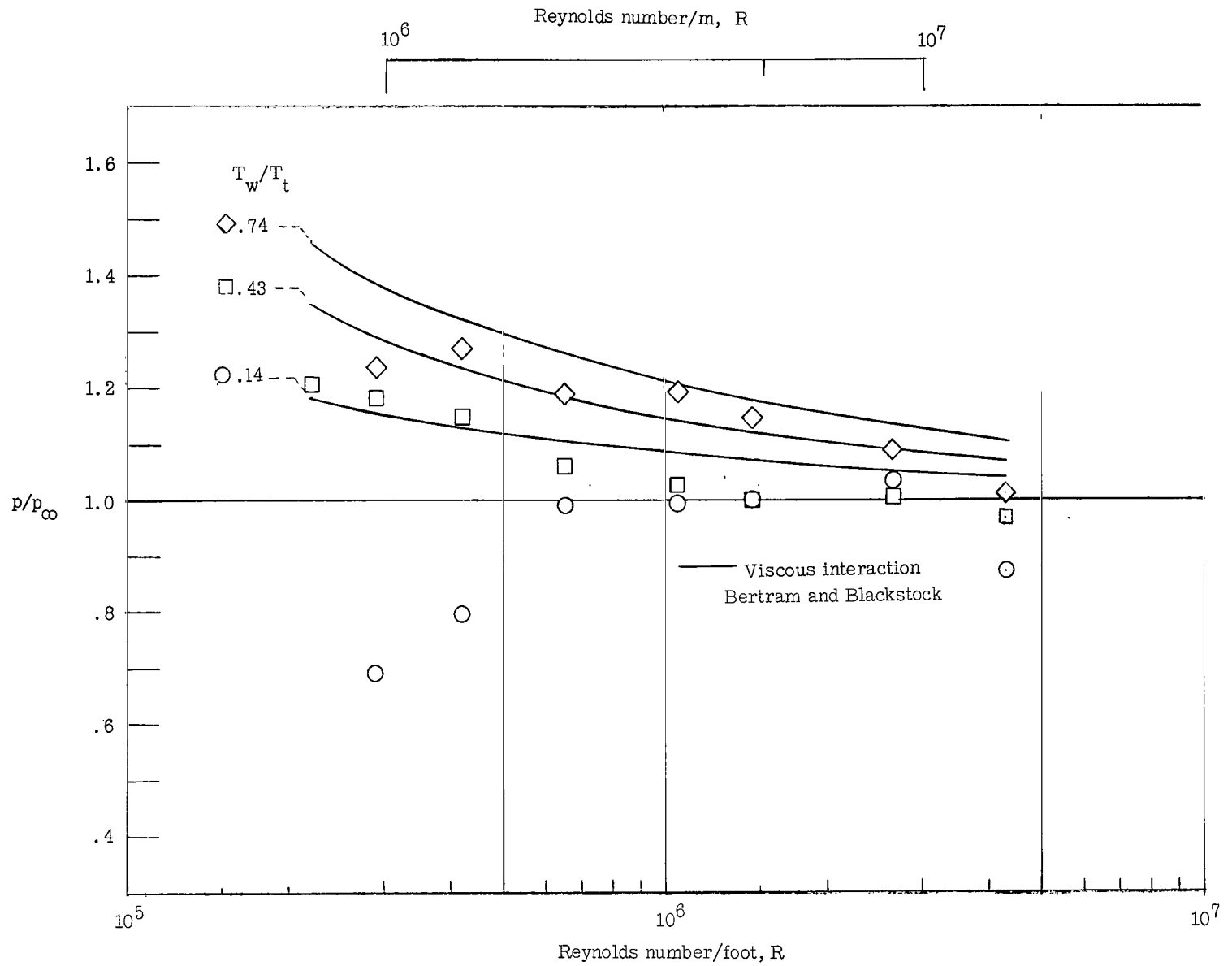


Figure 16.- The effect of wall temperature and Reynolds number on the induced flat plate pressure 5 inches from the leading edge.

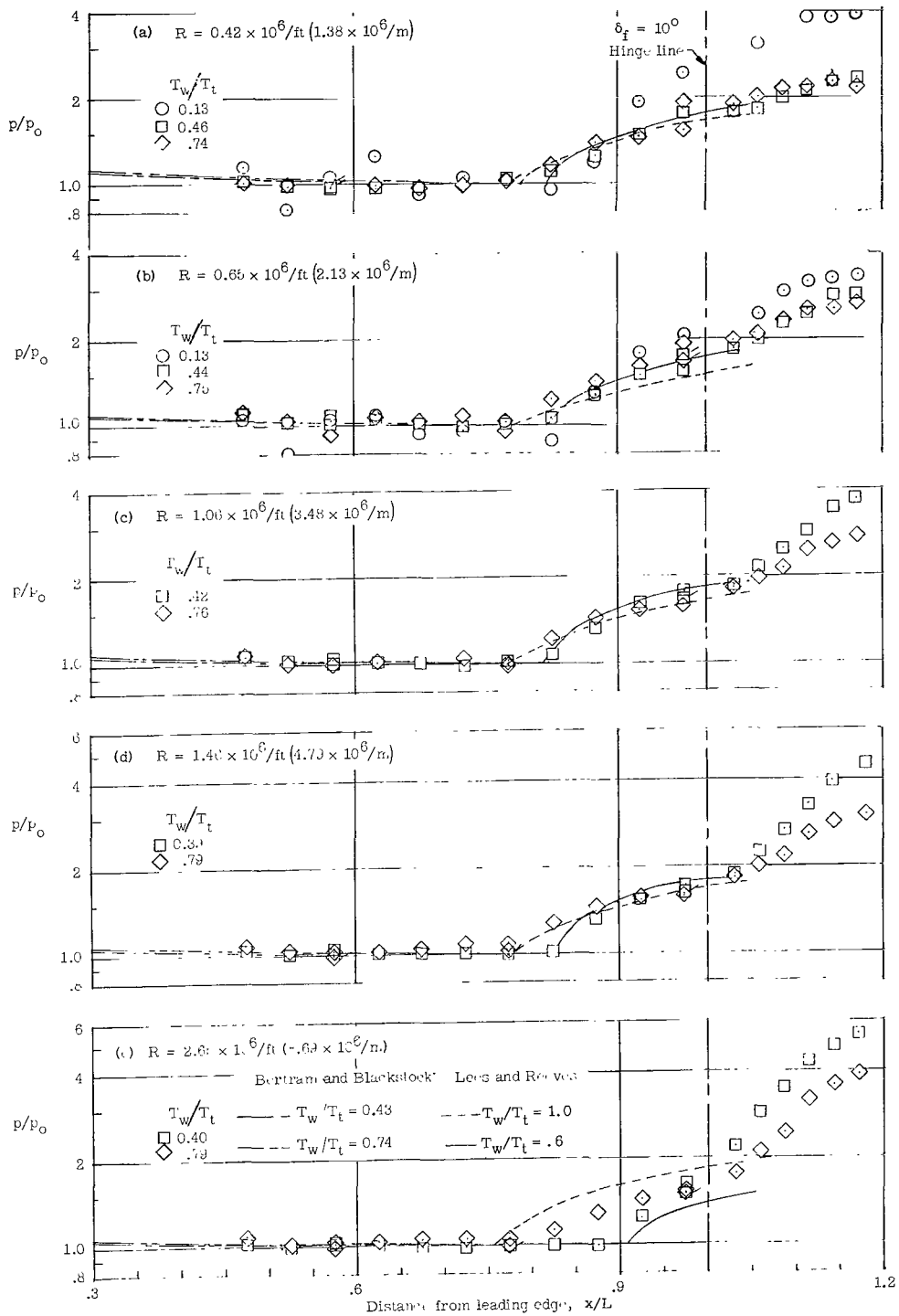


Figure 17.- The effect of wall temperature and Reynolds number on the pressure distribution at a flap angle of 10° .

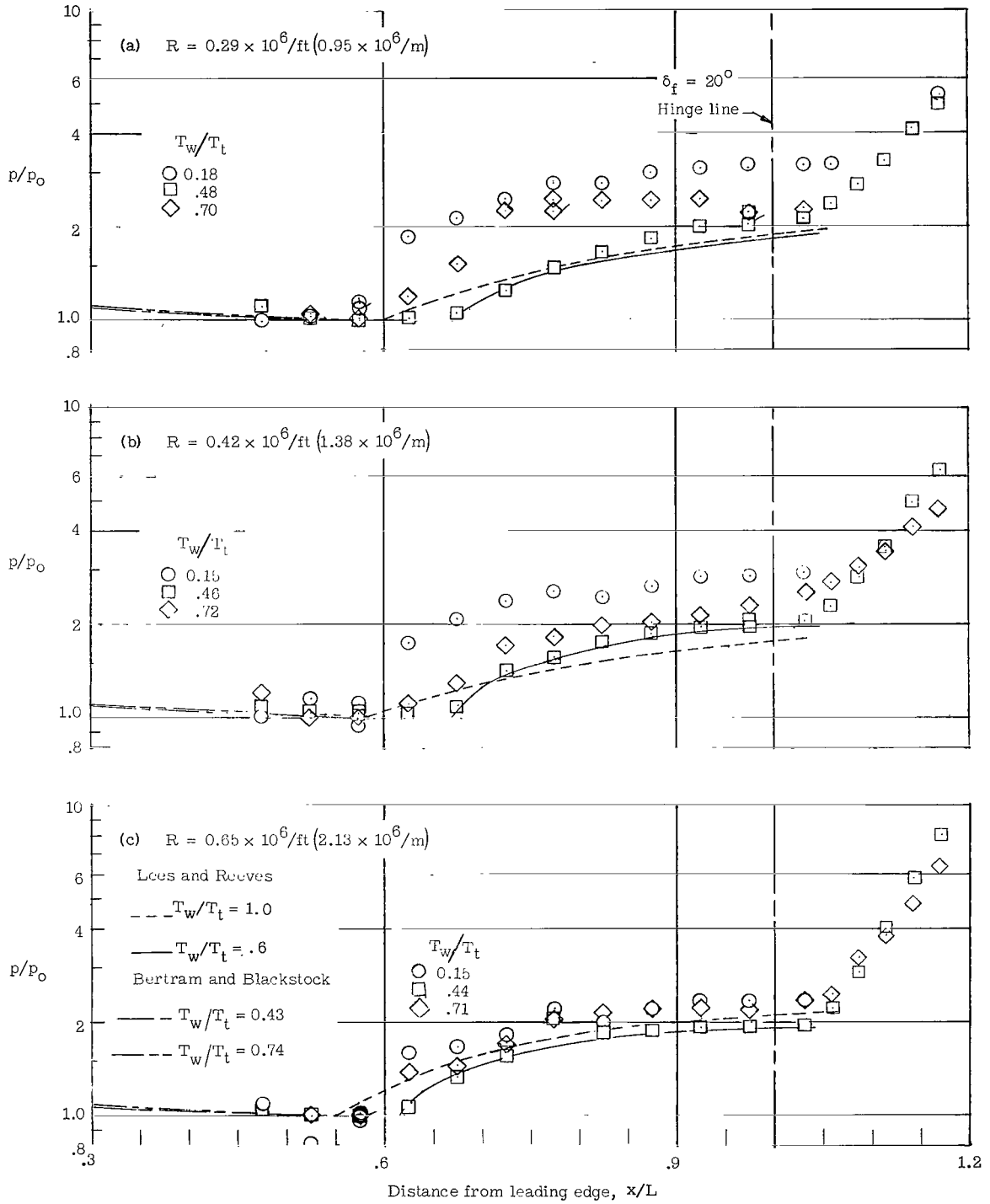


Figure 18.- The effect of wall temperature and Reynolds number on the pressure distribution at a flap angle of 20° .

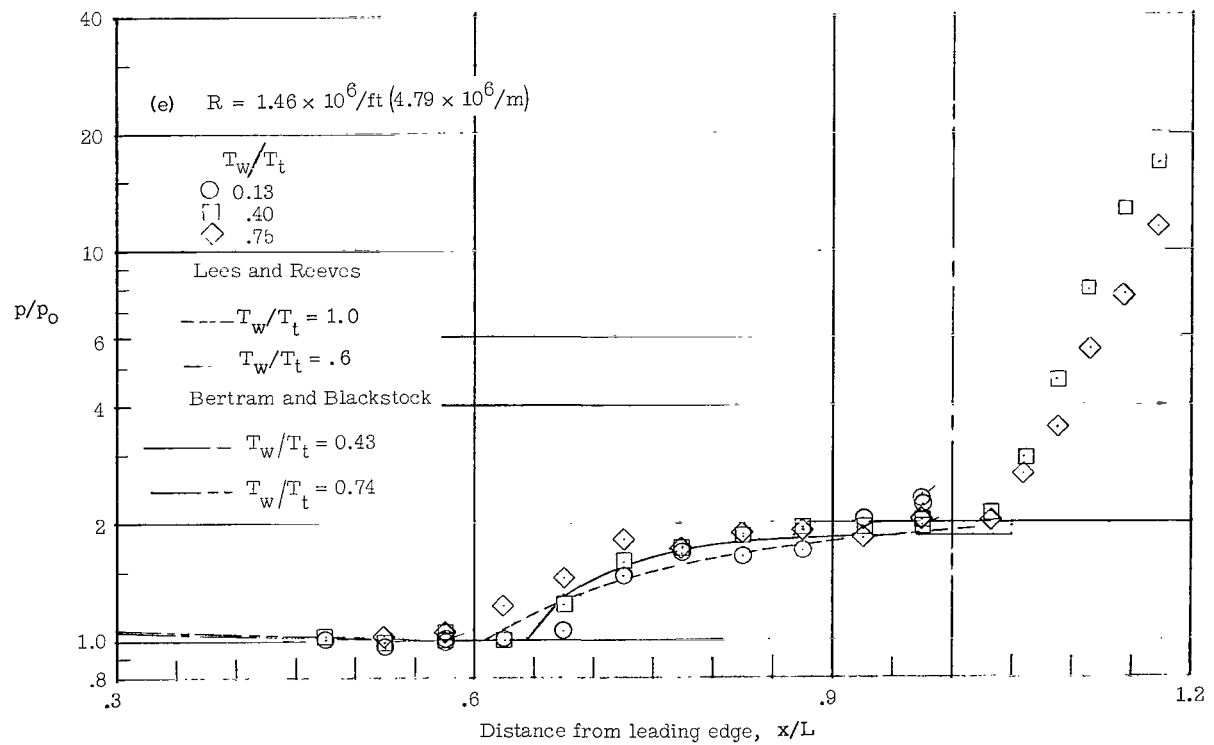
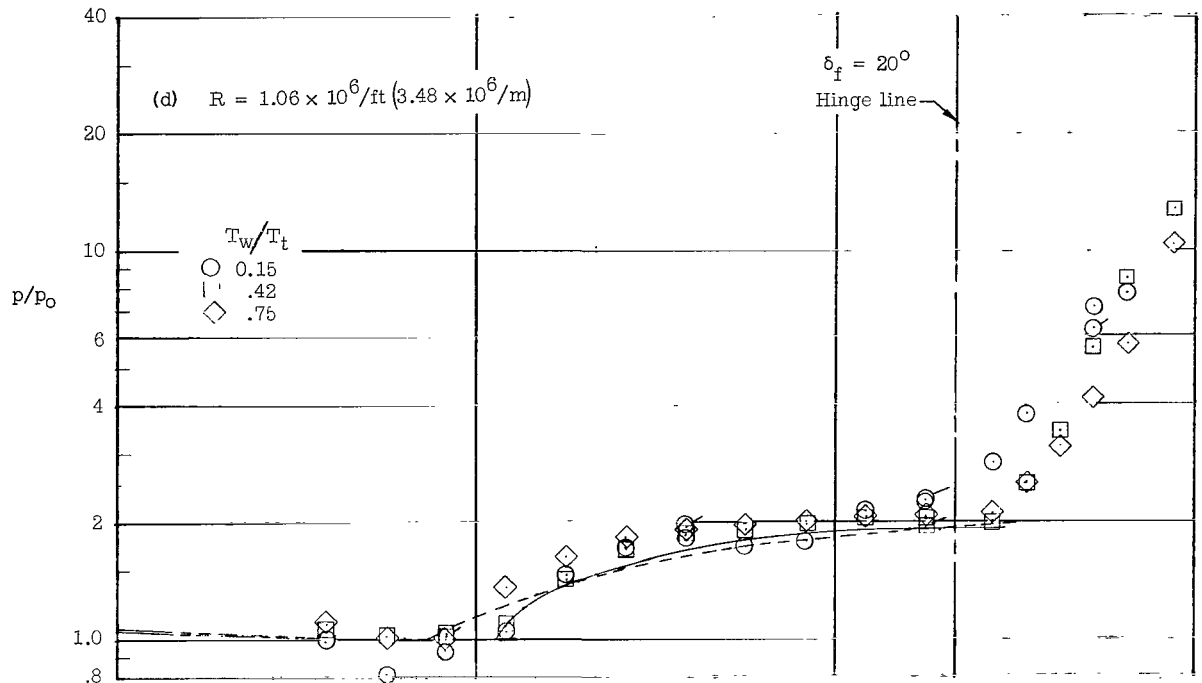


Figure 18.- Continued.

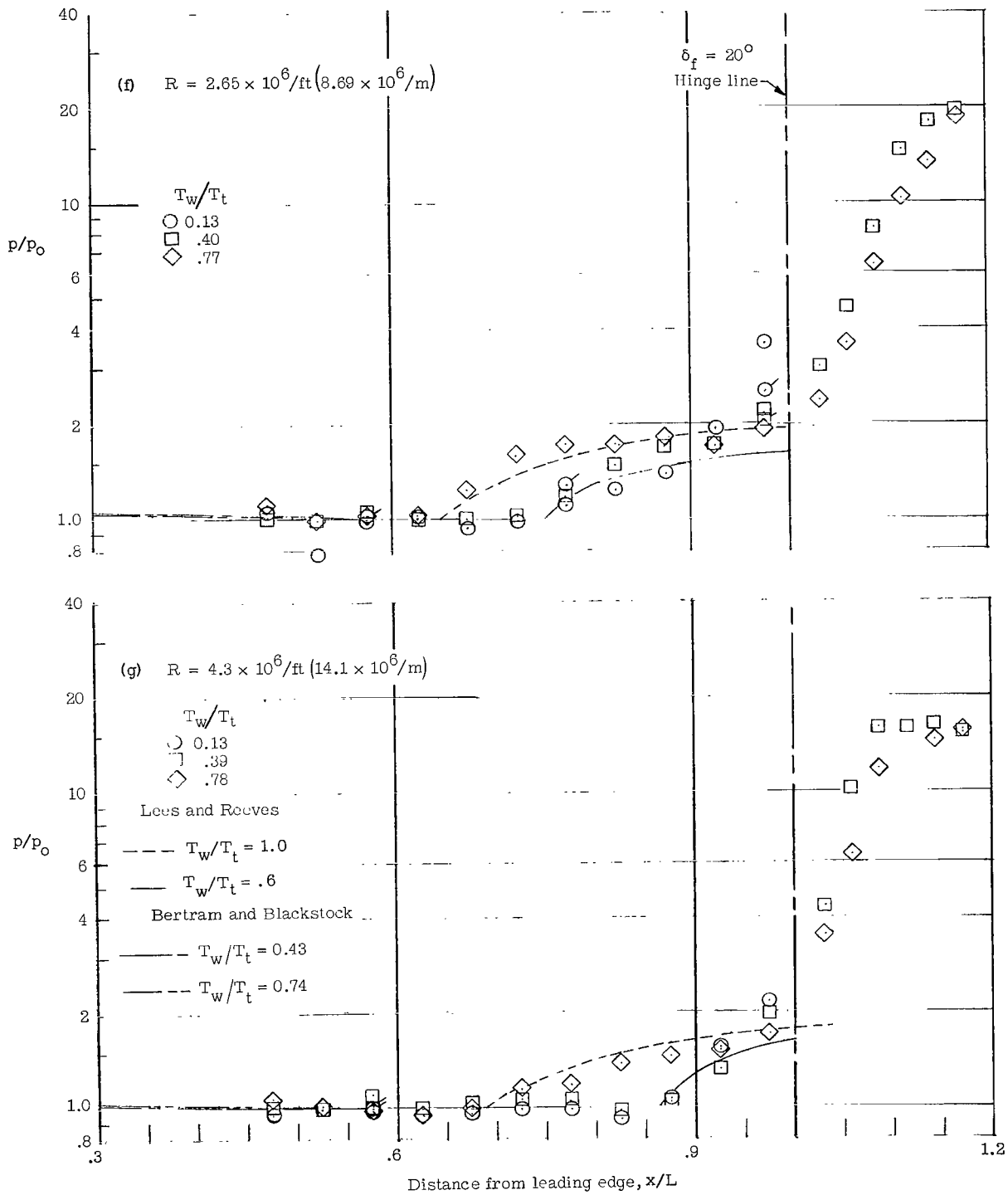


Figure 18.- Concluded.

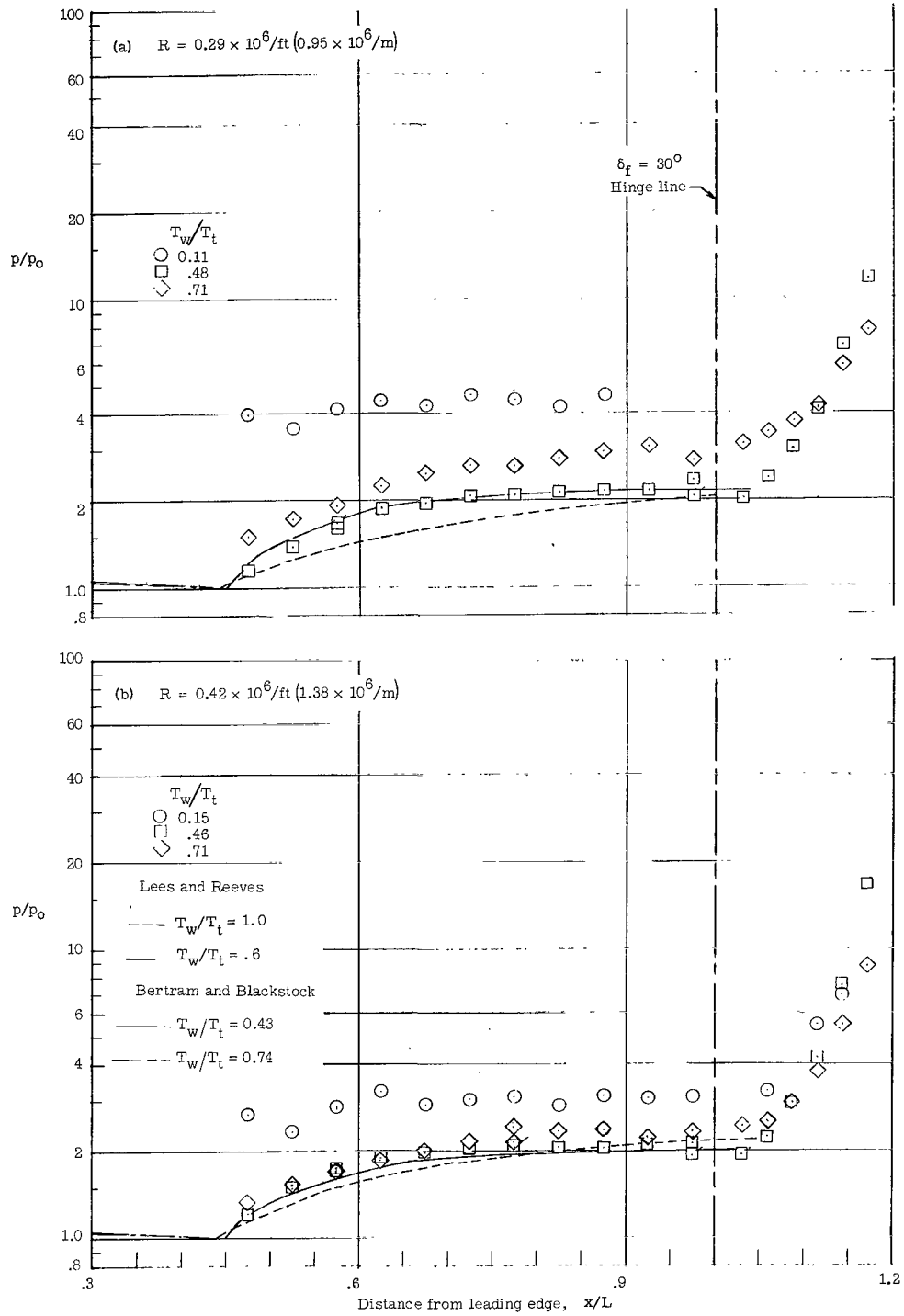


Figure 19.- The effect of wall temperature and Reynolds number on the pressure distribution at a flap angle of 30°.

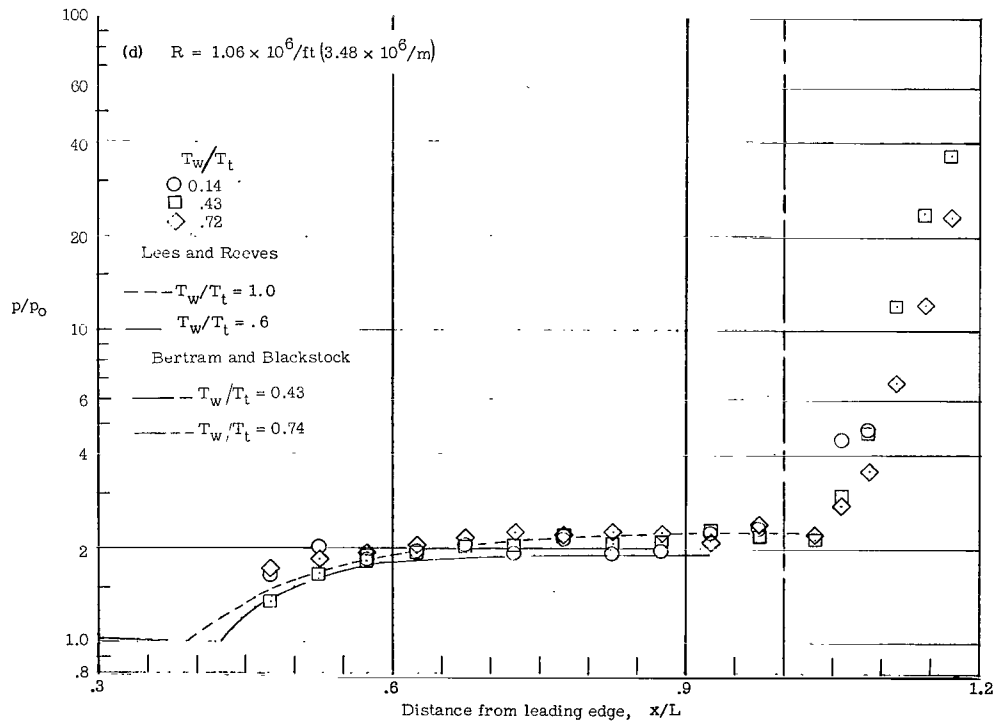
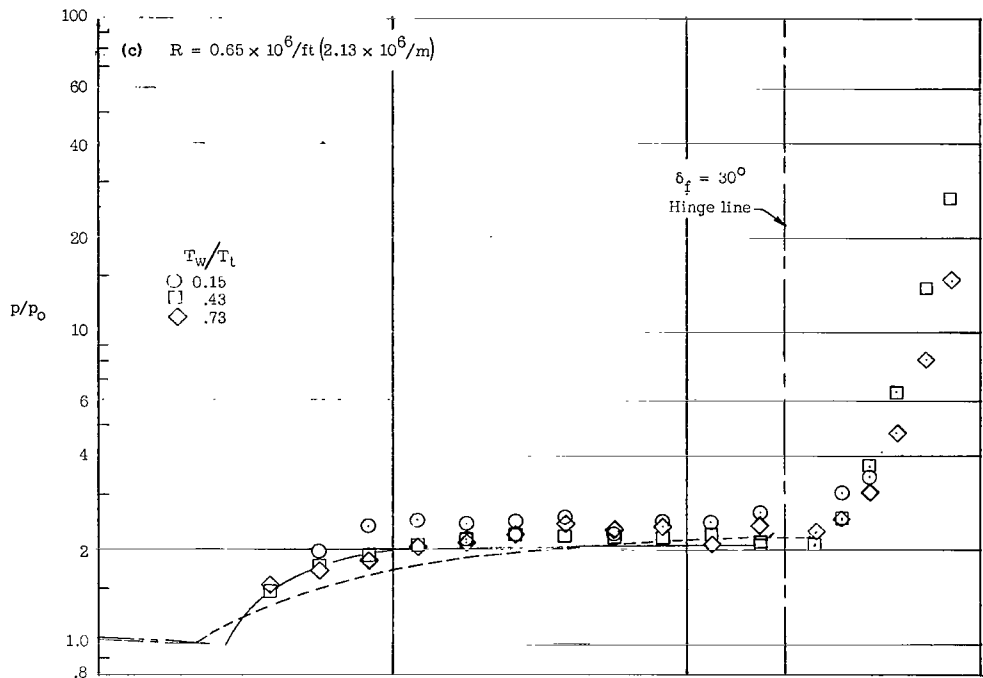


Figure 19.- Continued.

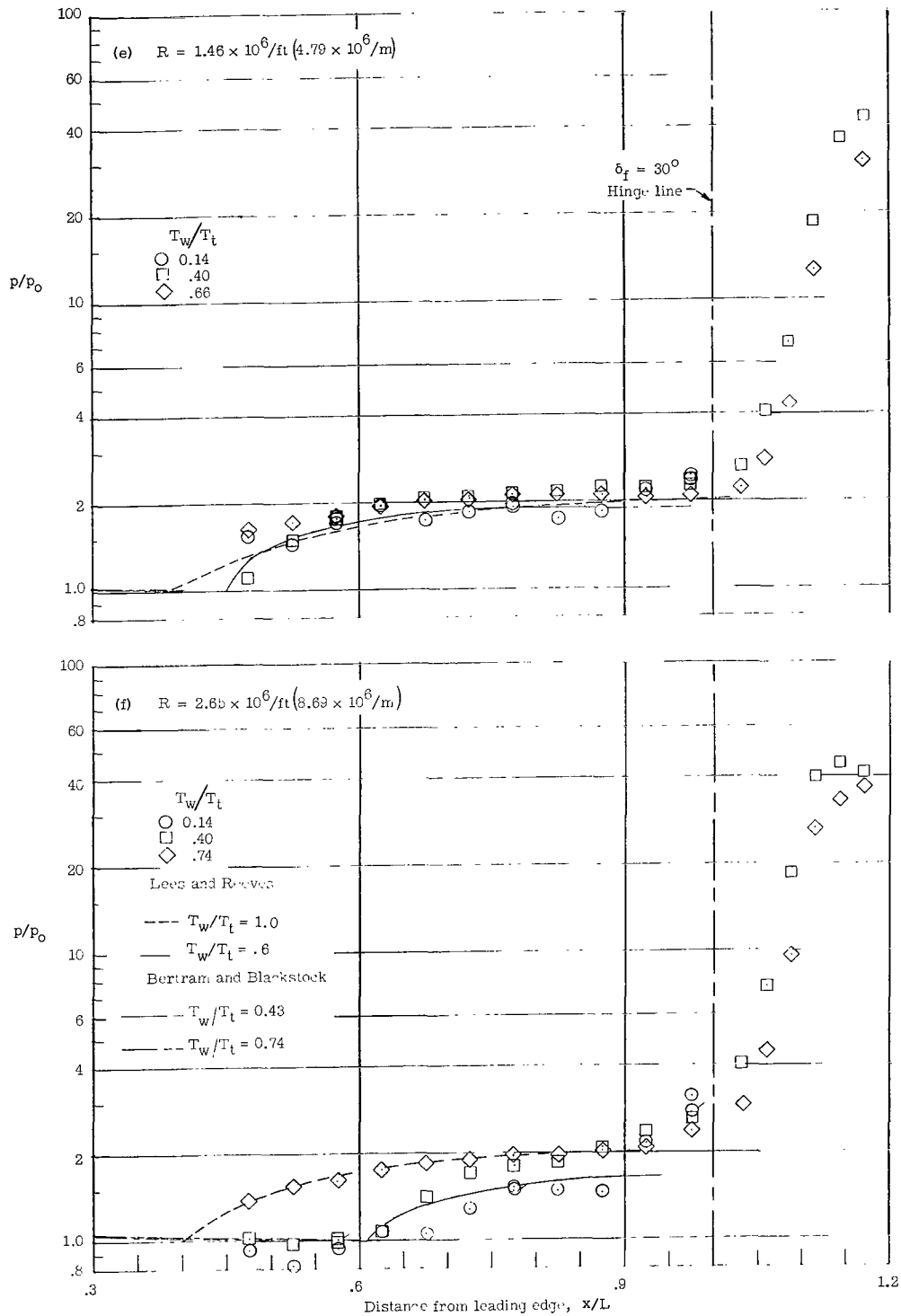


Figure 19.- Continued.

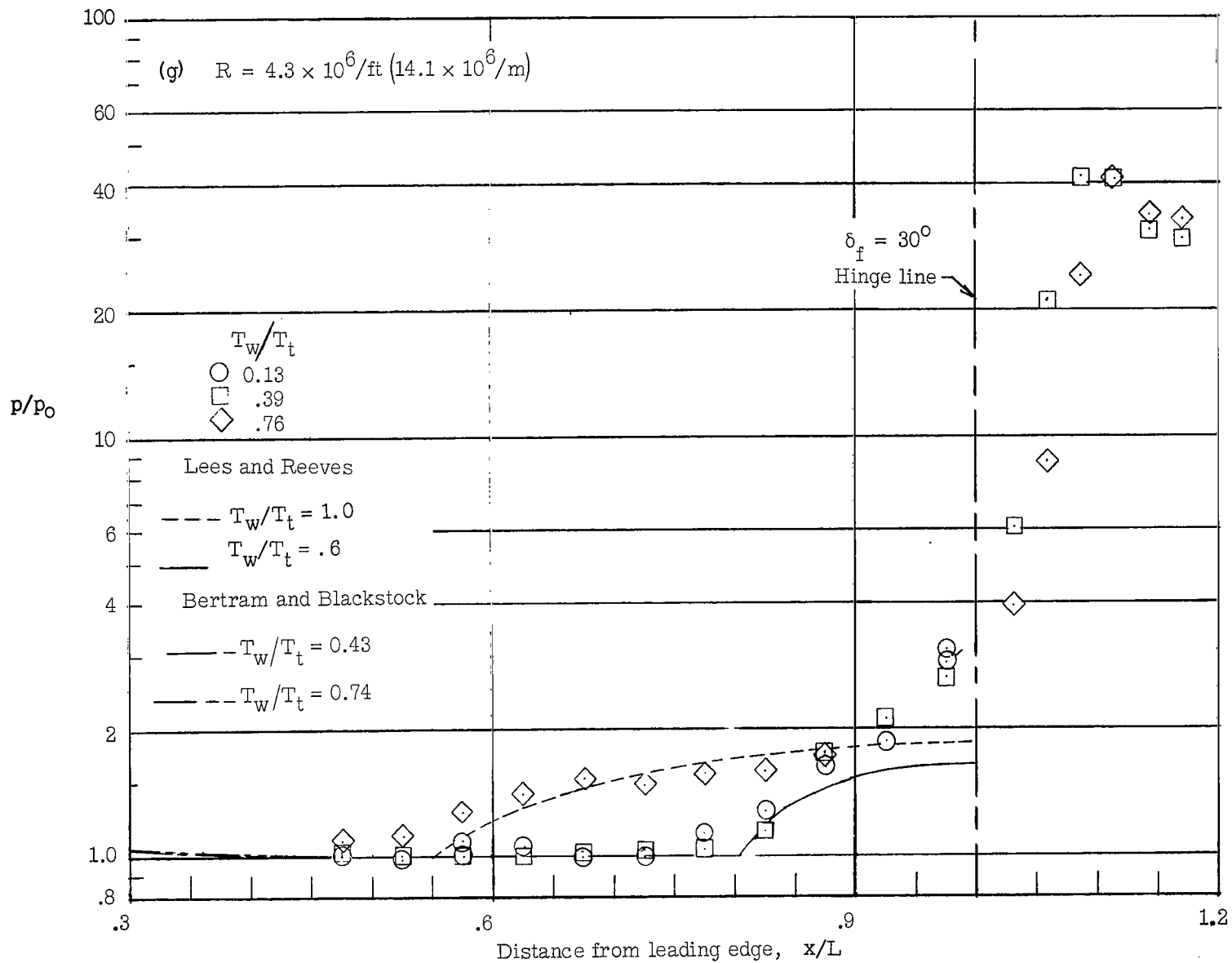


Figure 19.- Concluded.

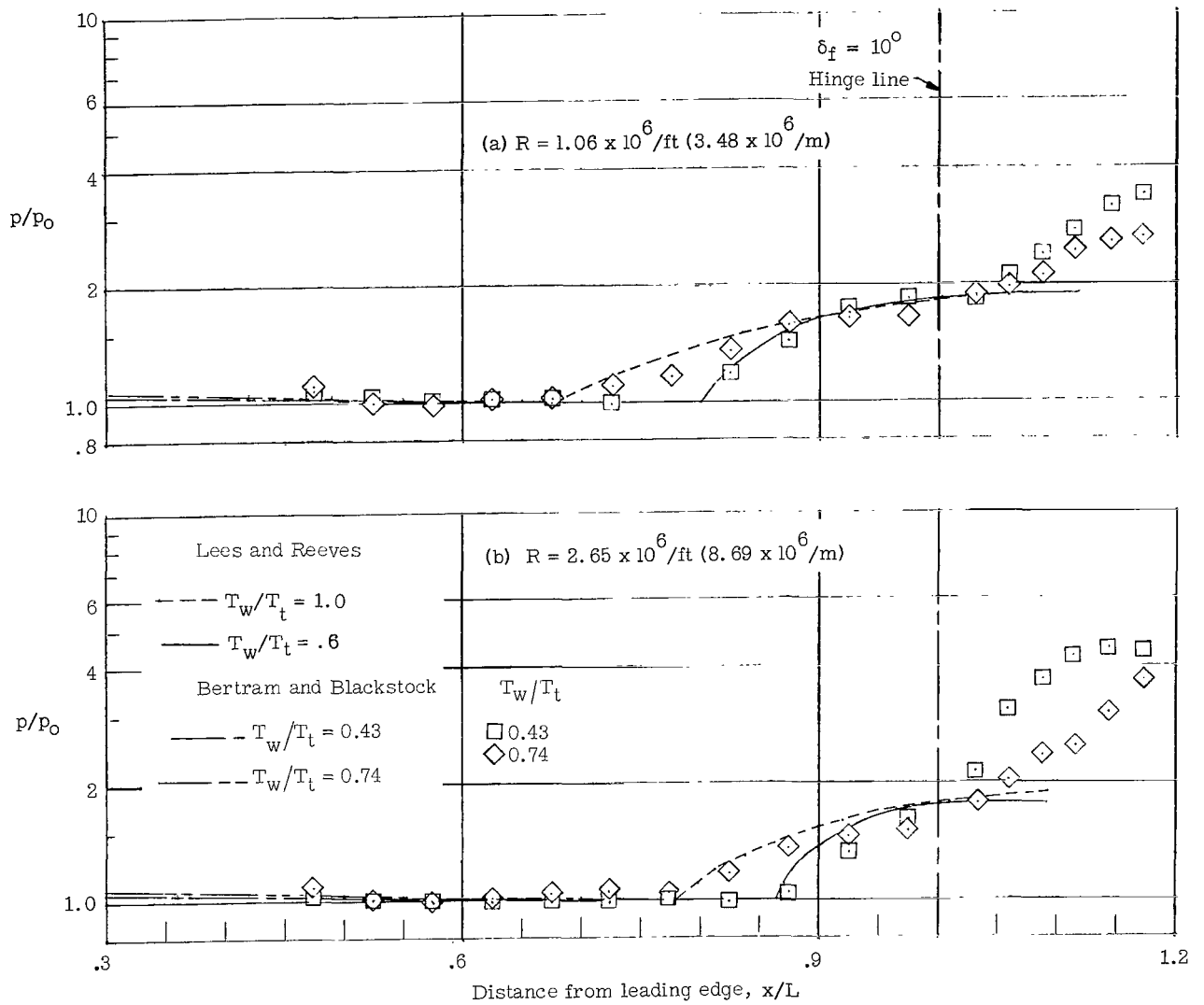


Figure 20.- The effect of wall temperature, Reynolds number on the pressure distribution at a flap angle of 10° . Side plates attached.

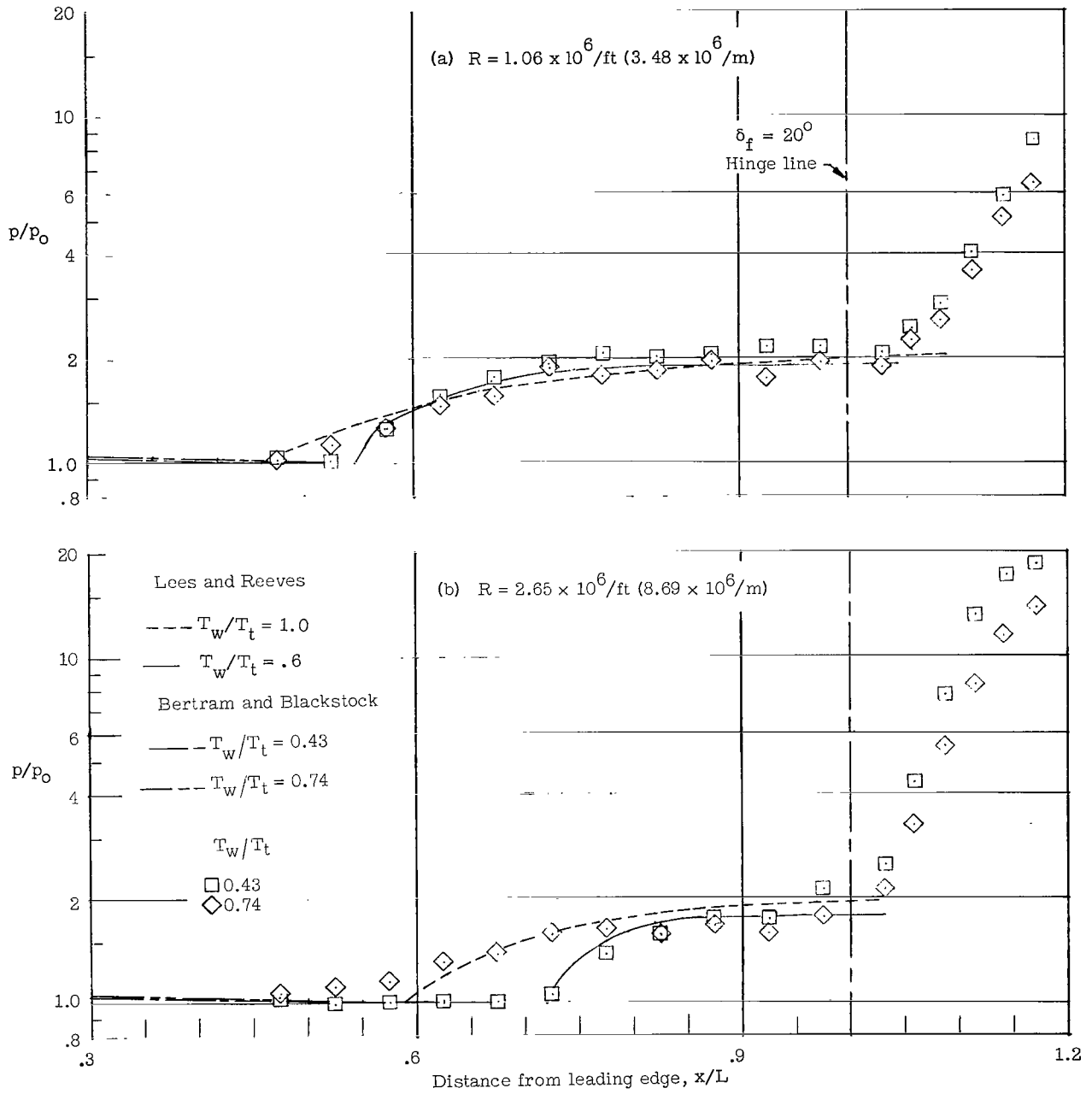


Figure 21.- The effect of wall temperature, Reynolds number, and side plates on the pressure distribution at a flap angle of 20° .

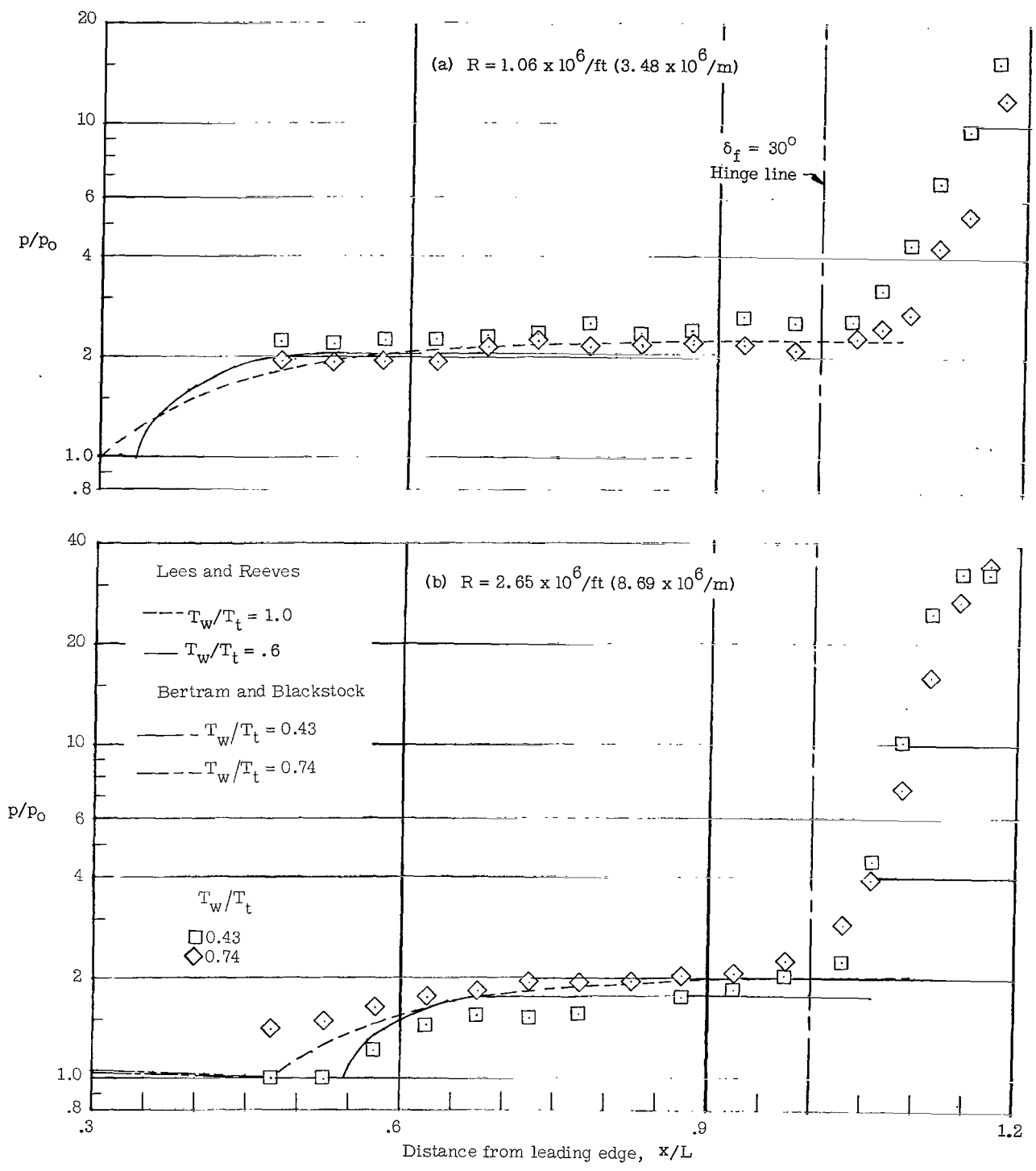
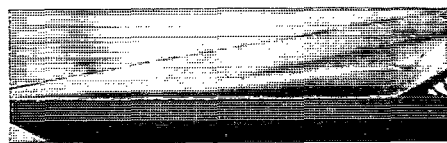


Figure 22.- The effect of wall temperature, Reynolds number, and side plates on the pressure distribution at a flap angle of 30° .



$$T_w/T_t = .51$$



$$T_w/T_t = .68$$

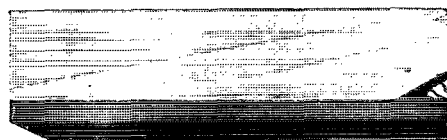
$$R = 0.220 \times 10^6 / \text{ft} (0.722 \times 10^6 / \text{m})$$



$$T_w/T_t = .11$$

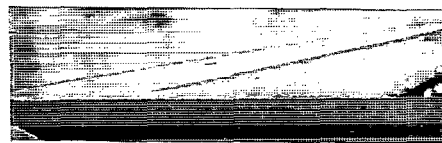


$$T_w/T_t = .48$$

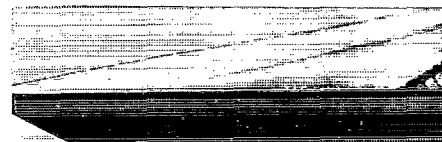


$$T_w/T_t = .71$$

$$R = 0.290 \times 10^6 / \text{ft} (0.950 \times 10^6 / \text{m})$$



$$T_w/T_t = .15$$

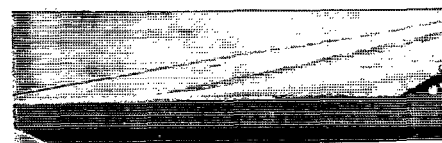


$$T_w/T_t = .46$$

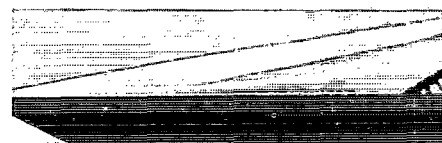


$$T_w/T_t = .71$$

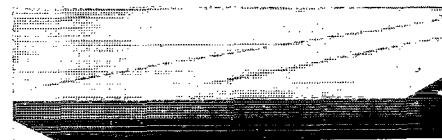
$$R = 0.420 \times 10^6 / \text{ft} (1.38 \times 10^6 / \text{m})$$



$$T_w/T_t = .15$$



$$T_w/T_t = .43$$



$$T_w/T_t = .73$$

$$R = 0.65 \times 10^6 / \text{ft} (2.13 \times 10^6 / \text{m})$$

(a) $\delta_f = 30^\circ$.

L-67-6602

Figure 23.- Schlieren photographs showing wall temperature effects at various Reynolds numbers and flap angles.



$$T_w/T_t = .14$$



$$T_w/T_t = .43$$

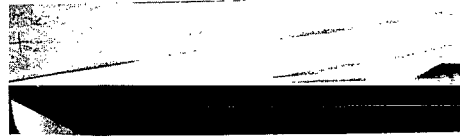


$$T_w/T_t = .72$$

$$R = 1.06 \times 10^6/\text{ft} (3.48 \times 10^6/\text{m})$$



$$T_w/T_t = .14$$



$$T_w/T_t = .40$$

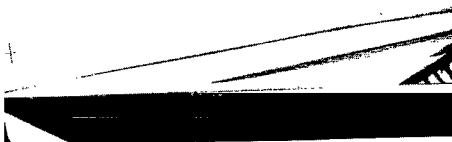


$$T_w/T_t = .74$$

$$R = 2.65 \times 10^6/\text{ft} (8.69 \times 10^6/\text{m})$$



$$T_w/T_t = .14$$

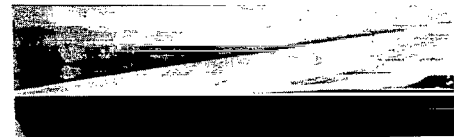


$$T_w/T_t = .40$$



$$T_w/T_t = .66$$

$$R = 1.46 \times 10^6/\text{ft} (4.79 \times 10^6/\text{m})$$



$$T_w/T_t = .13$$



$$T_w/T_t = .39$$



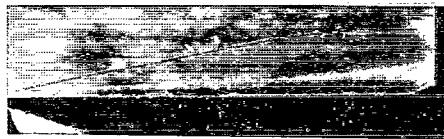
$$T_w/T_t = .76$$

$$R = 4.30 \times 10^6/\text{ft} (14.1 \times 10^6/\text{m})$$

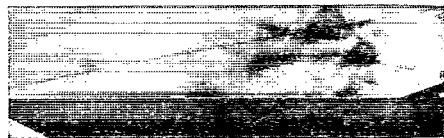
(a) $\delta_f = 30^\circ$ - Concluded.

L-67-6603

Figure 23.- Continued.



$$\tau_w/\tau_t = .51$$



$$\tau_w/\tau_t = .70$$

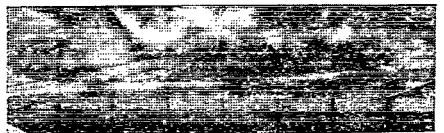
$$R = 0.220 \times 10^6/\text{ft} (0.722 \times 10^6/\text{m})$$



$$\tau_w/\tau_t = .18$$

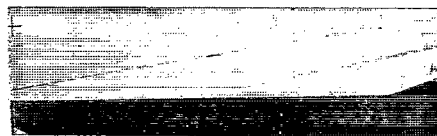


$$\tau_w/\tau_t = .48$$



$$\tau_w/\tau_t = .70$$

$$R = 0.290 \times 10^6/\text{ft} (0.950 \times 10^6/\text{m})$$



$$\tau_w/\tau_t = .15$$

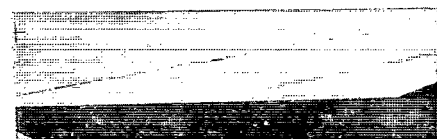


$$\tau_w/\tau_t = .46$$



$$\tau_w/\tau_t = .72$$

$$R = 0.420 \times 10^6/\text{ft} (1.38 \times 10^6/\text{m})$$



$$\tau_w/\tau_t = .15$$



$$\tau_w/\tau_t = .44$$



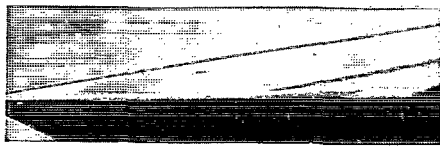
$$\tau_w/\tau_t = .71$$

$$R = 0.650 \times 10^6/\text{ft} (2.13 \times 10^6/\text{m})$$

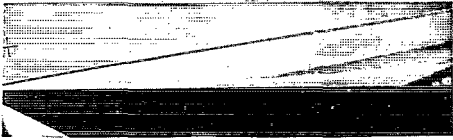
(b) $\delta_f = 20^\circ$.

L-67-6604

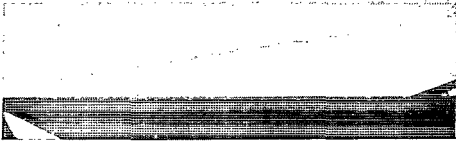
Figure 23.- Continued.



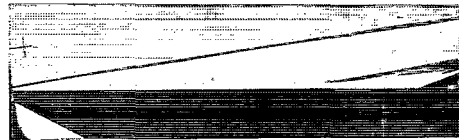
$$\tau_w/\tau_t = .15$$



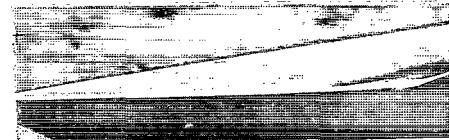
$$\tau_w/\tau_t = .42$$



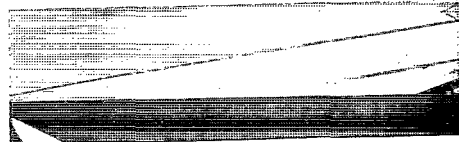
$$\tau_w/\tau_t = .75$$
$$R = 1.06 \times 10^6/\text{ft} (3.48 \times 10^6/\text{m})$$



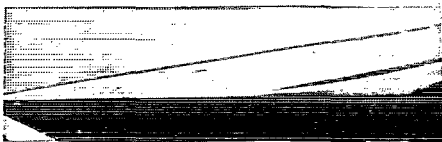
$$\tau_w/\tau_t = .13$$



$$\tau_w/\tau_t = .40$$



$$\tau_w/\tau_t = .77$$
$$R = 2.65 \times 10^6/\text{ft} (8.69 \times 10^6/\text{m})$$



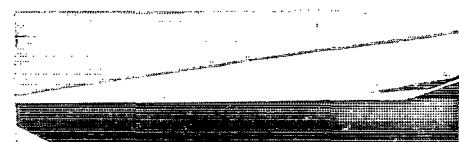
$$\tau_w/\tau_t = .13$$



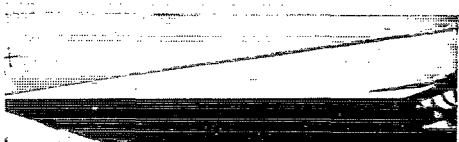
$$\tau_w/\tau_t = .40$$



$$\tau_w/\tau_t = .75$$
$$R = 1.46 \times 10^6/\text{ft} (4.79 \times 10^6/\text{m})$$



$$\tau_w/\tau_t = .13$$



$$\tau_w/\tau_t = .39$$



$$\tau_w/\tau_t = .78$$
$$R = 4.30 \times 10^6/\text{ft} (14.1 \times 10^6/\text{m})$$

(b) $\delta_f = 20^\circ$ - Concluded.

L-67-6605

Figure 23.- Concluded.

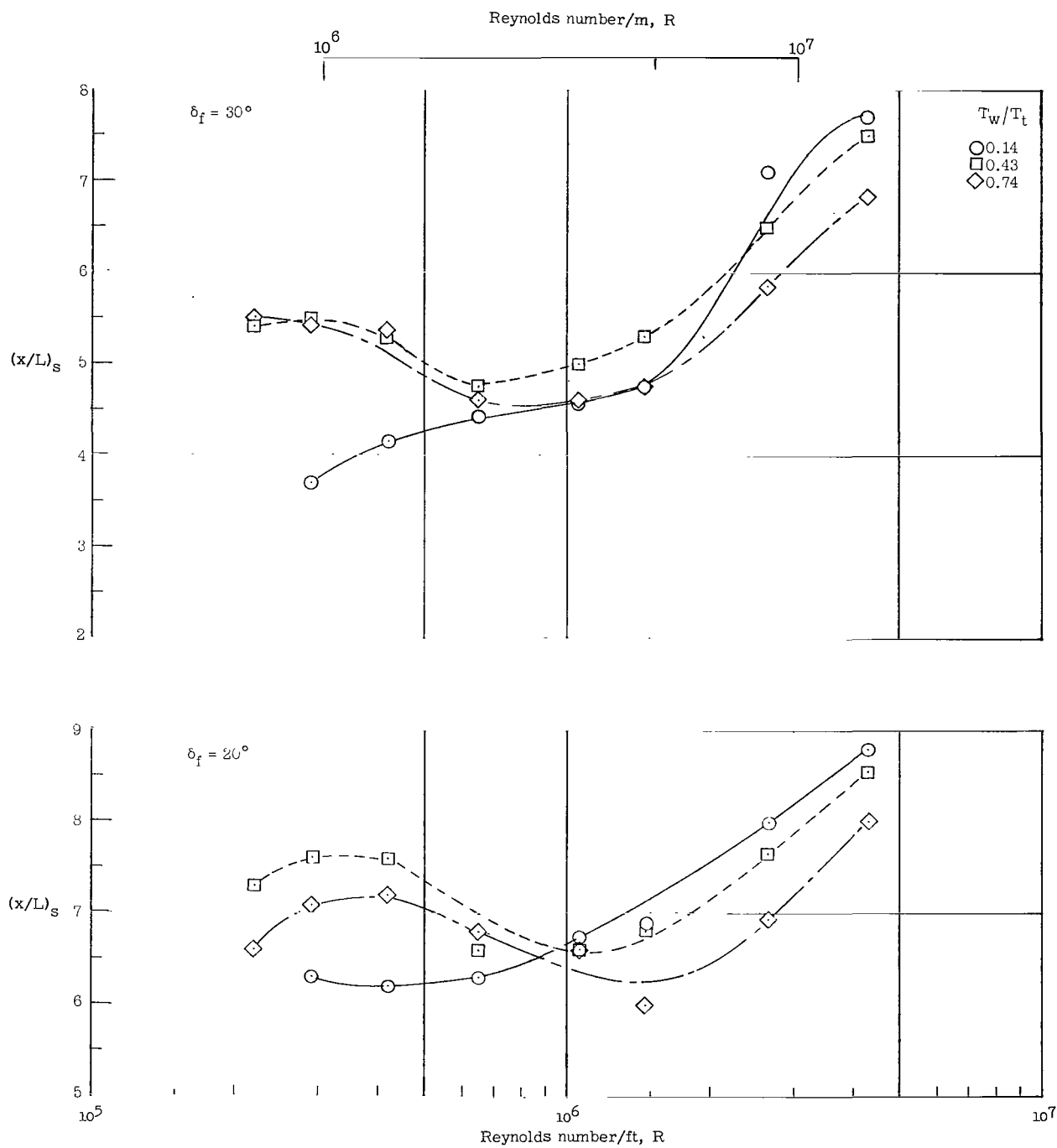


Figure 24.- The effect of Reynolds number, wall temperature, and flap angle on the location of the separation point on the plate surface.

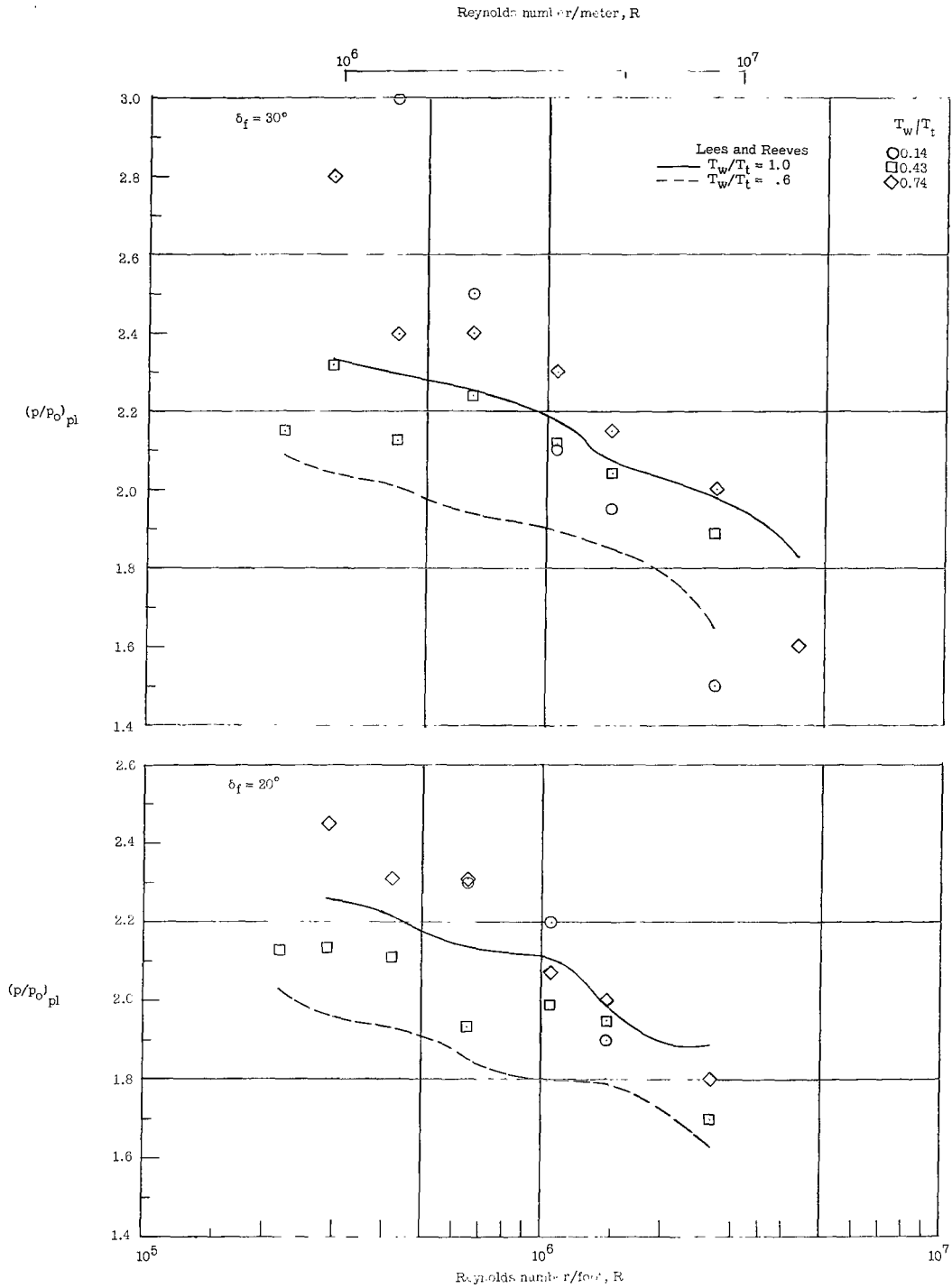


Figure 25.- The effect of Reynolds number, wall temperature, and flap angle on the value of plateau pressure.

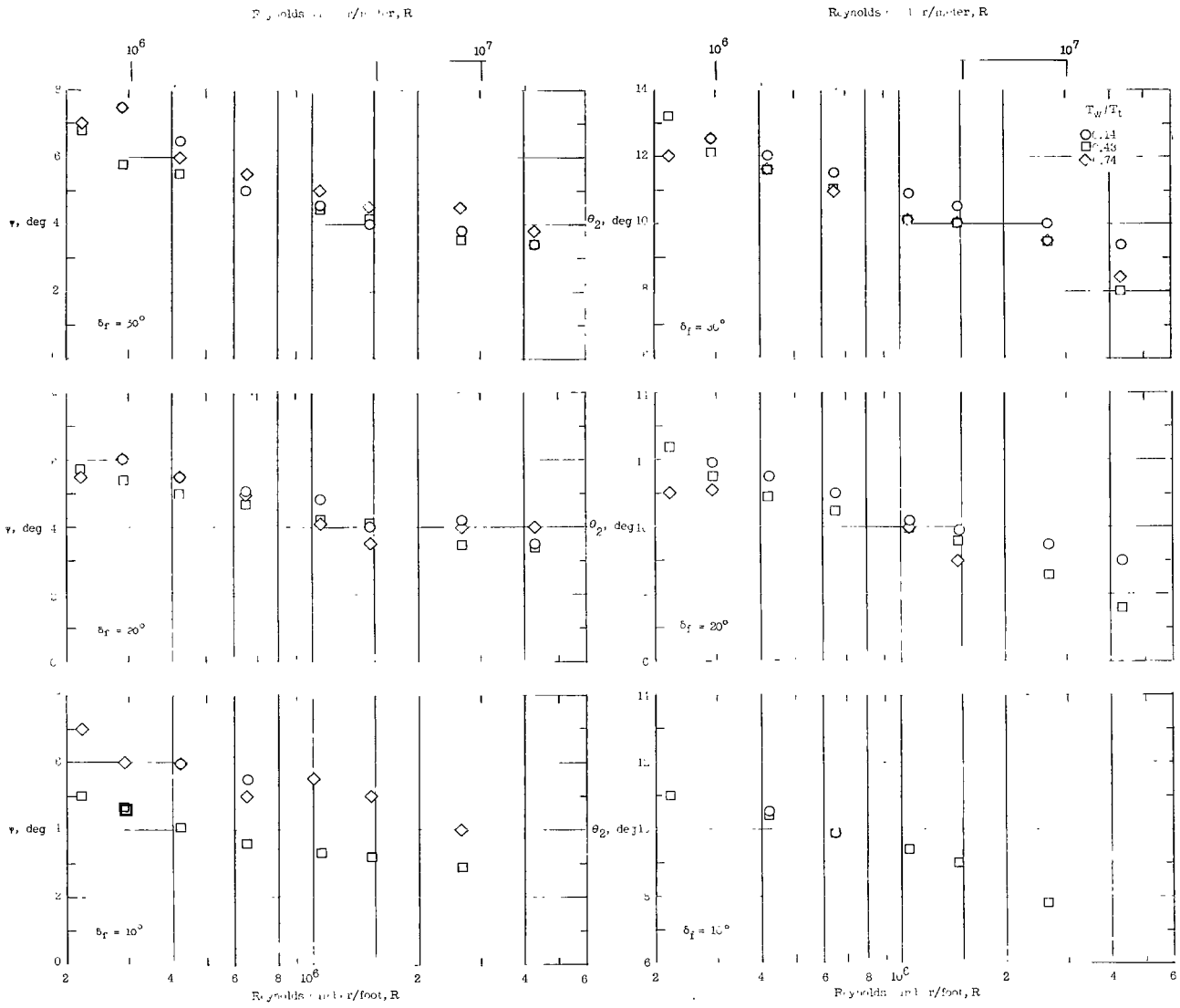


Figure 26.- The effect of Reynolds number, wall temperature, and flap angle on the indicated separation point flow deflection angle and the indicated separation shock wave angle.

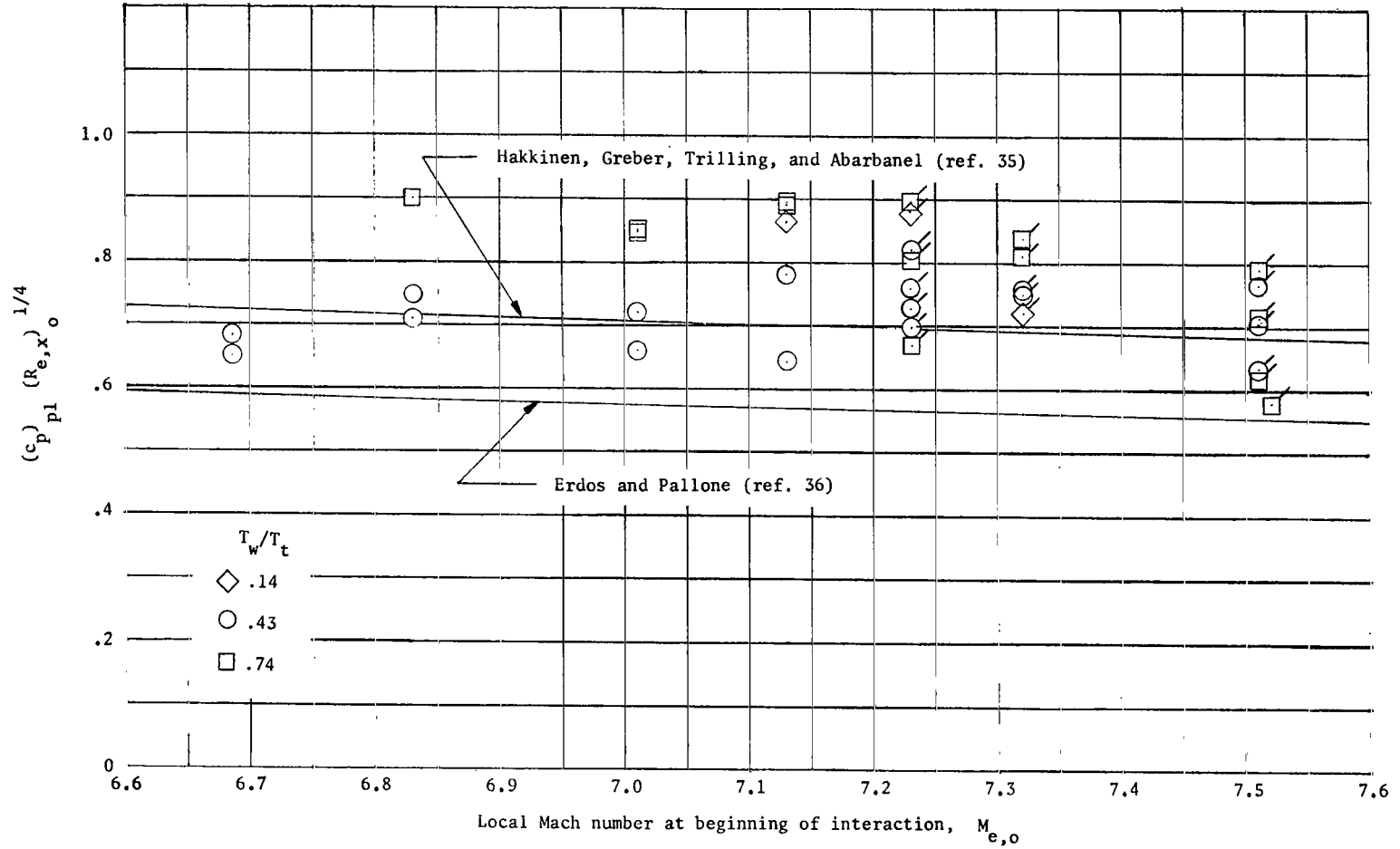


Figure 27.- The effect of wall temperature on the plateau pressure correlation. Flagged symbols indicate probable transition.

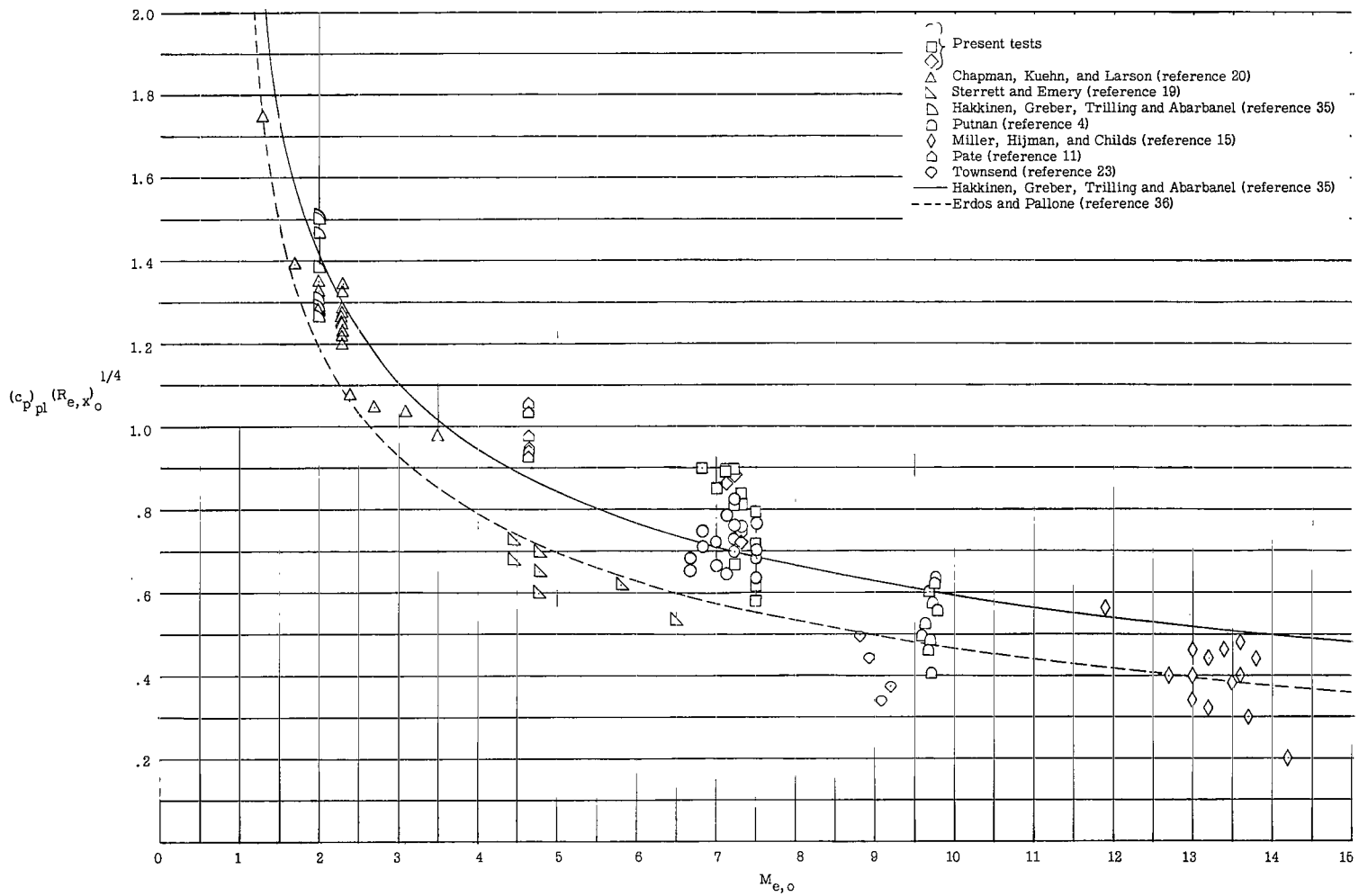


Figure 28.- A correlation of plateau pressure with Reynolds number and Mach number.

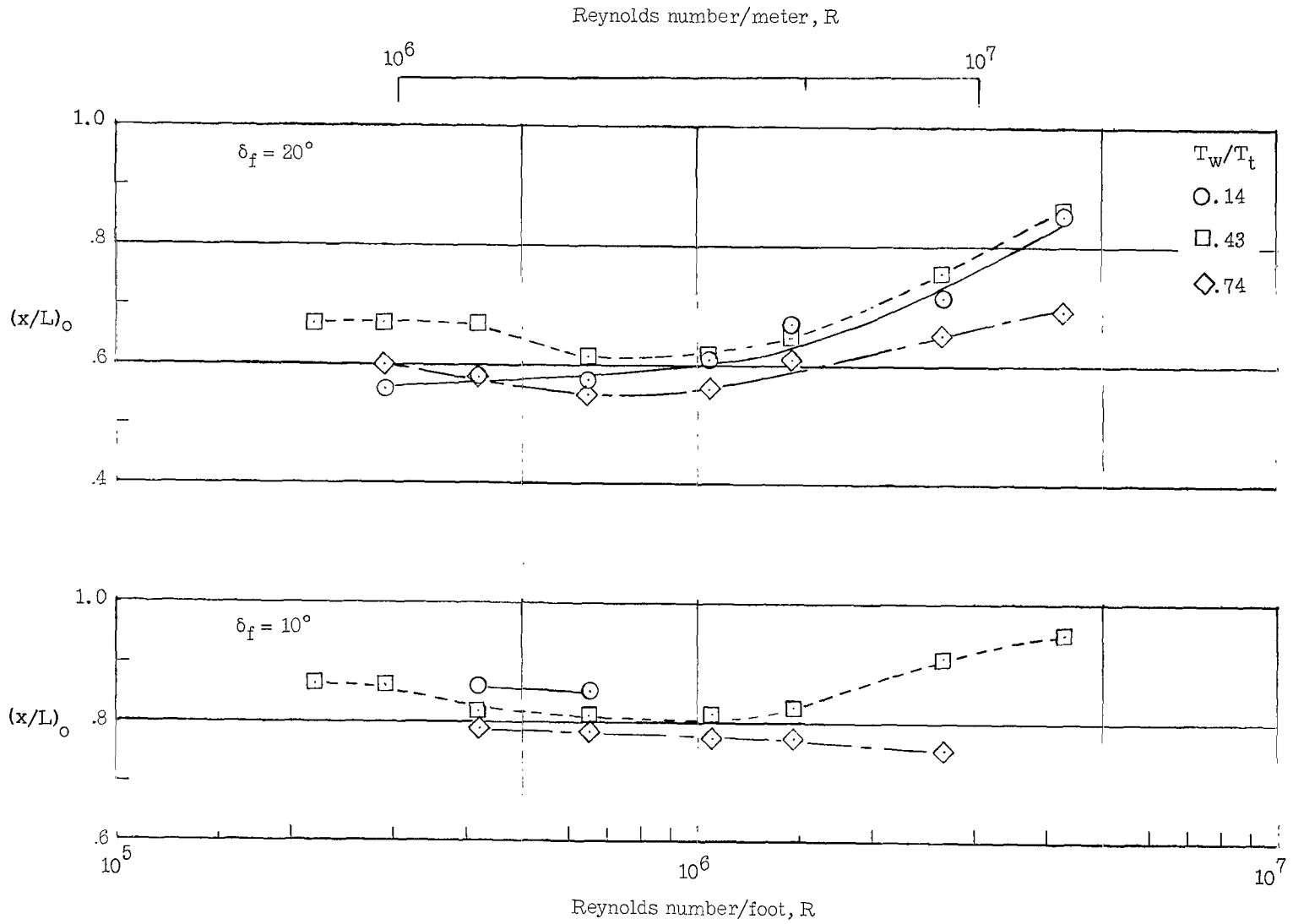


Figure 29.- The variation in the location of the beginning of the interaction region for two flap angles and three wall conditions at various unit Reynolds numbers.

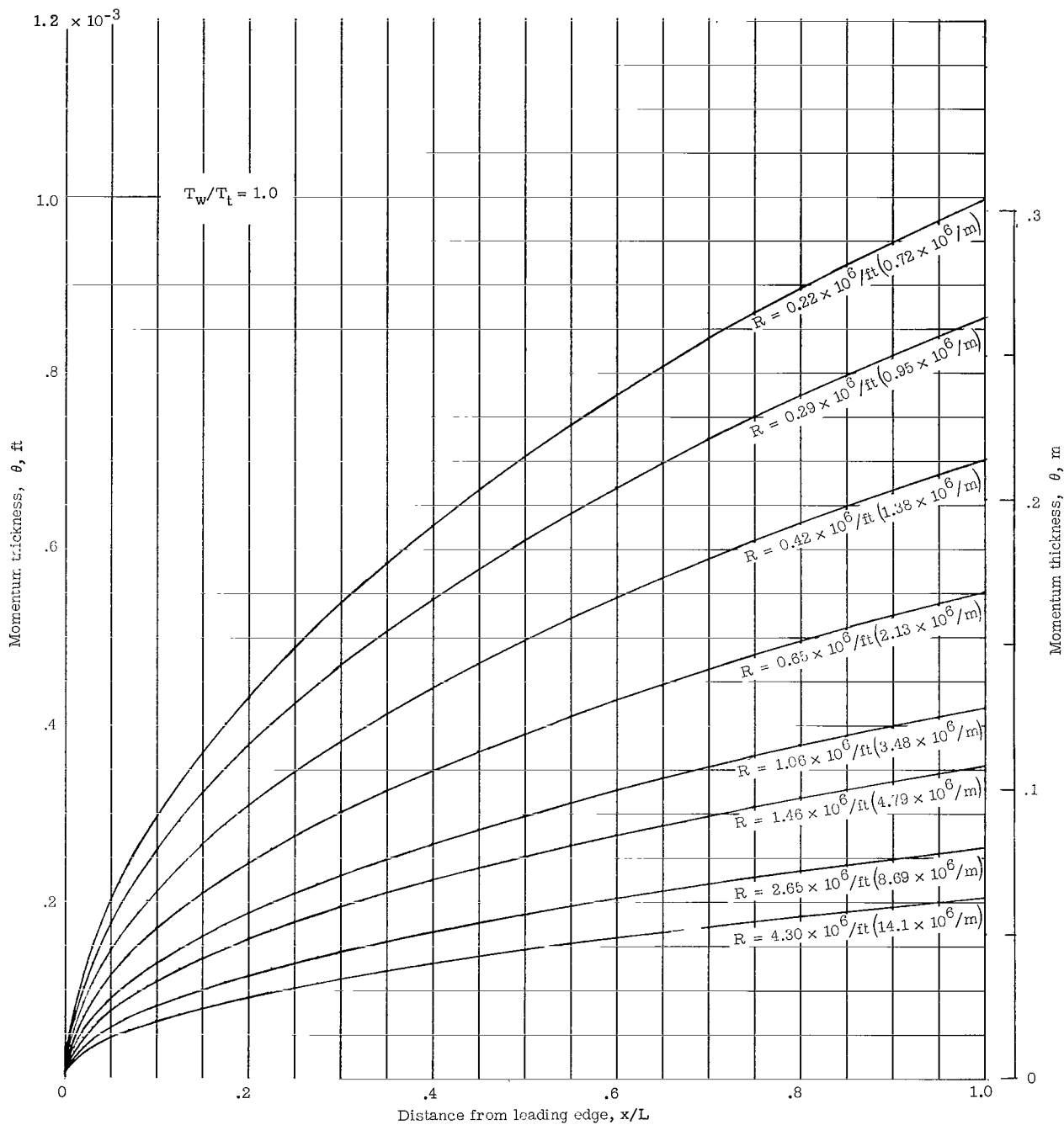


Figure 30.- The momentum thickness along a flat plate at a nominal Mach number of 8 for adiabatic wall conditions at various unit Reynolds numbers.

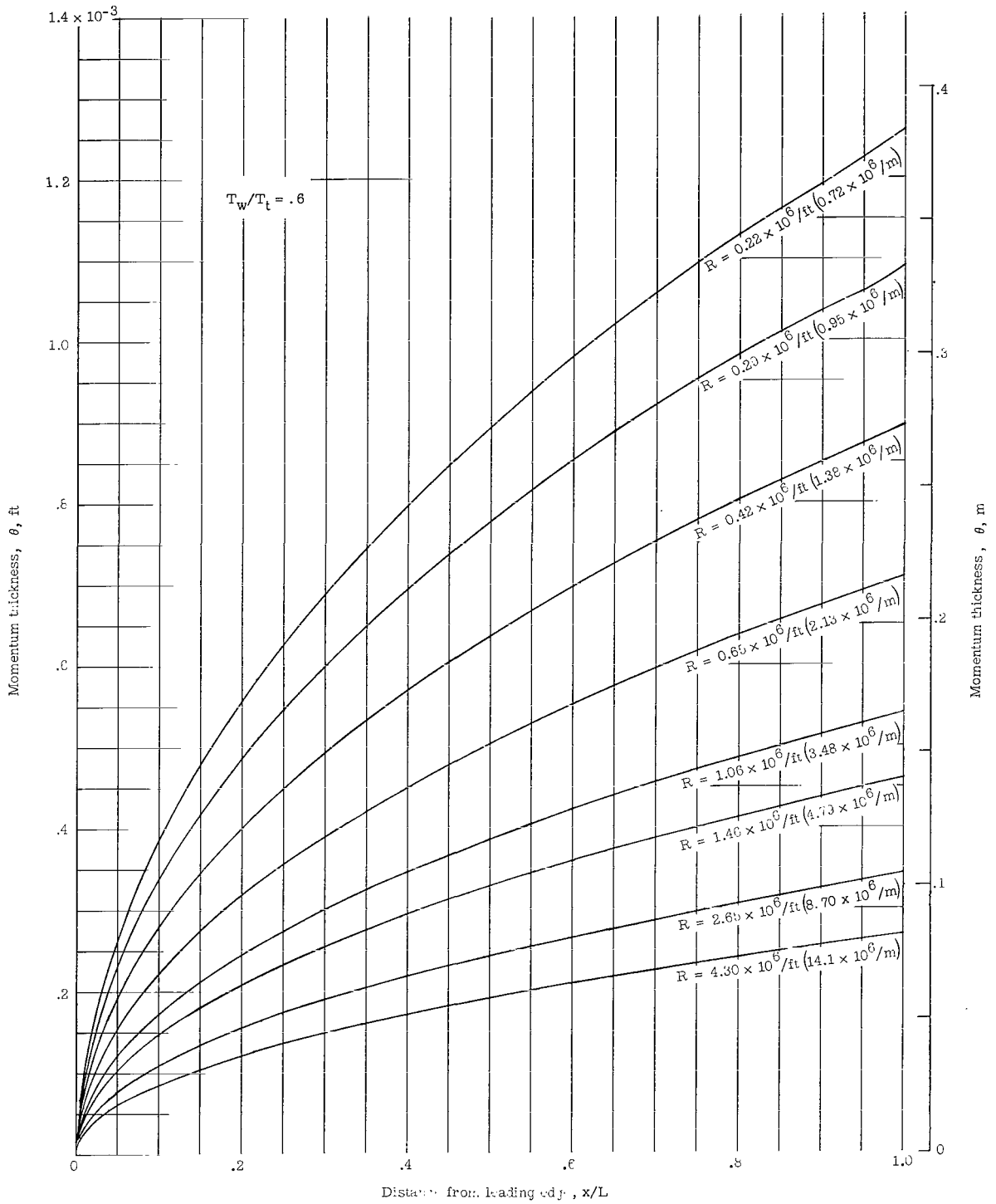


Figure 31.- The momentum thickness along a flat plate at a nominal Mach number of 8 for cool wall conditions at various unit Reynolds numbers.

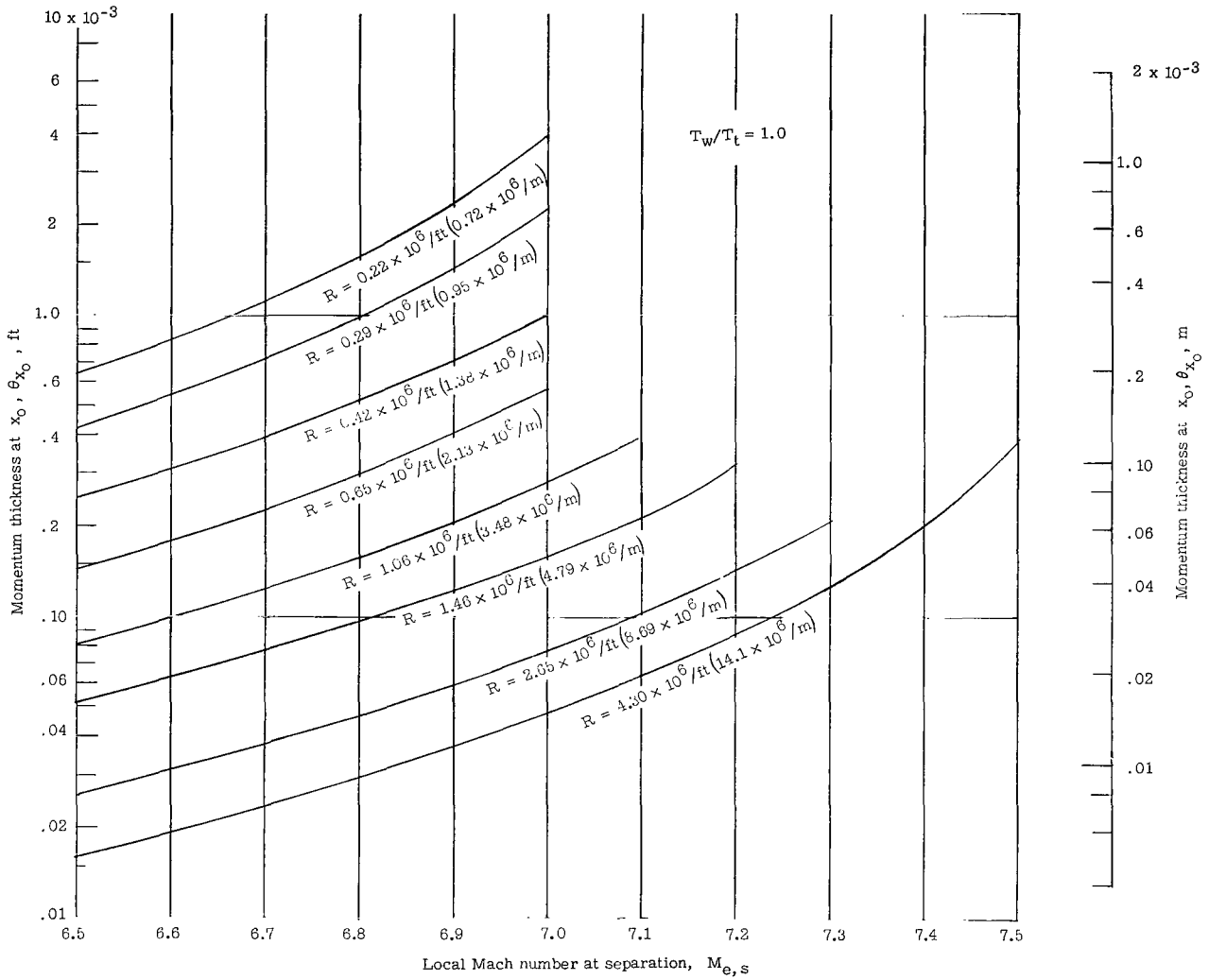


Figure 32.- The momentum thickness at beginning of interaction region plotted against local Mach number at separation for adiabatic wall conditions at various unit Reynolds numbers.

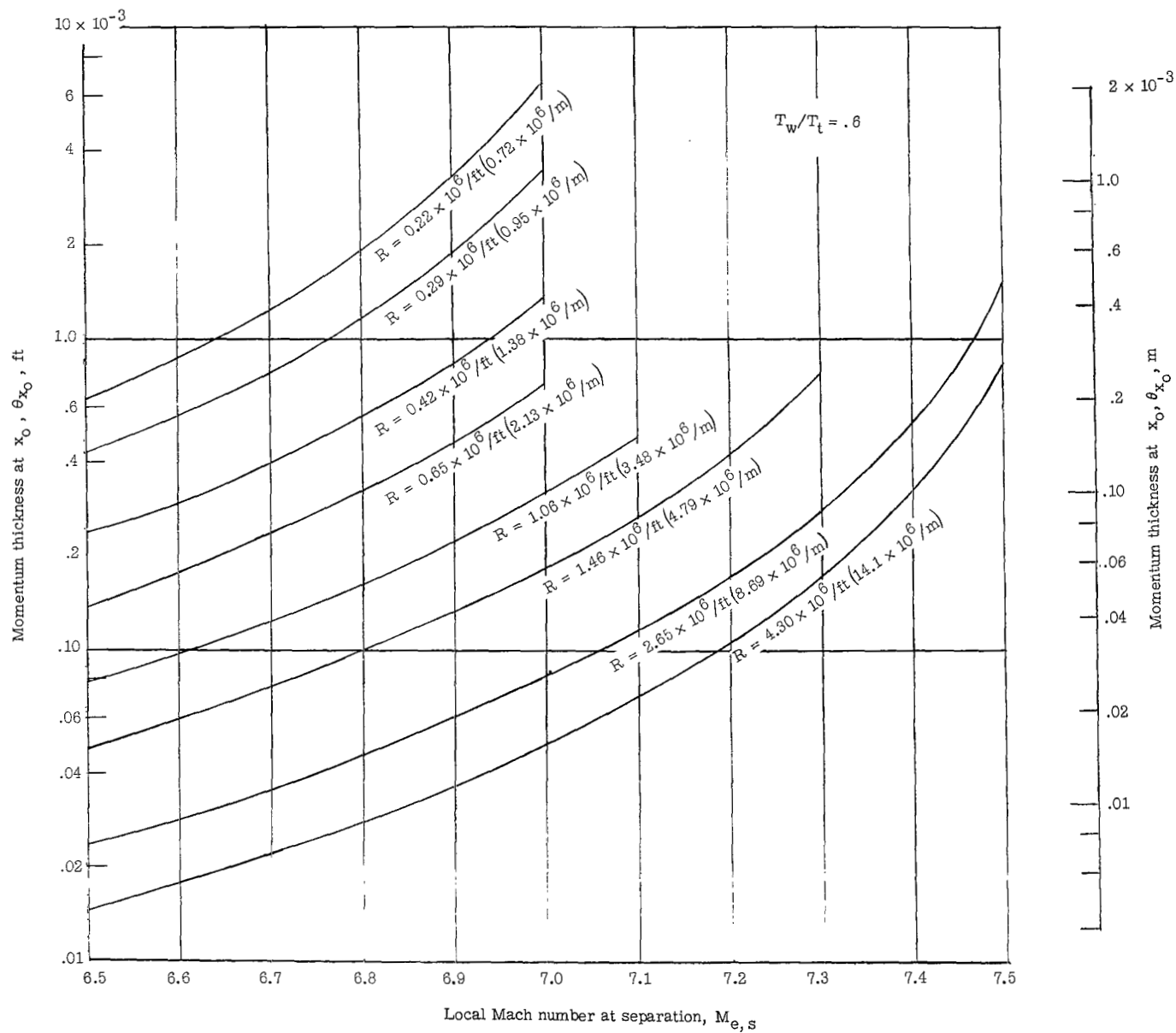


Figure 33.- The momentum thickness at the beginning of the interaction region versus the local Mach number at separation for cool wall conditions at various unit Reynolds numbers.

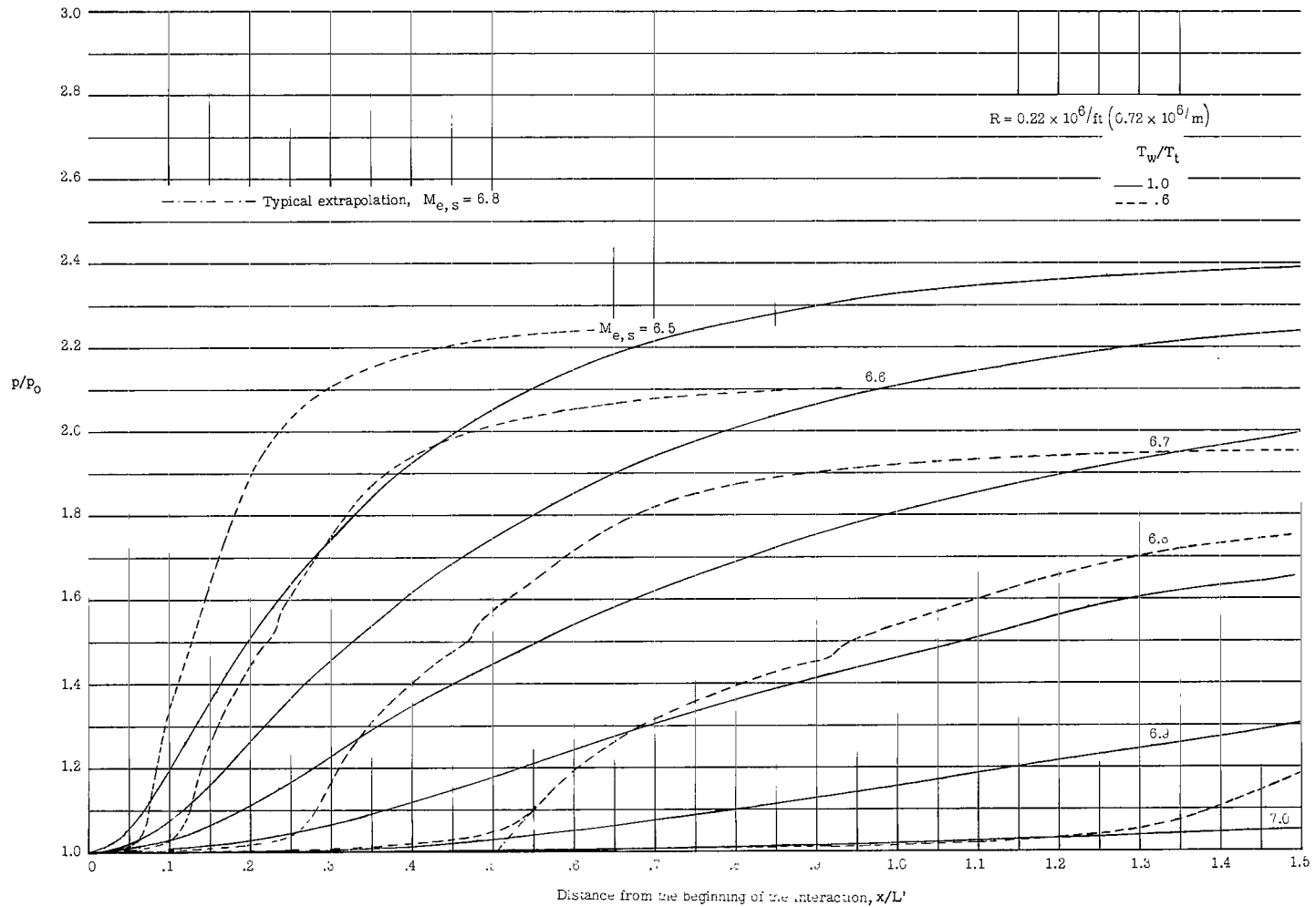


Figure 34.- The theoretical pressure rise due to separation for various local Mach numbers at separation for cool and adiabatic wall conditions at various unit Reynolds numbers.

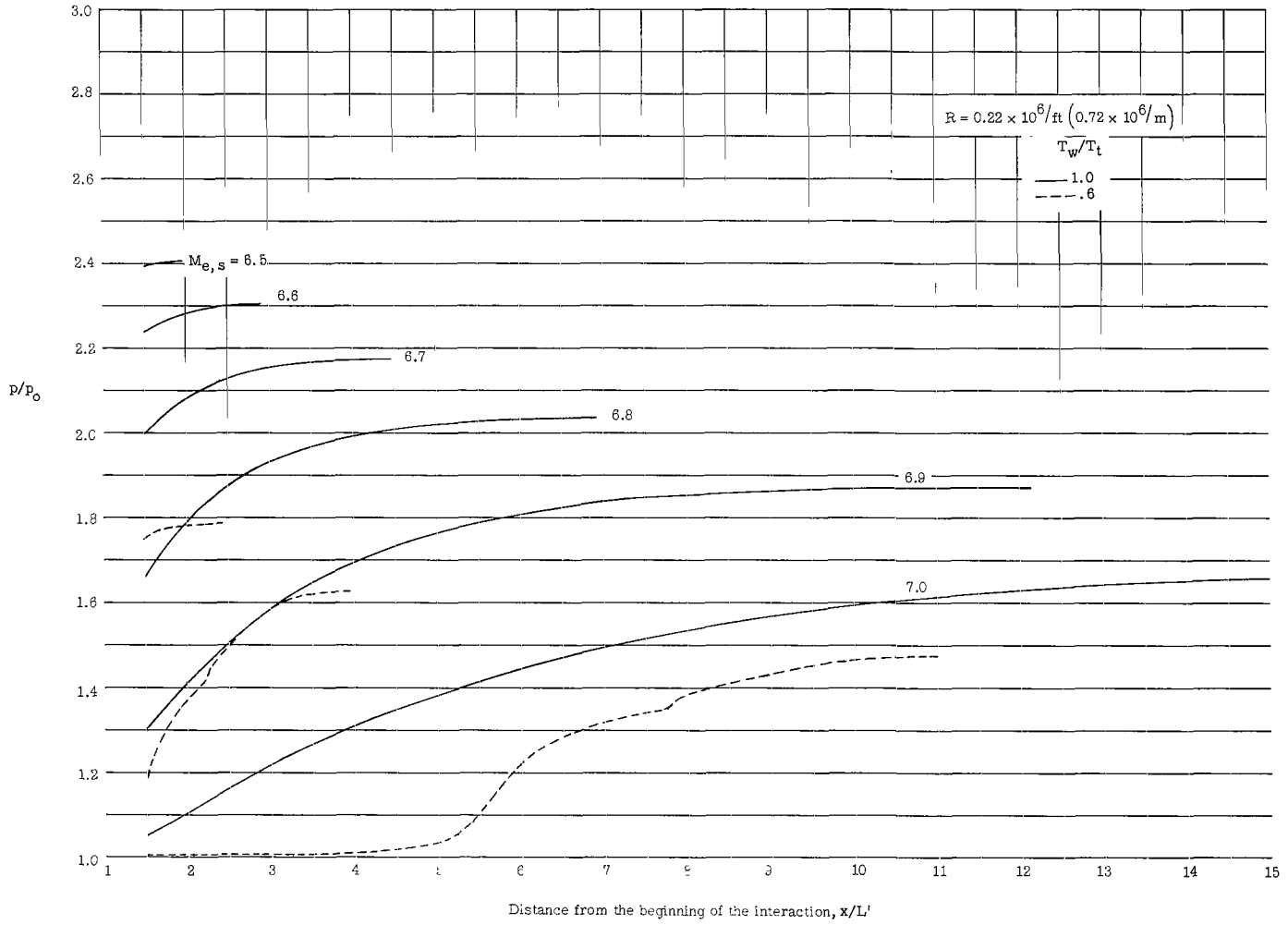


Figure 34.- Continued.

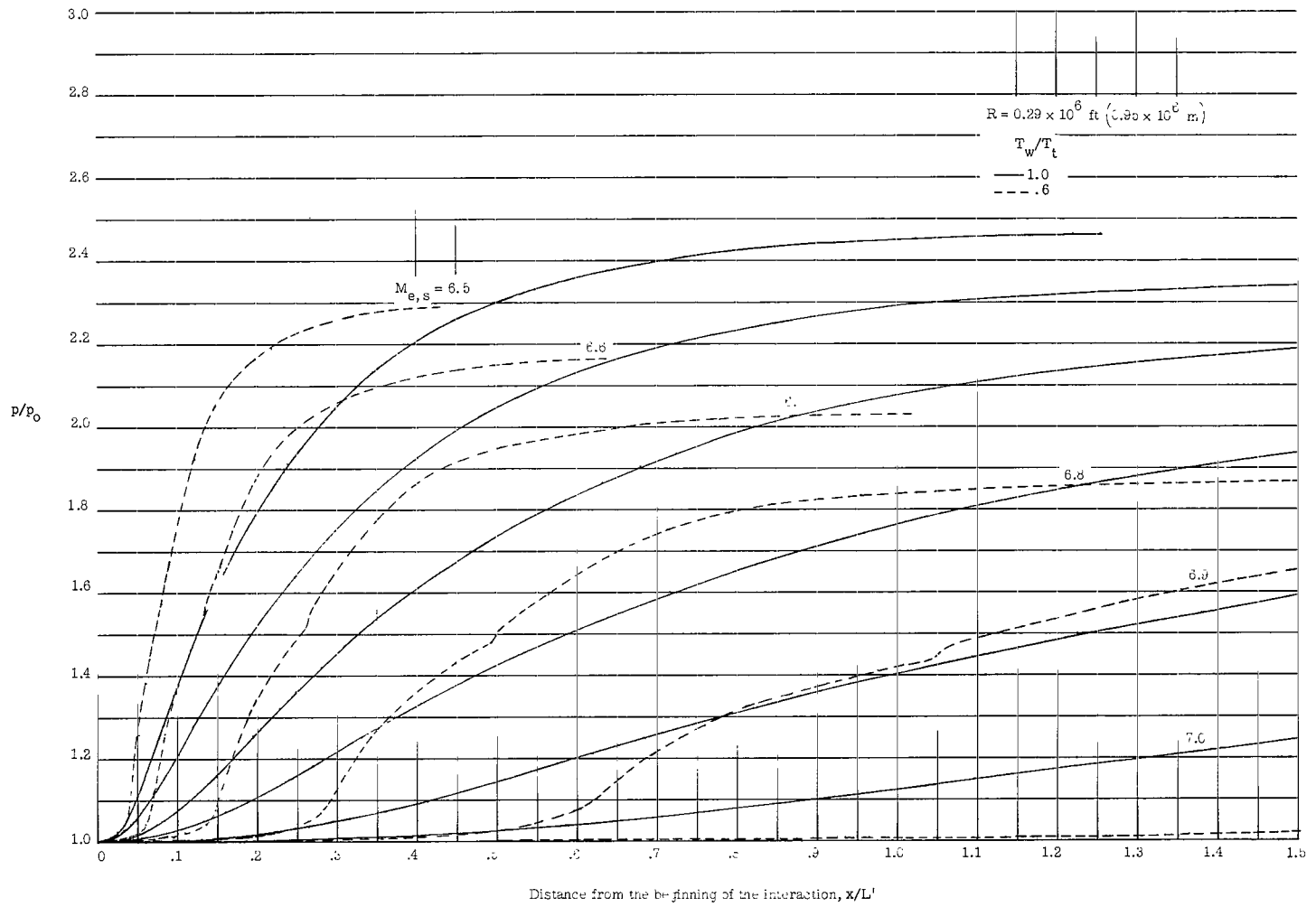


Figure 34.- Continued.

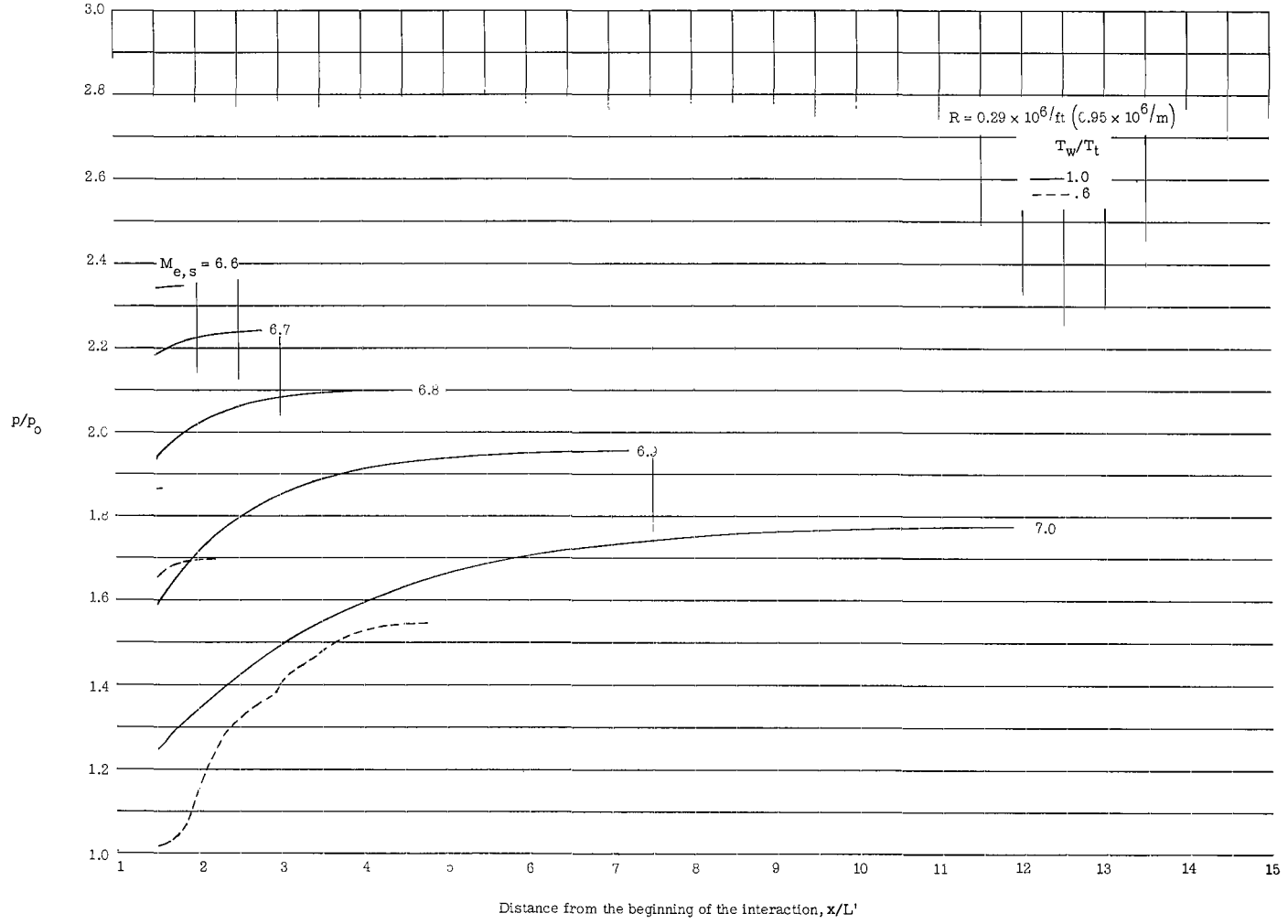
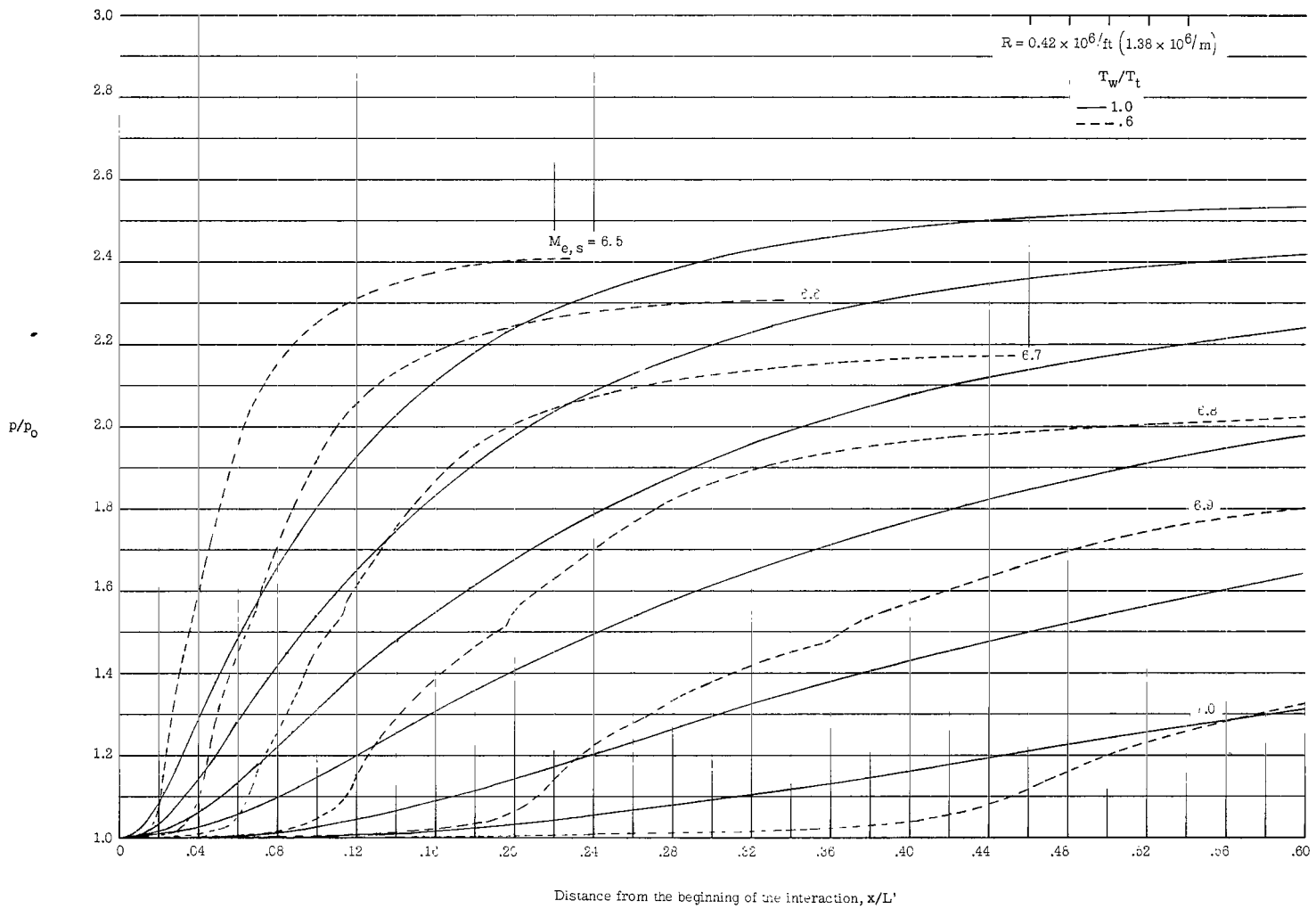


Figure 34.- Continued.



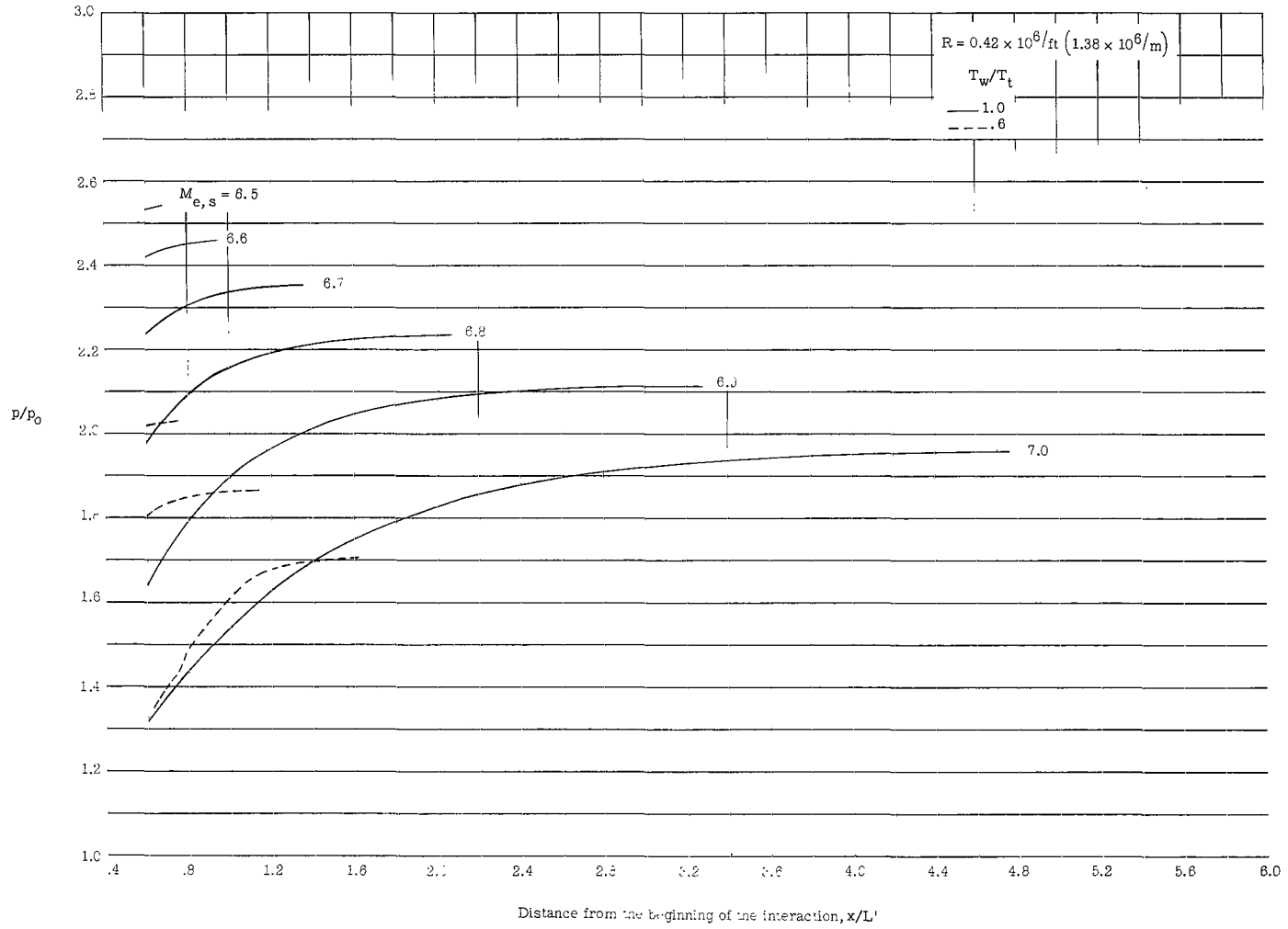


Figure 34.- Continued.

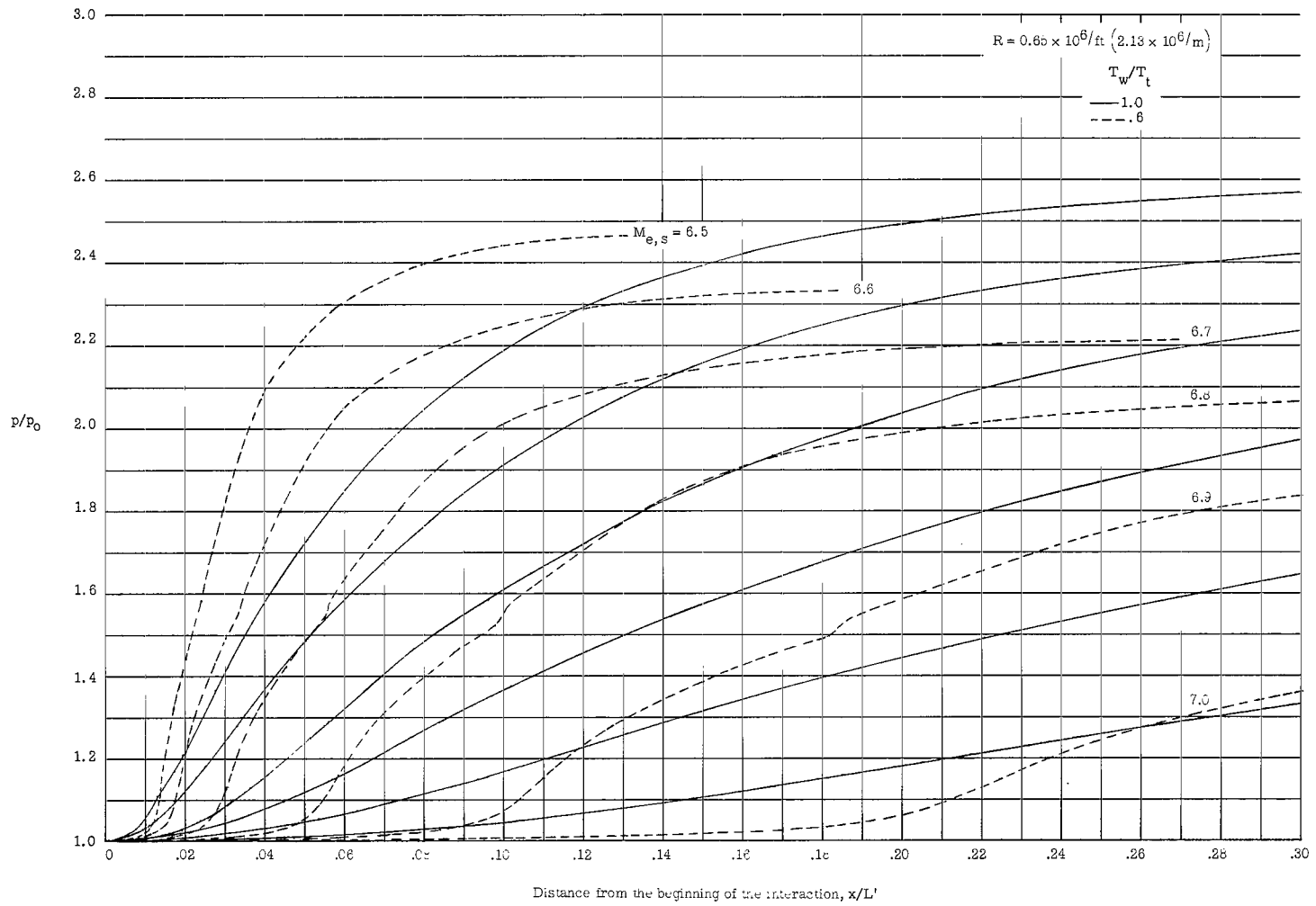


Figure 34.- Continued.

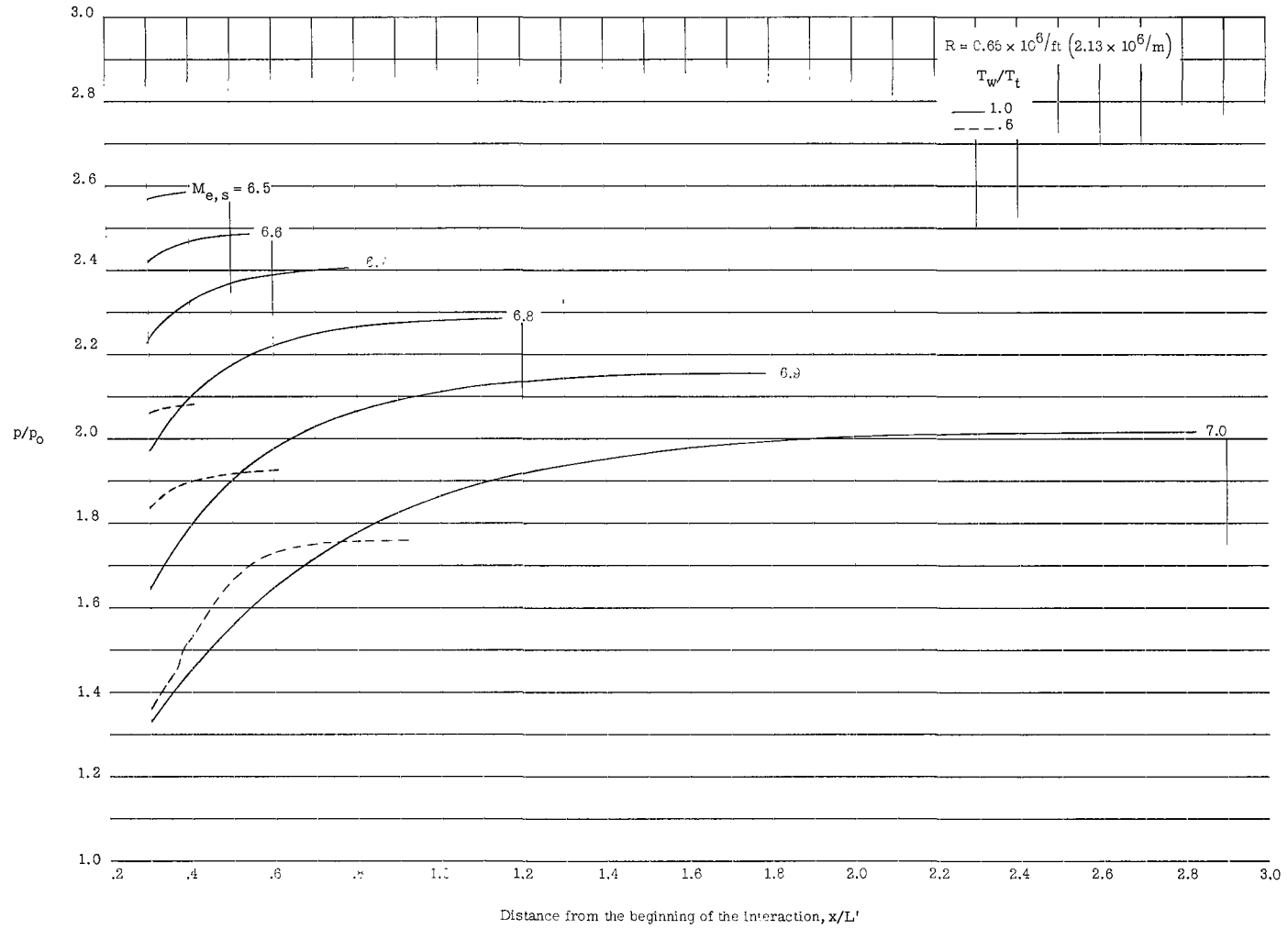


Figure 34.- Continued.

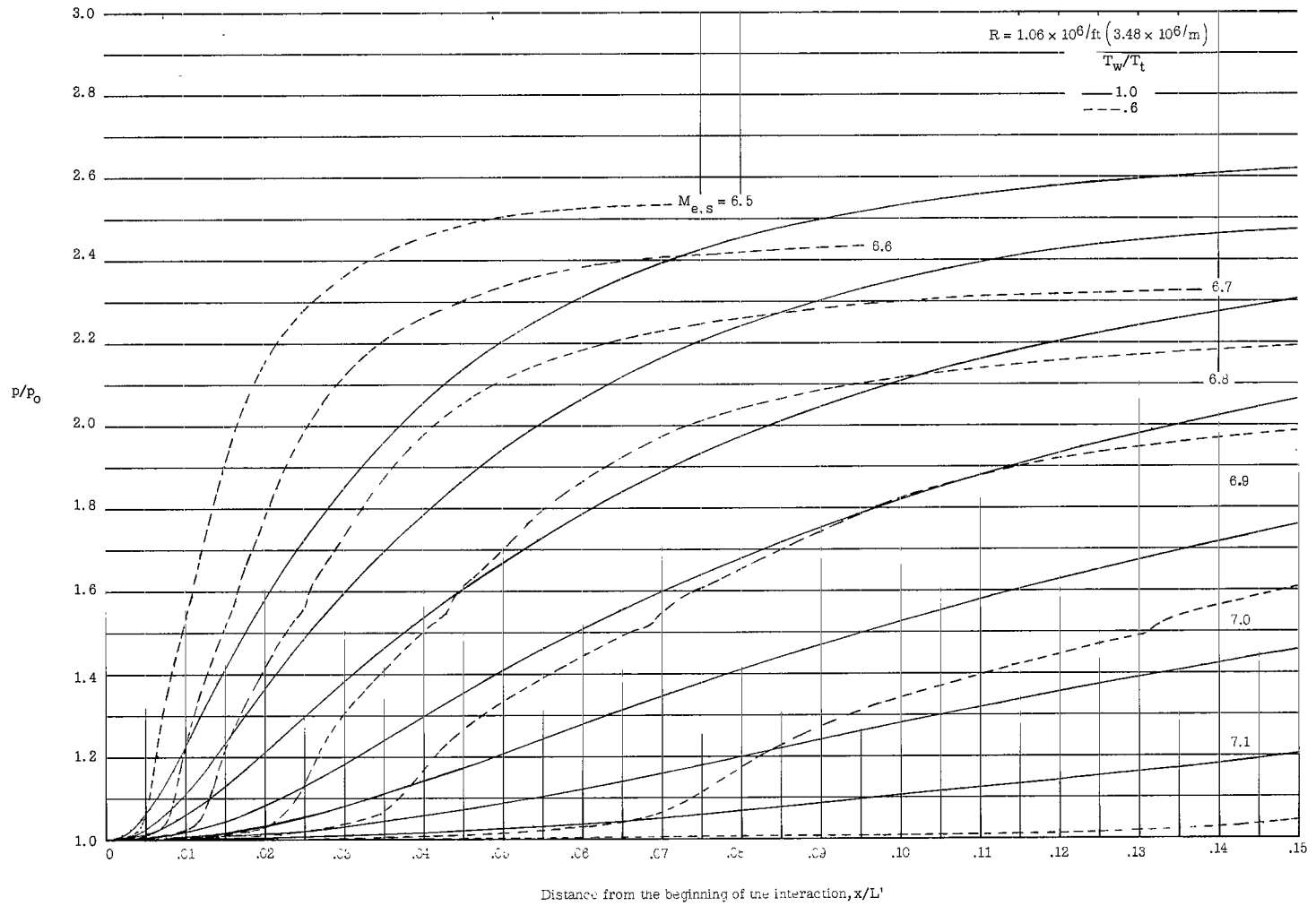


Figure 34.- Continued.

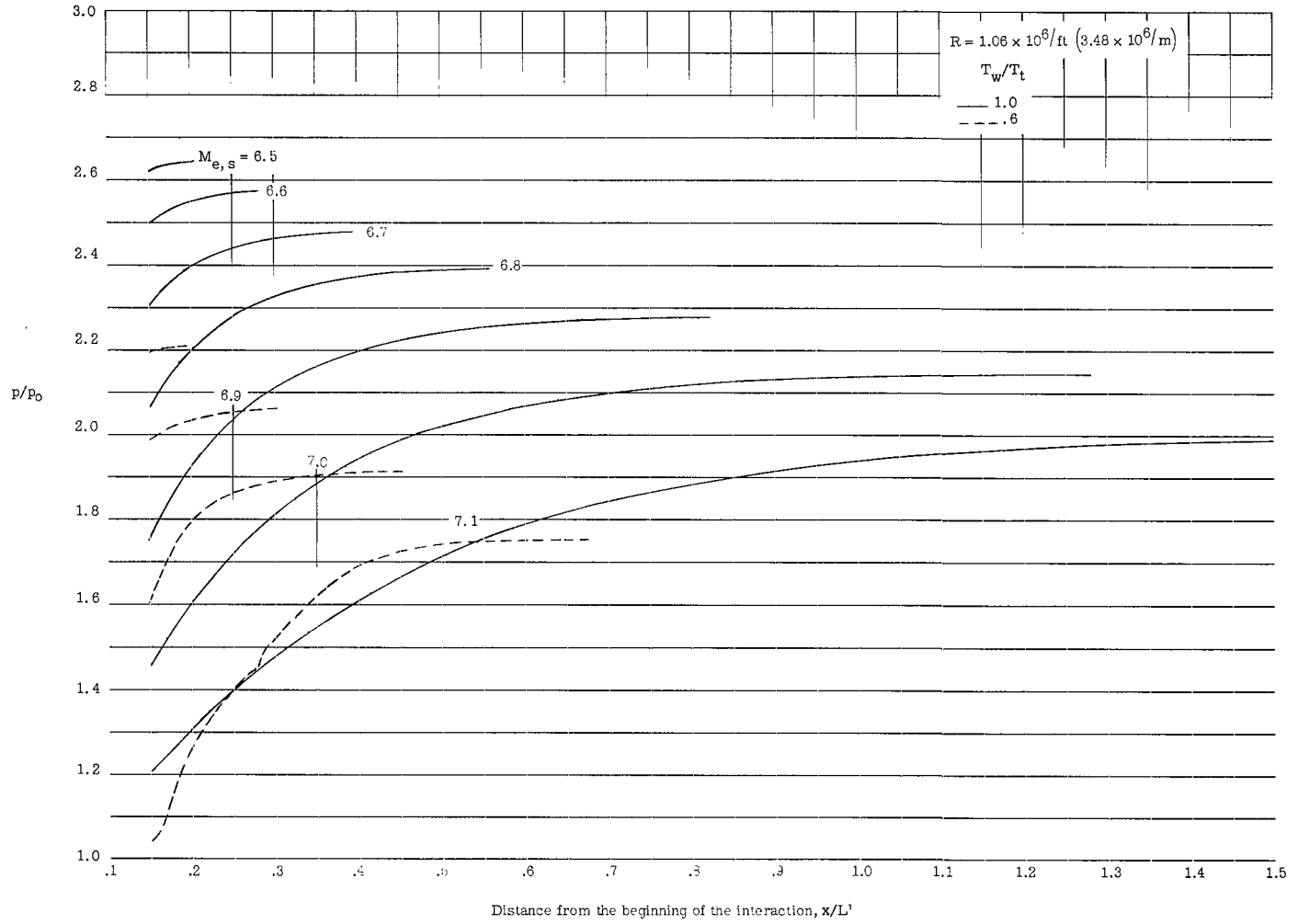


Figure 34.- Continued.

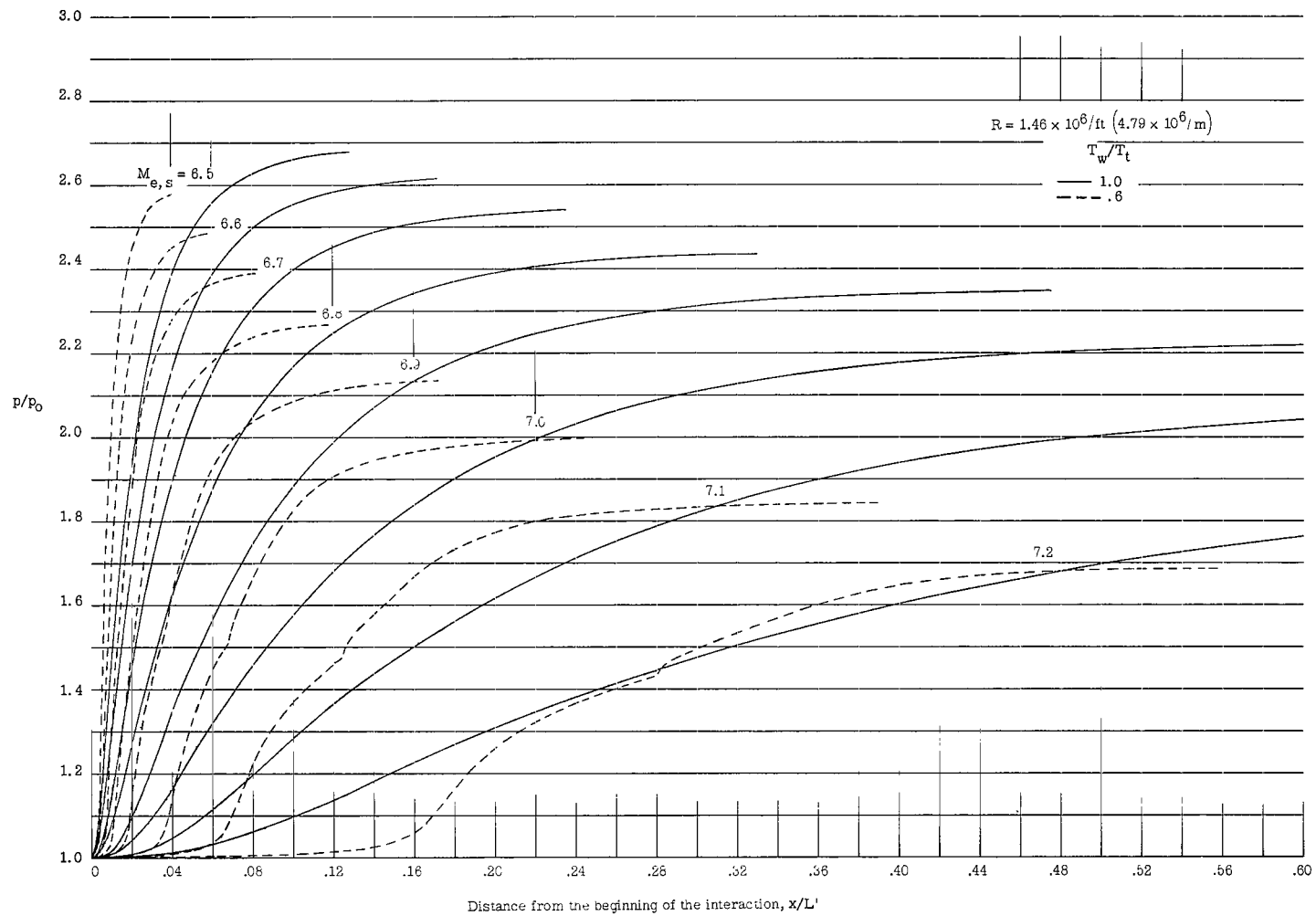


Figure 34.- Continued.

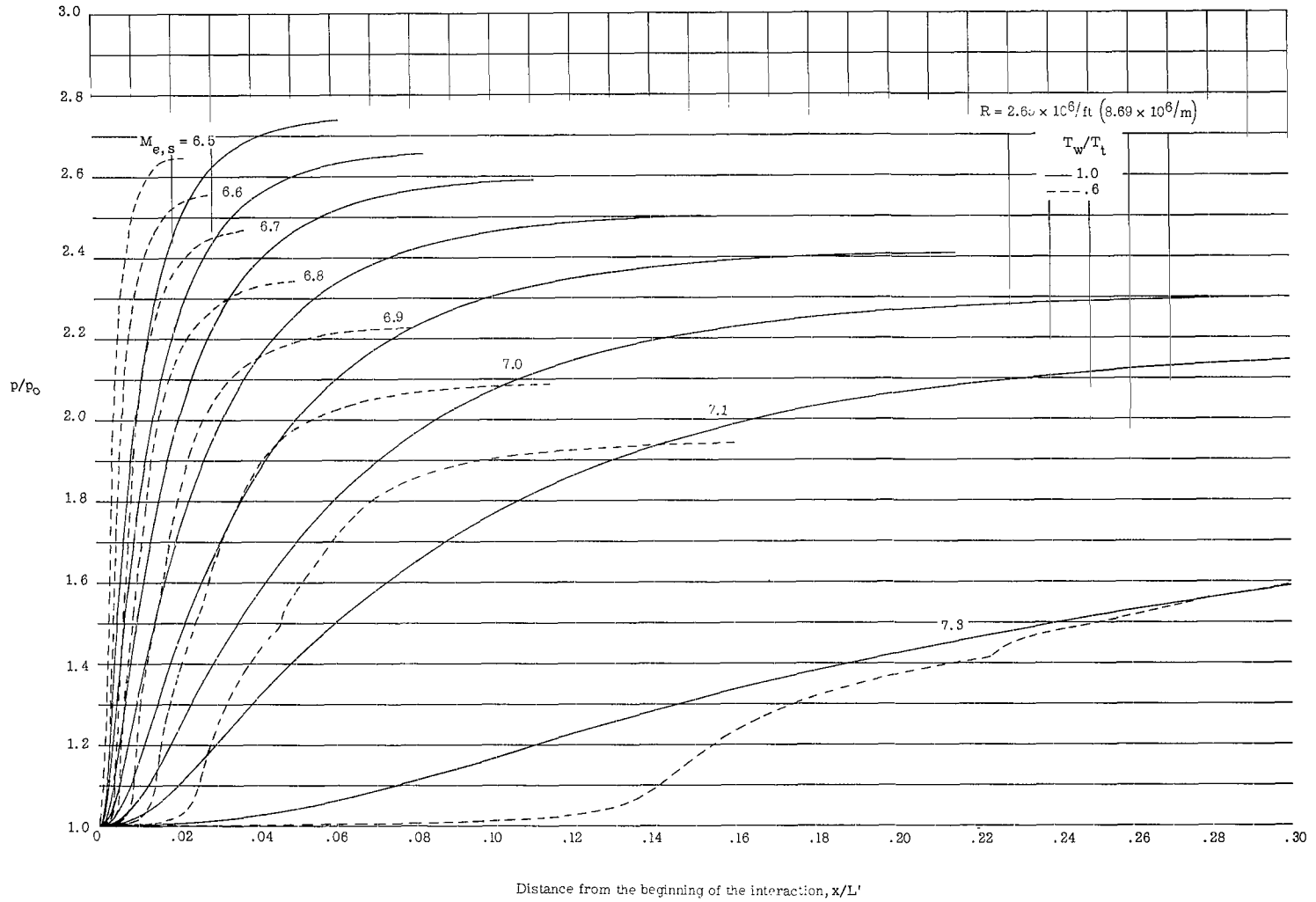


Figure 34.- Continued.

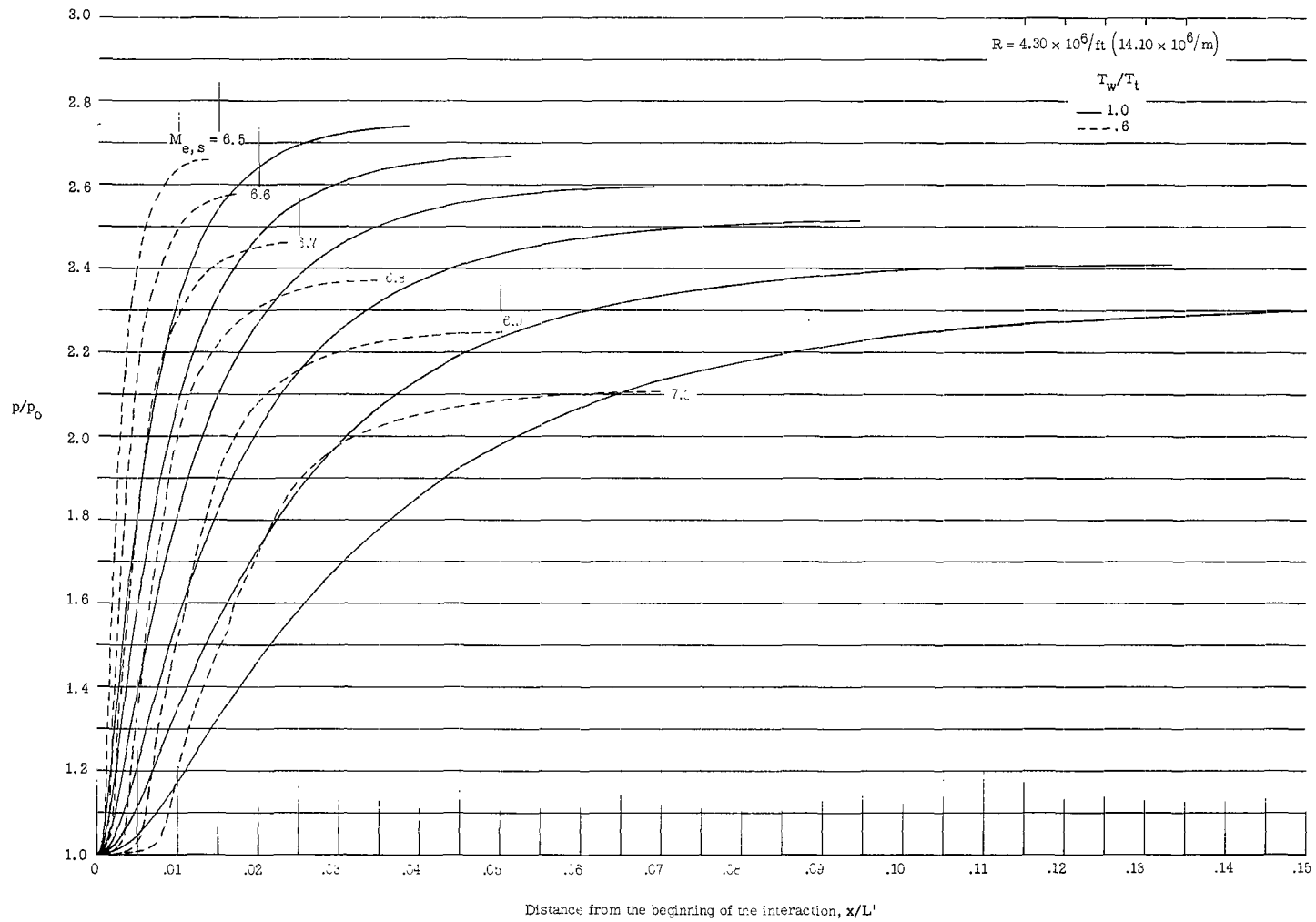


Figure 34.- Concluded.

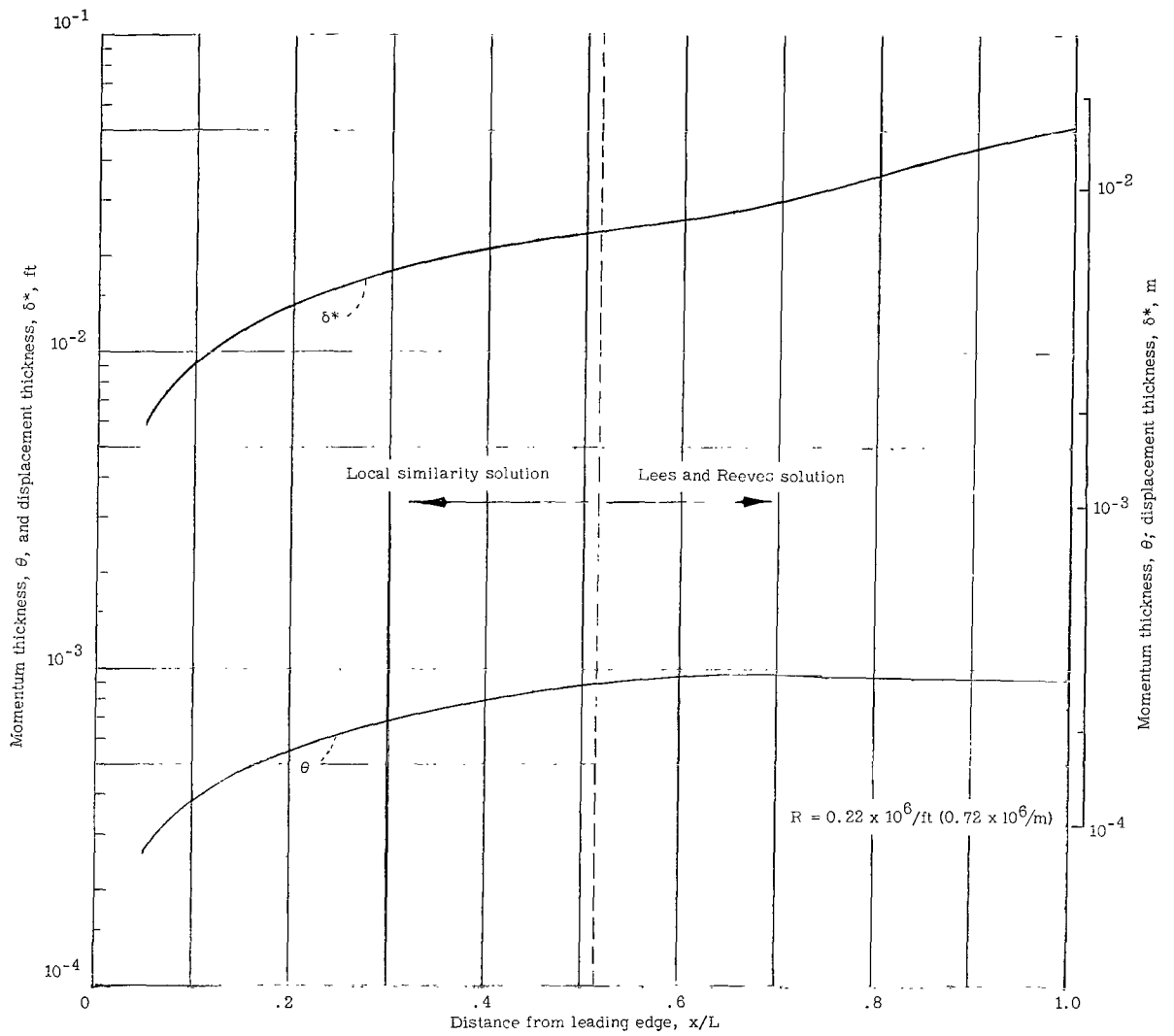


Figure 35.- A comparison of the growth of the momentum thickness and the displacement thickness over a flat plate with flow separation.

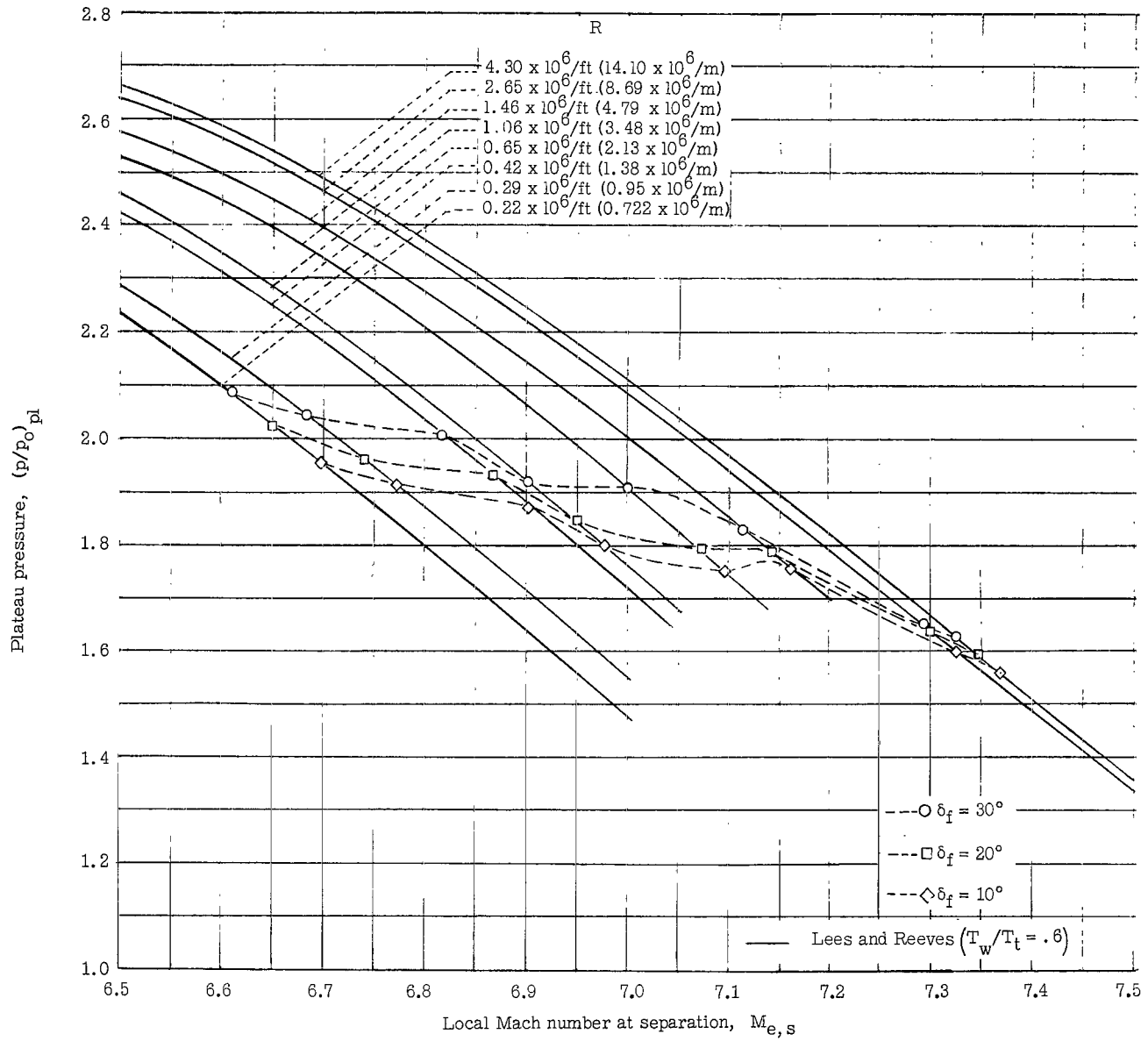


Figure 36.- The effect of Reynolds number and flap angle on the theoretical prediction of plateau pressure for cool walls.

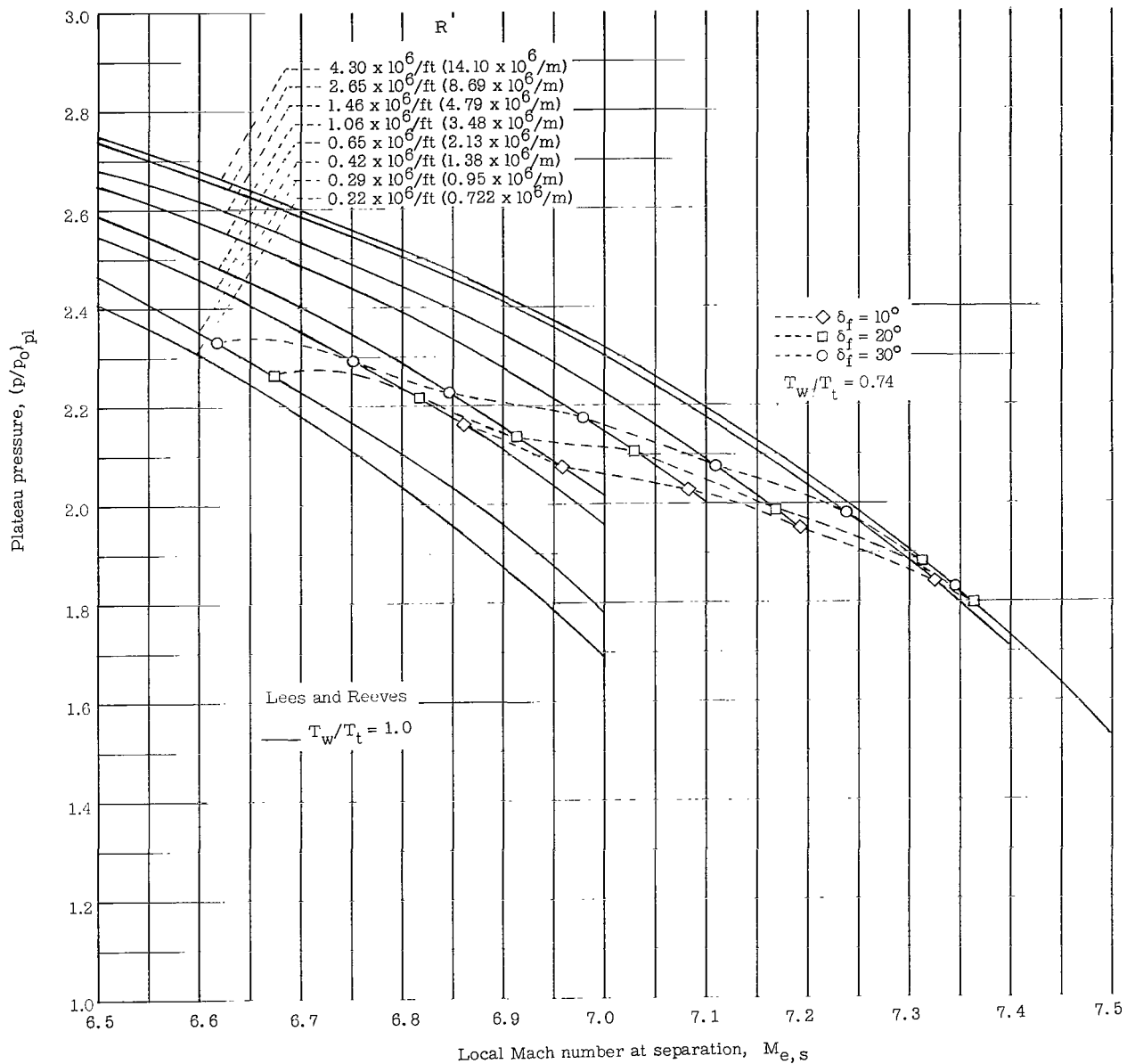


Figure 37.- The effect of Reynolds number and flap angle on the theoretical prediction of plateau pressure for adiabatic walls.

OFFICIAL BUSINESS

070 001 37 DL BDS 68044 00903
AIR FORCE WEAPONS LABORATORY/AFWL/
KIRTLAND AIR FORCE BASE, NEW MEXICO 87117

ATTN: MISS SUELENE T. CAMPA, CHIEF TECHNICAL
LIBRARY/AFWL

POSTMASTER: If Undeliverable (Section 158
Postal Manual) Do Not Return

"The aeronautical and space activities of the United States shall be conducted so as to contribute . . . to the expansion of human knowledge of phenomena in the atmosphere and space. The Administration shall provide for the widest practicable and appropriate dissemination of information concerning its activities and the results thereof."

—NATIONAL AERONAUTICS AND SPACE ACT OF 1958

NASA SCIENTIFIC AND TECHNICAL PUBLICATIONS

TECHNICAL REPORTS: Scientific and technical information considered important, complete, and a lasting contribution to existing knowledge.

TECHNICAL NOTES: Information less broad in scope but nevertheless of importance as a contribution to existing knowledge.

TECHNICAL MEMORANDUMS: Information receiving limited distribution because of preliminary data, security classification, or other reasons.

CONTRACTOR REPORTS: Scientific and technical information generated under a NASA contract or grant and considered an important contribution to existing knowledge.

TECHNICAL TRANSLATIONS: Information published in a foreign language considered to merit NASA distribution in English.

SPECIAL PUBLICATIONS: Information derived from or of value to NASA activities. Publications include conference proceedings, monographs, data compilations, handbooks, sourcebooks, and special bibliographies.

TECHNOLOGY UTILIZATION PUBLICATIONS: Information on technology used by NASA that may be of particular interest in commercial and other non-aerospace applications. Publications include Tech Briefs, Technology Utilization Reports and Notes, and Technology Surveys.

Details on the availability of these publications may be obtained from:

SCIENTIFIC AND TECHNICAL INFORMATION DIVISION
NATIONAL AERONAUTICS AND SPACE ADMINISTRATION

Washington, D.C. 20546